

ABSTRACT

Title of Document: INVESTIGATION OF A CABLE-DRIVEN
PARALLEL MECHANISM FOR PRESSURE
SUIT ARM RESIZING AND MOTION
ASSISTANCE

Elizabeth Ann Benson, Master of Science, 2007

Directed By: Professor David L. Akin
Department of Aerospace Engineering

The fit of a spacesuit has been identified as a crucial factor that will determine its usability. Therefore, because one-size-fits-all spacesuits seldom fit any wearer well, and because individually tailored spacesuits are costly, the University of Maryland has conducted research into a resizable Extravehicular Activity (EVA) suit. This resizing is accomplished through a series of cable-driven parallel manipulators, which are used to adjust the distance between plates and rings built into a soft space suit. These actuators, as well as enabling passive suit resizing, could be used to actively assist the astronaut's motion, decreasing the torques that must be applied for movement in a pressurized suit. This thesis details the development and testing of an arm test section, which is used to better understand the dynamics of a more complex torso-limb system.

Investigation of a Cable-Driven Parallel Mechanism for Pressure Suit Arm Resizing
and Motion Assistance

By

Elizabeth Ann Benson

Thesis submitted to the Faculty of the Graduate School of the
University of Maryland, College Park, in partial fulfillment
of the requirements for the degree of
Master of Science
2007

Advisory Committee:

Associate Professor David L. Akin

Associate Professor Robert M. Sanner

Dr. Mary Bowden

© Copyright by
Space Systems Laboratory
2007

Dedication

This thesis is dedicated to the memory of my grandfather, Lee Ashby Benson, who passed away suddenly earlier this year. He had grand plans for each of his twenty grandchildren, and never once doubted that they would come true. Even as his health began to fail, he continued to clip out any article mentioning NASA in any of the many publications he read, and send it along in the mail. His interest in my dreams, and his unwavering belief in me, have always been inspirational and humbling. I hope that I will continue to make him proud, and will work twice as hard as ever, to be half the engineer that he was.

Acknowledgments

Where do I even begin? I have so many people to be thankful for. First of all, my family has stood by me through thick and thin, through all the highs and lows of life as a graduate student. All your thoughts and prayers were appreciated more than you can imagine. Thanks for dragging the whole family out to Goddard and the Air and Space Museum so many times, to satisfy my need to ogle NASA artifacts. Thanks for always telling me that things would work out OK, even when it didn't seem possible.

Thanks also to my thesis advisor, Dr. David Akin. Thanks especially for being patient with me as I searched for a thesis topic, and for providing such an amazing place to work and grow. This really has been an amazing experience for me, and has opened doors that I didn't even know existed. After all, where else can a student scuba dive with robots? I cannot begin to say how amazing this place is – I was made to feel at home, the minute I walked through the door.

I also owe a great deal of thanks to the other members of my thesis committee: Dr. Mary Bowden and Dr. Robert Sanner. Thanks for taking the time out of your busy schedules to read my thesis and preside at my defense, during a week crammed with thesis defenses.

Thanks also to Kiwi, the guy who keeps our servers running despite our apparent efforts to bring everything to a grinding halt. Thanks for finding the time to answer questions between crises.

Last but not least, I have to thank all of the SSLers. Thanks to the old guard who provided much needed support and advice, the incoming students who quickly became new friends, and the class I entered with, who are now scattering to their separate parts of the world. The moment I arrived at this lab, I knew I had come to a pretty amazing place (again, scuba diving with a space suit comes to mind), but not just because of the awesome facilities. The main thing that attracted me to this lab when I visited, was the friendliness of its students. The atmosphere lived up to my expectations, and now I am sad to leave behind so many amazing friends. I'm going to miss all of you very much. Best of luck to you in the future, and may we all meet again some day... perhaps in Houston?

Table of Contents

Dedication.....	ii
Acknowledgments.....	iii
List of Figures.....	vii
Chapter 1 : Introduction.....	1
1.1 The Reconfigurable Suit Concept.....	1
1.2 The Morphing Upper Torso (MUT).....	5
1.3 A Simplified Test Section.....	6
Chapter 2 : Background and Literature Review.....	8
2.1 The Need for a New Planetary Suit.....	8
2.1.1 The Apollo Planetary Suit: A7L.....	10
2.1.2 NASA’s Workhorse: The Shuttle EMU.....	14
2.2 Advanced Suit Prototypes.....	18
2.2.1 The AX-5: A Hard Suit.....	19
2.2.2 An Elegant Compromise? The Mk-III.....	22
2.2.3 I-Suit: Perfecting the Art of Soft Mobility Joints.....	25
2.3 Hard Suit or Soft?.....	27
2.4 The Properties of a Soft Suit.....	27
2.4.1 The Importance of Fit.....	28
2.4.2 The Behavior of Soft Mobility Joints.....	30
2.4.3 Constraints on Internal Pressure.....	34
2.5 Upgrades to the Soft Suit.....	36
2.5.1 Joint Actuation Assistance.....	37
2.5.2 A System for Active Resizing and Motion Assistance.....	38
2.6 The Stewart Platform.....	42
2.7 Tendon Based Parallel Manipulators.....	47
Chapter 3 : Initial Investigations.....	49
3.1 Early Prototypes.....	49
3.2 Single-Link Wrist Joint.....	50
3.3 Rotational Interference Model.....	54
3.4 Whole-Arm Mockup.....	58
Chapter 4 : Test Setup.....	61
4.1 Construction of the Test Section.....	61
4.1.1 Fabricating the Pressurized Sleeve.....	63
4.1.2 Method for Connecting a Fabric Cylinder to a Metal Plate.....	63
4.1.3 Heat Sealing the Pressure Bladder.....	65
4.1.4 Assembling the Test Section.....	68
4.2 Pressurizing the Test Section.....	69
4.3 Attaching Links to the Plates.....	70
4.4 Node Measurement Setup.....	73
4.4.1 FAROArm Calibration.....	74
4.4.2 Taking Measurements Using the FAROArm.....	76
4.5 Load Measurement Setup.....	77
4.5.1 Amplification of Load Cell Signal.....	77

Chapter 5 : Inverse Kinematics for the Stewart Platform	80
5.1 Definition of Coordinate Systems	80
5.2 MATLAB Code	82
5.2.1 Vector Representations of Node Locations	82
5.2.2 Transformation of Platform Nodes to Base Coordinate System.....	83
Chapter 6 : Results	85
6.1 Qualitative Results	85
6.1.1 Node Numbering Convention	85
6.1.2 Labeling Convention: Link Length vs. Node-Node Distance	86
6.1.3 Pressurization with Parallel Plates	89
6.1.4 Pressurization at More Complex Configurations.....	94
6.2 Quantitative Results	96
6.2.1 Error in Platform Center Location	96
6.2.2 Euler Angle Calculation.....	106
6.2.3 Accuracy and Precision in Position and Orientation of Platform	110
6.2.4 Measurement of Link Tension	114
6.2.5 Application of Inverse Kinematics to Arm Length Changes.....	119
Chapter 7 : Conclusions and Future Work.....	122
7.1 Conclusions	122
7.2 Future Work	123
7.2.1 Testing to be Conducted with the Test Section	123
7.2.2 Modifications to the Test Section	124
7.2.3 Application to the MX-II	125
References.....	134

List of Figures

Figure 1: Resizing of a Space Suit Arm.....	2
Figure 2: Stewart Platform Configuration	3
Figure 3: Morphing Arm Configuration, and Deflection of Wires.....	4
Figure 4: Morphing Upper Torso in Expanded and Resized Configurations[MUT Paper]	5
Figure 5: Pressure Constrained Stewart Platform Test Section	7
Figure 6: Artist Concept of Lunar Operations, Vision for Space Exploration [VSE Report]	9
Figure 7: The Apollo A7L, with and without protective outer layer (TMG) [Wiki,ALSJ].....	11
Figure 8: Apollo Glove and Wrist Segment [Apollo 14 Mission Report].....	13
Figure 9: Shuttle EMU [CapcomeSpace.net,].....	15
Figure 10: The EMU Hard Upper Torso (HUT) [SUT]	16
Figure 11: EMU Suit Donning Procedure [Tiger Team]	17
Figure 12: The AX-5 Suit [HowStuffWorks, DivingHeritage.com]	19
Figure 13: The MK-III Zero Prebreathe Suit [NASA.gov,Spaceflight.NASA.gov] ..	22
Figure 14: Rear Entry (Left) and Waist Entry (Right) I-Suit [DRATS,I Suit Advanced].....	25
Figure 15: The Layers of a Shuttle EMU [madehow.com]	28
Figure 16: Convolute Joint.....	31
Figure 17: Gored Joint	32
Figure 18: Power Assisted Glove [00635330].....	38
Figure 19: SUT Shape when Undeformed (Left) and Reconfigured (Right) [SUT] ..	39
Figure 20: Resizing of the I-Suit SUT [MUT].....	40
Figure 21: Influence of Fabric on Wire Shape [MUT]	41
Figure 22: A Cappel Flight Simulator [Parallemic.com].....	43
Figure 23: Platform Degrees of Freedom	44
Figure 24: A Simple Example.....	45
Figure 25: Possible table configurations.....	46
Figure 26: Example of a tendon-based parallel robot [Tendon Based]	47
Figure 27: Initial Prototype of Manipulator.....	49
Figure 28: Correct Measurement Location for Wrist-Sized Ring	50
Figure 29: Single-Linkage Wrist at 0 and 90 degree Rotations.....	51
Figure 30: Pitch and Yaw Flexibility of Manipulator.....	52
Figure 31: Novel Rotational Joint on the A7L Shoulder [ALSJ]	52
Figure 32: Wires Crossing into Interior of Ring (at 30 Degree Rotation)	53
Figure 33: Top Down View of the Wrist (Ellipse), Forearm (Circle), Outer Rings (Dashed Line), Inner Ring (Dotted Lin) and Links (Solid Lines)	54
Figure 34: Arm Mockup	58
Figure 35: 'Horseshoe' Ring Placement and Shape.....	59
Figure 36: Horseshoe Ring, Showing Reinforcement	60
Figure 37: Elbow Joint Interference	60
Figure 38: Pressurized Test Section.....	62

Figure 39: A test sleeve, turned inside out to show flange tabs.....	63
Figure 40: End Plate (Left) and Flange (Right)	64
Figure 41: Heat Sealing Tool.....	65
Figure 42: Top Left: Urethane coated (white) and uncoated (blue) sides of fabric. Top Right: Heat Sealing the Test Section. Bottom: Testing the seam of the test section	66
Figure 43: Heat Sealing the Flange.....	67
Figure 44: Compressor, Pressurized Line into Test Section, Regulator and Pressure Gauge	69
Figure 45: Link Attachment.....	70
Figure 46: Line Extending from Either Side of Washer	71
Figure 47: Turnbuckle.....	72
Figure 48: Test Section, with Turnbuckles Integrated.....	72
Figure 49: Left: FAROArm with Workstation. Top Right: FAROArm in Use. Bottom Right: FAROArm Probe	74
Figure 50: Calibration of FAROArm.....	75
Figure 51: Amplification Circuit	78
Figure 52: Load Cell Calibration Curve	78
Figure 53: Load Cell Integration.....	79
Figure 54: Left: Top Down View of Platform in Neutral Position. Center: Node Numbering Right: Base and Platform Coordinate Systems.....	81
Figure 55: Relationship Between Nodes in A and B Coordinate Systems	81
Figure 56: Node Numbering Convention	86
Figure 57: Test Section Labeling.....	86
Figure 58: Exaggerated cross section of undeformed (left) and pressurized (right) test segment	87
Figure 59: Initial Pressurization of Test Section. A.) Section Viewed from the Left. B.) Section Viewed from the Front. C.) Section Viewed from the Back	90
Figure 60: Pressurization with 10" Wires	90
Figure 61: 10" Wires, Pressurization 2	92
Figure 62: 1st and 2nd Pressurizations Compared.....	92
Figure 63: Pressurization w/ 12" Wires, Showing Slack	93
Figure 64: Location of Slack Wires, and Resultant Behavior	94
Figure 65: Plate at Drastic Angle Led to Loading of Fabric Sleeve.....	95
Figure 66: Pressurized Section at 13 degrees beta, 3 degrees gamma.....	95
Figure 67: Uniform Deformation Forced by Introduction of Convolutes	98
Figure 68: Section with convolutes (Left) and without (Right).....	100
Figure 69: Change in Shape Between Three Successive Pressurizations.....	101
Figure 70: Pressurization at 6,10 and 60.....	103
Figure 71: Angled Platform with Convolutes Added to Force Uniform Deformation	104
Figure 72: Deformation of Section With and Without Convolutes	106
Figure 73: Calculation of Unit Vectors for Platform Orientation.....	107
Figure 74: Calculation of Correct Angle	108
Figure 75: View of Platform and Nodes Relative to Base, for Verification.....	109
Figure 76: Initial Pressurization, Separation A.....	111

Figure 77: Separation A, Pressurized with Convulutes	113
Figure 78 : Test Section with Load Cell Attached.....	115
Figure 79: Deformation of Wire Links During Measurement of Load on Link 14 (Left) and Link 35 (Right and Center).....	117
Figure 80: Bulging of Fabric Causing Large Side Loads on Load Cell	118
Figure 81: Wire Deformation.....	119
Figure 82: Example ring configuration.....	120
Figure 83: The MX-II [spacecraft.ssl.umd.edu]	126
Figure 84: Addition of Resizing Rings to MX-II. Left: MX-II Torso. Center: Addition of rings. Right: Addition of links connecting rings	127
Figure 85: Sleeve segmentation (cutting the pressure bladder, or leaving it intact). 128	
Figure 86: Indexing: Pressure bladder and restraint layer sleeves stitched together at 'X'	128
Figure 87 : 'Bridge' used to attach wires.....	129
Figure 88: Pressurized MX-II Arm [spacecraft.ssl.umd.edu].....	130

Chapter 1 : Introduction

Since President Bush's "Vision for Space Exploration" speech in 2004, the U.S. space program has been ramping up to return to the moon. In preparation for this endeavor, space suit designers are working to develop the next generation of space suits, which will be needed for operations on the lunar surface and beyond. This suit would ideally be flexible, lightweight, easily maintained, and capable of fitting a wide range of crew members. All of these qualities could potentially be achieved by taking a soft space suit, and actively changing its shape to move in concert with the wearer. This chapter of the paper introduces the concept of the morphing suit, and describes the motivation for the research that was conducted.

1.1 The Reconfigurable Suit Concept

Contradictorily, a suit is easiest to climb into if it is slightly big, but is most mobile and easiest to work in if it fits the wearer tightly. For this reason, researchers at the University of Maryland and ILC Dover have developed the idea of a morphing suit.

A so-called 'soft goods' spacesuit will take the shape of its restraint layer, a fabric enclosure with a high tensile strength. (Imagine blowing a balloon up inside a spherical net, which would then take the pressure loads and dictate the shape of the balloon). If rings could be integrated into this fabric enclosure, its shape could be changed by varying the distance between the rings.

Imagine, for instance, the arm of a spacesuit. Resizing is generally done through the addition or removal of resizing bands, or by adjusting the length of restraint lines (lengths of tubular webbing that take the longitudinal load along a joint). If a series of circumferential rings were built into the restraint layer of the arm, the distance between these rings could be altered to vary the length of the sleeve (Figure 1). This way, the elbow joint could be collocated with the wearer's elbow, and the gloves could be kept in close proximity to the hands (sleeves that are too long can quickly lead to fatigue, since the astronaut must actuate gloves using only the tips of their fingers).

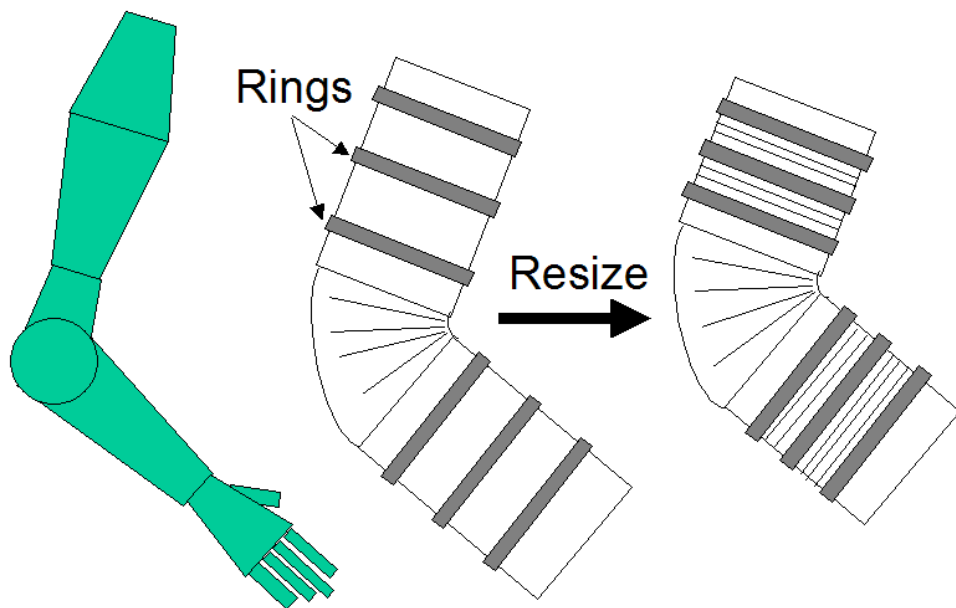


Figure 1: Resizing of a Space Suit Arm

The rings could be connected with cables in a symmetric Stewart Platform configuration, which allows high rigidity and positioning accuracy. In this configuration, three points on one ring are attached by cables to three opposing points on another ring (see Figure 2). The internal pressure maintains the separation

between the rings, keeping the cables in tension. Changing the lengths of these cables would adjust the relative position and orientation of the rings.

A symmetric Stewart Platform configuration (with attachment points spaced symmetrically around the circumference of the plate) is shown in Figure 2. Each of the attachment points (hereafter referred to as a ‘node’) is numbered for easier identification of links. For example, the link connecting nodes 1 and 4 is designated as link 14.

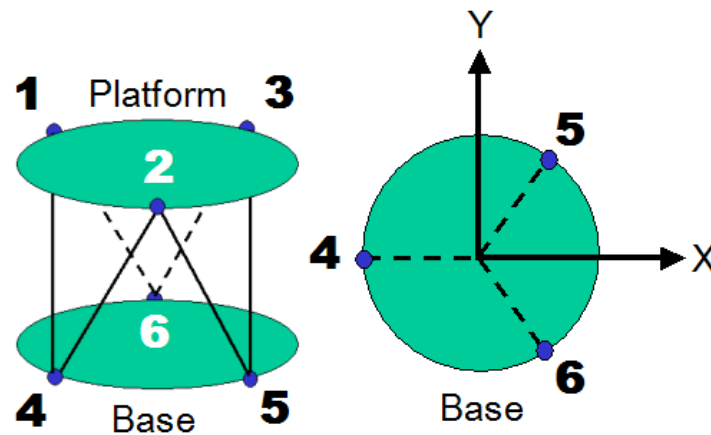


Figure 2: Stewart Platform Configuration

In a Stewart Platform, the bottom plate is designated as the ‘Base’, and considered to be stationary. The top plate is called the ‘Platform’, and is assumed to move relative to the base. This distinction is less apparent when Stewart Platforms are connected in series (since the base will not necessarily be stationary), but the important factor to be considered is still the platform’s motion relative to the base. Figure 3 shows how the Stewart Platforms would be connected in series to form the arm.

A classical Stewart Platform involves six linear actuators, connected between the base and platform. In the morphing suit concept, the links are flexible cables kept in tension by the suit's internal pressure, which applies circumferential and longitudinal loads along the arm. The circumferential load actually causes the fabric sleeve to expand outwards, bowing out the cables that connect the rings. The influence of the pressurized fabric is shown in

Figure 3, which illustrates the ideal and deformed configurations of the links.

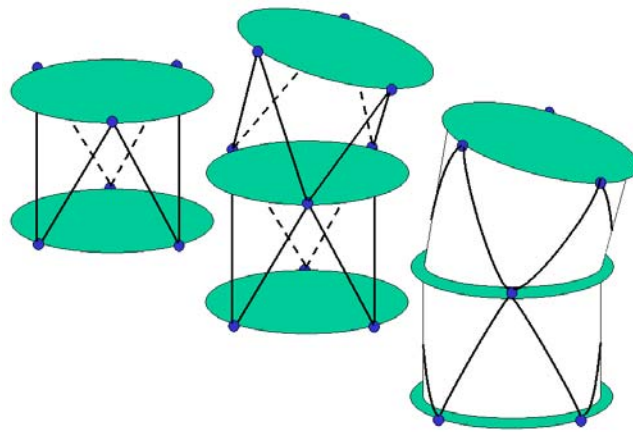


Figure 3: Morphing Arm Configuration, and Deflection of Wires

The behavior of the pressurized fabric is very difficult to quantify, because textiles have very complex material properties, which can vary based on manufacturing technique, previous load history, and the bias of the fabric (direction of weave and warp threads). There is also localized buckling and wrinkling, which can lead to non uniform bulging in the sleeve.

1.2 The Morphing Upper Torso (MUT)

The morphing concept can be adapted to fit any component of a suit, and has already been applied to reshape the upper torso of a space suit. In 2005, researchers at the University of Maryland Space Systems Lab, in cooperation with ILC Dover, built a prototype Morphing Upper Torso (MUT) [1]. In this concept, cables control the positions and orientations of the suit torso's hard components: a helmet ring, back hatch, two scye rings, and a waist ring (see Figure 4). Any adjustment in link lengths will change the positions of the rings relative to the back hatch.

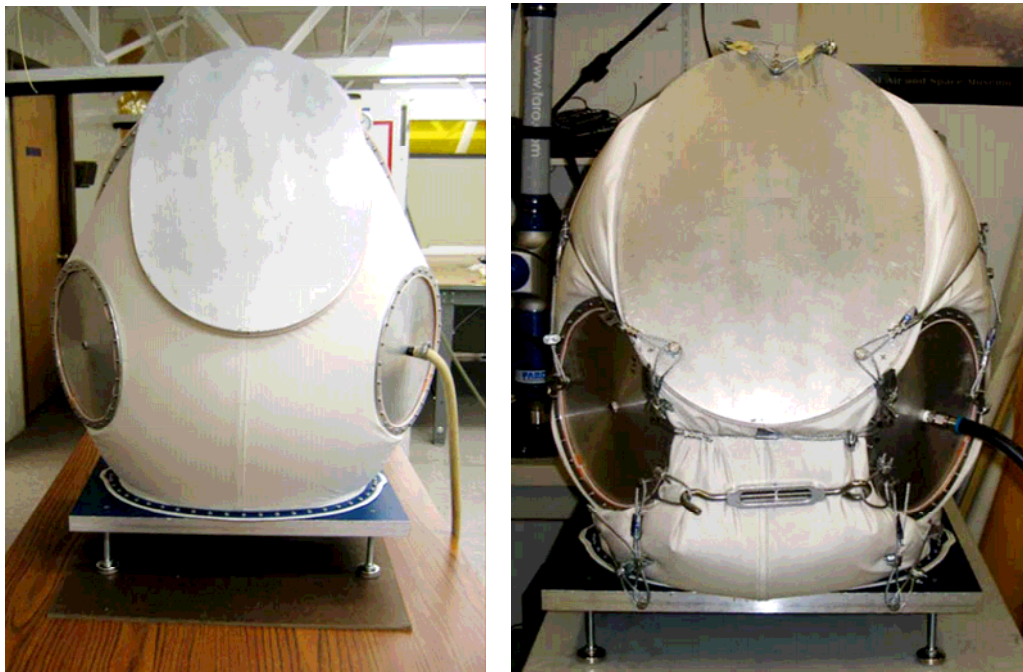


Figure 4: Morphing Upper Torso in Expanded and Resized Configurations[MUT Paper]

The experiments conducted at the University of Maryland helped establish the morphing suit as a concept that merited further research. The upper torso was successfully resized, and some crucial data was collected: loads on links, required

changes in link length to vary the configuration, and sensitivity of the link lengths to changes in plate orientation. Nevertheless, there still remained many unknowns about the behavior of the system. For instance, with what accuracy were the plates being positioned? Would this plate positioning be repeatable, or would the configuration change with each repressurization, as the pressurized fabric shifted into a different configuration? How does the behavior of this system differ from the behavior of a traditional Stewart Platform with rigid links? The following list of properties should be determined, before a morphing arm is built.

1. Accuracy and Precision in Controlling the Location of the Platform
2. Accuracy and Precision in Controlling the Orientation of the Platform
3. Influence of Fabric on Wires (Error in Length)
4. Effect of Pressure on Amount of Wire Impingement
5. Effectiveness of Methods Reducing Fabric Impingement on Wires
6. Sensitivity of Platform Configuration to Errors in Link Length
7. Constraints on Platform's Rotation
8. Required Change in Link Length for Resizing based on Wearer
9. Wearability Issues (Impingement of Wires on Human, e.g.)
10. Determine Loads in Links Based on Platform Configurations

1.3 A Simplified Test Section

The morphing Upper Torso is an extremely complex system, since all of the rings are interconnected (for instance, the helmet is attached to the back plate, but also to the two rings at the shoulders). Any motion of one ring leads to deflection of the other rings, so predicting the dynamics of the system is extremely difficult. The

prototype is so complex, in fact, that it is difficult to characterize the system and obtain a general understanding of its behavior. For this reason, a simplified test section was constructed. This section was composed of two plates spanned by a section of sleeve, and linked together using wires (Figure 5). This configuration should allow testing of the previously listed parameters, as well as a better intuitive understanding of the behavior of a pressure-constrained Stewart Platform.

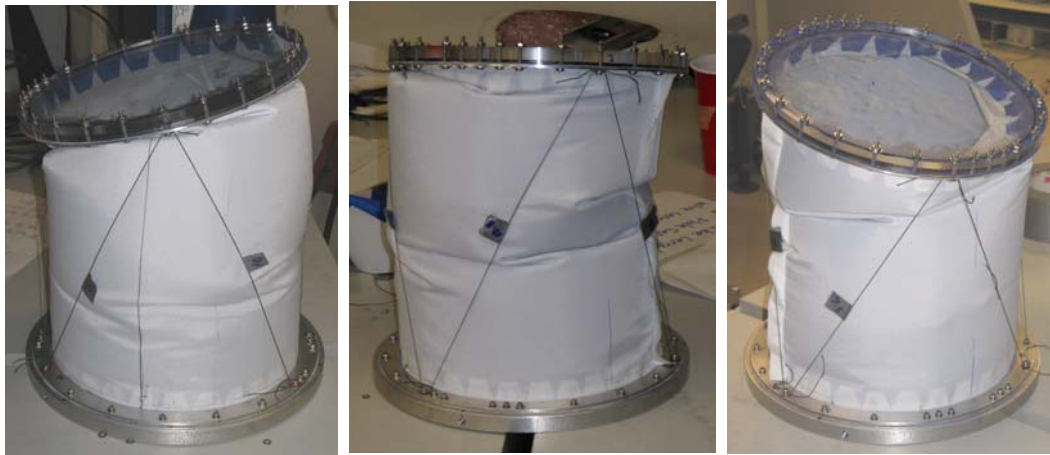


Figure 5: Pressure Constrained Stewart Platform Test Section

The following section describes the immediate need for a planetary suit, introduces concepts that will help the reader understand the behavior of contemporary space suits, and provides details of past research into the topic of reconfigurable suits. This should serve to explain the motivation for the current research: a ‘Morphing’ suit that can be resized to fit a wide range of crewmembers, and which could potentially be actuated to assist or event augment the astronaut’s movement in the suit.

Chapter 2 : Background and Literature Review

This chapter will discuss the current state of space suits, and explain why the currently operational suits would be inadequate for the upcoming exploration program. Several concept suits are introduced, and the limitations and strengths of each are presented. At the same time, basic suit properties such as mobility and actuation torque are introduced, and example values are given. This discussion leads into the selection of a likely suit architecture, which then segues into the motivation of this research: investigation into the actuation and resizing of an all-soft space suit for planetary exploration. The chapter first justifies the use of a soft space suit, and then suggests ways to improve upon the suit's performance.

2.1 The Need for a New Planetary Suit

In January 2004, President Bush unveiled his “Vision for Space Exploration,” an ambitious plan that includes the establishment of a permanent manned base on the moon, with the eventual goal of extending man's exploration to Mars and beyond, according to the report released in 2004 [2]. An artist's conception from the VSE report is shown in Figure 6. This agenda will require the development of an entirely new system of spacecraft to take astronauts to the moon and Mars, as well as the space suits that they will use to explore once they arrive. Although manned lunar operations have been conducted in the past, the president's proposed exploration architecture calls for an entirely new breed of endeavor: long term manned operations on another terrestrial body.

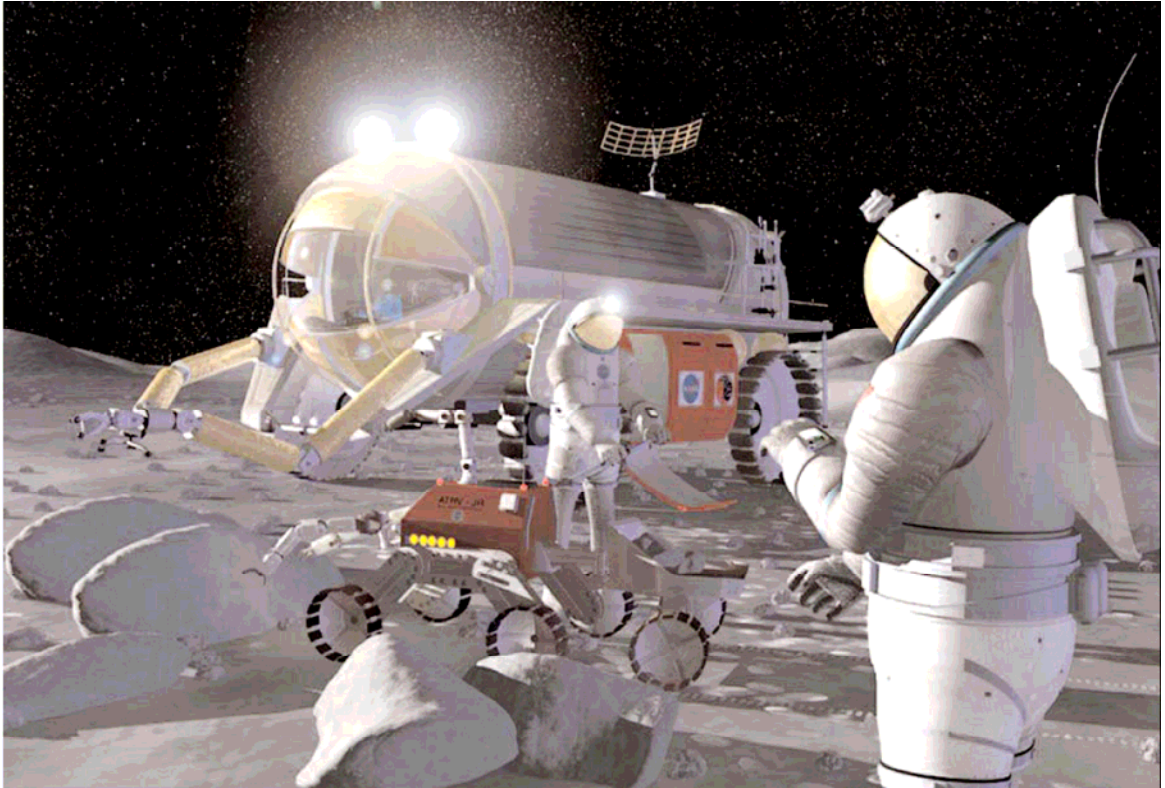


Figure 6: Artist Concept of Lunar Operations, Vision for Space Exploration [VSE Report]

The construction and operation of a base on the Moon will require extensive Extravehicular Activity (EVA) on the lunar surface, which will mandate suits that are durable and easily maintained on site. A trip to Mars would involve a similarly packed EVA schedule, since the long journey could best be justified if significant time was spent on the surface after arrival. In addition to being easily maintained and repaired, a planetary suit would have to be lightweight, since the astronaut would have to support the weight of the suit during moonwalks.

Although the reduced gravity on the moon would decrease the apparent weight of a suit, a heavy suit could still lead to unacceptably high workloads during an eight hour EVA. In addition, a lighter suit concept would be welcomed by design engineers, since any pound saved in EVA suits is a pound that can be used for another

system. Launch vehicle and capsule sizes also place tight restrictions on volume, so an easily stowable suit (for instance, an all-fabric suit that could be packed in a vacuum bag) would be preferable over a suit with a large fixed volume.

The next generation planetary suit would also have to be resistant to the fine, abrasive dust on the surface of the moon and Mars. This layer of dust can jam closures, foul up bearings, and generally wreak havoc with every moving part on the suit.

In addition, planetary suits should be able to fit a wide range of subjects, to minimize the number of suit sizes that must be supplied on a mission. In the past, this requirement has generally been met through modularity (supplying suit segments in a variety of sizes, that can then be combined to fit various crewmembers) or sizing segments integrated into the suit (e.g. the sizing bands on the Apollo A7L).

Although some might point to the Apollo A7L as a planetary suit that has been used in the past, that suit would not fulfill all of the previously mentioned requirements, although it worked very well for the mission it was designed for

2.1.1 The Apollo Planetary Suit: A7L

The Apollo program's answer to a planetary space suit, the A7L (Figure 7) was a marvelous example of engineering, that has since been highly praised by the men who wore it.

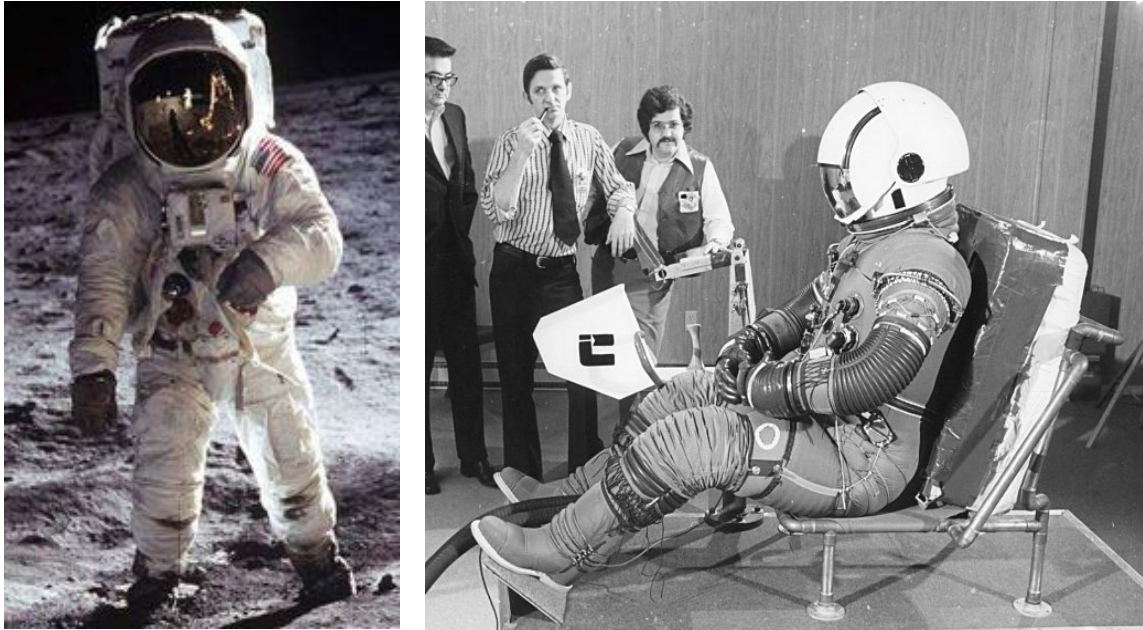


Figure 7: The Apollo A7L, with and without protective outer layer (TMG) [Wiki,ALSJ]

The suit evolved as the program progressed, to react to the changing needs of the astronauts, and to solve unforeseen issues that arose. For instance, when the astronauts were first ‘integrated’ into the couches of the Apollo capsule in pressurized suits, the men had a hard time operating instruments on the control panel, because the shoulders of their suits were too wide, leading to interference with their neighbors [3]. For this reason, the early Apollo suits, and the Command Module Pilot’s suit for all future missions, did not include arm bearings. Other improvements to the suit included a ‘nose scratcher’ (a piece of strategically placed Velcro inside the helmet), and the integration of a waist mobility joint to allow the astronauts to sit on the lunar rover.

A board of eight former Apollo astronauts, when interviewed 30 years later, were quick to point out the strengths of the suit that had kept them alive during their moonwalks [4]. They stressed that the suit was exactly as flexible as it needed to be,

and in general had been designed to do a specific set of routine tasks, which it accomplished as desired. A new suit, they suggested, should be designed similarly, instead of trying to anticipate any possible functionality that might be required (beyond simple emergencies). They found the Apollo suit reliable, and believed that it had all the functionality they needed. Contemporary crew debriefings revealed similar appreciation of the Apollo suit, although to be fair, these men didn't have any suits to compare it to at the time.

Although well suited to the tasks at hand, the Apollo suit did have significant limitations. Perhaps the biggest disadvantage of the Apollo suit was its lack of interchangeability between crewmembers. If a suit was designed for Jack Lousma, anyone else who wanted to wear the suit would have to be very close to Jack Lousma's size. Each of the suits, as well as the multiple backups and training suits, were sewn by a small army of highly skilled seamstresses. If an astronaut wanted his suit to fit right, he would have to go through a whole series of fit checks to make sure the suit was properly tailored. Apollo 15 Commander David Scott underlined this point, while discussing a transcript of the mission [5]. He seemed to have had none of his colleagues' problems with suit flexibility, and attributed this to his extensive time spent with tailors, a lesson he learned from his experience in the Gemini program.

Another problem with the Apollo space suit was a lack of mobility. Due to the inflexibility of the pressurized suit, the astronauts had to apply very large torques to move the joints of the suit. Especially troublesome were the gloves of the suit, which led to scraped knuckles, finger fatigue and overall discomfort, due to the large

loads that had to be applied to effect motion. Tools were difficult to grip, especially for long periods of time. During Apollo 14, the glove (Figure 8) actually settled into an awkward position, and bent the crewmembers' wrist back at an uncomfortable angle [6].

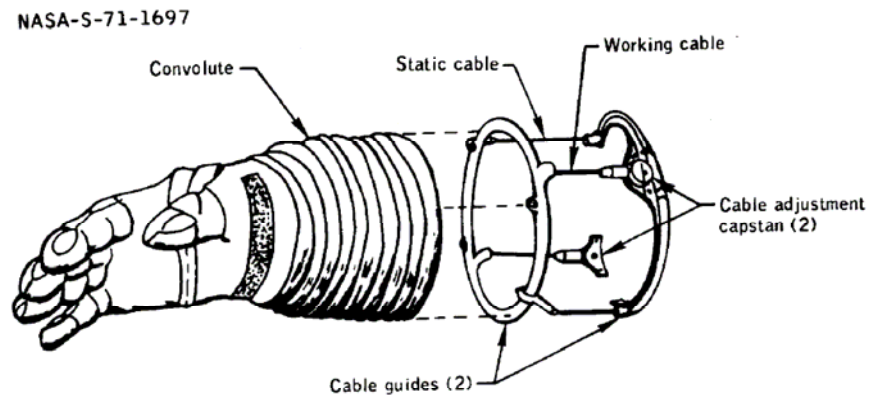


Figure 8: Apollo Glove and Wrist Segment [Apollo 14 Mission Report]

The astronauts initially assumed that one of the restraint cables had broken, but it turned out that this was actually one of the neutral positions of the joint. The cable system shown involved one sliding and two static cables, that allowed some pitch and yaw of the wrist convolute joint.

Another area of concern was the low mobility of the hips and lower legs, which made it very difficult to work close to the ground [7]. Of particular concern was the astronauts' difficulty in recovering from a supine (lying down) position on the lunar surface. They found it rather troublesome to rise to a standing position after falling, without the help of a fellow crewman.

The suit also had a number of mechanical connections that quickly became fouled with dust. Zippers were jammed, wrist bearings scraped and stuck, and air connections became difficult to open and close []. Although some dust problems

could be alleviated by careful cleaning of all connections, the issue would likely grow as time progressed. A next generation space suit would ideally integrate technologies that would protect important closures from dust buildup, especially given the long duration expected for future missions. The abrasive dust also chafed the fabric components of the suit, leading to lower pressure retention and concerns about suit integrity.

Given these concerns with the Apollo EMU, an observer might suggest the use of a slightly more modern suit, that has been developed in the interval between Apollo and the new VSE architecture. The space shuttle Extravehicular Mobility Unit (EMU) is a readily available technology has seen thousands of hours of flight use. However, the shuttle EMU is optimized for on-orbit use, and has several design features that make it unsuitable for planetary EVA.

2.1.2 NASA's Workhorse: The Shuttle EMU

While the Apollo suit was designed specifically for planetary EVA (with limited orbital EVA capabilities, in the case of the Command Module Pilot's slightly different configuration), the shuttle EMU (Figure 9) was designed specifically for on-orbit servicing, to support shuttle and station operations. As a result, the shuttle EMU has a configuration that would be extremely impractical for use on a planet's surface.

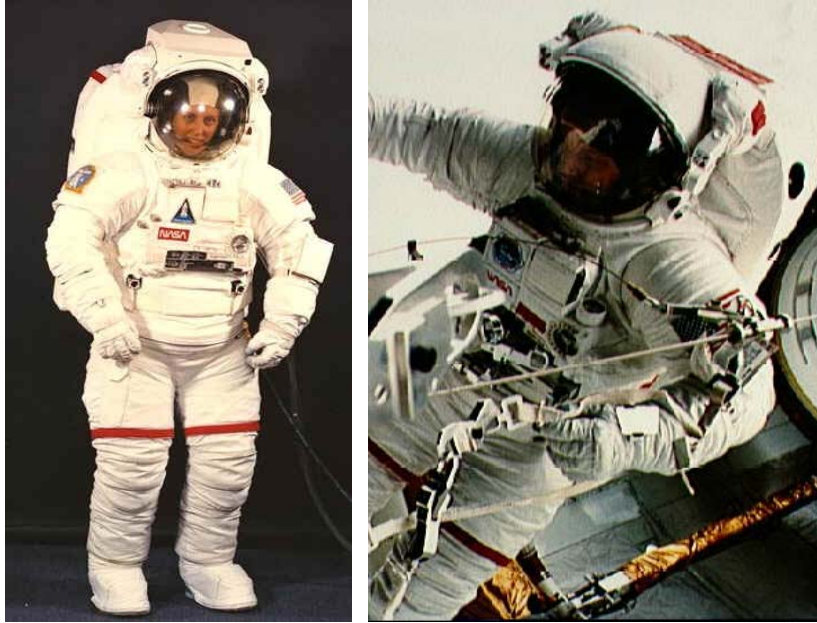


Figure 9: Shuttle EMU [CapcomeSpace.net,]

The most restrictive aspect of the shuttle EMU is its weight: 102 lbs with its Portable Life Support System (PLSS), a backpack that supplies the astronaut with air and cooling []. Although this weight is not an issue on orbit, it would be prohibitive for planetary operations, even given the reduced gravity of the moon or Mars. During walk-back studies (meant to determine how far an astronaut could walk back from a disabled rover), suit subjects found it difficult to stand, not to mention walk, in the current EMU.

Another issue with the shuttle EMU is its lack of lower torso mobility. Some suit designers contest that this low mobility is actually a design feature, since astronauts can lock themselves into foot restraints, and then use the stiff lower torso to resist loads. For instance, a suited astronaut, when applying a large torque as he deploys a satellite, can react this load through the foot restraints, instead of having to apply large counter-torques with his legs. However, some might argue that this use of

the suit as a fixed installation is putting very high man-loads on a suit that is being used for longer and longer periods between refurbishments.

In addition, the EMU only fits a small range of people, and these people tend to have a great deal of difficulty ingressing the suit. One of the driving factors of suit fit is the suit's Hard Upper Torso (HUT), which only comes in three sizes: medium, large, and extra large. Although small and extra small torsos were originally planned, these were never built for a variety of reasons. One of the reasons was relatively straightforward: there are simply less small (usually female) astronauts, so it was hard to justify spending the money on design, tooling and manufacture to fit an additional 10% of the astronaut corps.

Another reason for the small range of sizes, is inherent in the design of the HUT: the fixed location of the scye bearings (see Figure 10).



Figure 10: The EMU Hard Upper Torso (HUT) [SUT]

These bearings must fit as closely as possible to an astronaut's body (essentially, from just under his armpit to just above his shoulder), to prevent a loss of mobility. If the scye bearings were too far away from the astronaut's natural

shoulders, he would contact them as he swung his arms inward or upward, restricting his range of motion. Because these scye bearings must be so close to the shoulders, donning a hard upper torso requires a series of careful contortions (Figure 11).



Figure 11: EMU Suit Donning Procedure [Tiger Team]

The astronaut must essentially insert their arms through the arm bearings, and then snake upwards through the narrow waist opening of the HUT, until at last their head and fingers emerge through their respective openings. Given the well-documented difficulty in donning the standard sizes of hard upper torsos, it was decided not to pursue design of the smaller torsos, since so few people would be able to climb into such a tight enclosure.

The issues associated with donning are documented in a 2003 report by a “Tiger Team,” an eclectic team of medical personnel and EVA operations specialists,

which investigated suit donning procedures as one of many potential cause of shoulder injuries in EVA training [8]. Although they blamed the majority of injuries on inverted operations in an EMU (working upside down while doing underwater training), they included donning as a possible culprit for some number of injuries (around 3%, according to astronauts who were asked to rank possible causes of shoulder injuries). More revealingly, they blamed the majority of the shoulder injuries on the design of the HUT's shoulder joint. Their primary recommendation was to direct funds towards the development of the next generation suit, and they specified that "these development activities should incorporate the design of new suit soft goods, including [the] upper torso, an area of immediate priority due to the frequency, severity, and diversity of injury associated with the current suit." [8, p. 70]

The HUT is the main piece of the EMU that is switched out between sizes of astronaut, but other components are also available in a range of sizes, in an attempt to fit a wide range of candidates. Resizing rings are provided for some degree of on-orbit resizing, but these allegedly take multiple hours to change out.

2.2 Advanced Suit Prototypes

If both the Apollo and shuttle space suits would be insufficient for EVA on the moon and Mars, what other suit options are available? The primary suit contractors (including Hamilton Sundstrand, ILC Dover and David Clark) have been busy during the past few decades, turning out an impressive range of space suit prototypes with varying levels of success. Some of the more highly developed concepts include the AX-5 (a hard suit), the MK-III (a suit with a combination of hard and soft components), and the I-Suit (an all-soft suit with multiple bearings and

advanced mobility joints). Each of these suits has its advantages and disadvantages, which have varying impact on the suit's planetary operation.

2.2.1 The AX-5: A Hard Suit

The AX-5 (Figure 12) was an advanced space suit concept developed by Vic Vykukal of the Ames Research Center. Gary Harris's book on space suit design [9] has an entire section devoted to the AX-5, which will be summarized in the next section.

The AX-5's main claim to fame was its flexibility, which was (in some cases), *higher* than the 'nude body' mobility that is the Holy Grail of suit designers.



Figure 12: The AX-5 Suit [HowStuffWorks, DivingHeritage.com]

However, there are several factors that would make the AX-5 a somewhat impractical planetary suit. This is understandable, considering that the suit was initially designed for orbital EVA in close proximity to military satellites, in an

environment that could involve contact with toxic fuels. These fuels would soak into a fabric suit, and could then outgas in the cabin of a spacecraft. The suit was also designed to protect the astronaut from impact, which could be a danger when working in such close proximity to other spacecraft (Harris).

The main advantage of the AX-5 was its flexibility, and the low torque required to actuate its myriad of swiveling joints. This flexibility was a result of the suit's constant volume design: the joints did not change in volume, so none of the astronaut's effort was going into changing the shape of a pressurized volume.

Proponents of the hard suit say that the system could be manufactured within strict tolerances, reducing the variability that is a drawback of soft suits (even the best seamstress can miss a stitch occasionally, and no two sewn pieces are going to be the same). Because multiple interchangeable pieces could be run off of an assembly line, replacement parts could be made with relative ease. Because the suit was composed of so many parts, these segments could also be varied for different sizes of people. The designers alleged that they could fit suit subjects ranging in height from 6'4" to 5'.

The main drawback of the AX-5 was its weight. It was designed as a so-called zero prebreathe suit (ZPS), which meant that astronauts could move from a spacecraft of a standard Earth atmospheric pressure and composition (14.7 psi, 79% nitrogen, 21% oxygen), directly to a pressurized spacesuit without risking decompression sickness. To have this functionality, the suit was pressurized to 8.3 psi, and required components that were sized to take this load. When integrated with a specialized dual-gas life support system, the suit was predicted to weigh upwards of

250 lbs (even as much as 350). This weight would not be a problem in microgravity (for which the suit was designed), but would be prohibitive during a long moonwalk.

Another problem, strangely enough, was the suit's extreme flexibility. Suit subjects had to work hard just to stand upright, since there was no stiffness inherent in the legs. The myriad of bearings rotated at will, leading to instabilities that made operation on the ground problematic. The suit also exhibited a behavior known as 'programming.' Some sections of the AX-5 had a preferred path, and unnatural, additional motions were sometimes needed to complete a simple motion. For instance, an astronaut would find that he had to rotate his legs outward to bend his legs at the hips for sitting, or would be unable to simply reach over his head in a natural motion. There was even a potential for injury to the wearer, since the suit could potentially rotate past his natural joint limits.

In addition, it has already been shown that moving parts are prone to failure in the dusty lunar environment. A suit that is composed entirely of swiveling and rotating sections, would seem to be excluded for this reason alone. Unless each joint was covered with an impervious boot, there would seem to be a very great danger in the suit fouling up after exposure to dust.

A whole list of other problems seem to weigh heavily against the suit's advantages. For instance, current NASA guidelines suggest using one suit for both planetary EVA and launch and entry, with some switch-out of parts. The hard suit, unless extensively padded, would seem to be a poor choice for a launch and entry suit (current guidelines and common sense stress the elimination of hard points that the astronauts would be forced against during ascent). The suit also imposes some strict

constraints on stowage volume, since it is essentially a fixed size, which might take up an unacceptable portion of a capsule or habitat.

It would seem that the hard suit has some advantages (mainly flexibility and low torque), but that it would not be well suited for planetary EVA (high weight, excessive flexibility and dust protection being the primary concerns). One very successful suit prototype attempted to combine the advantages inherent in a hard suit, with the lower weight and greater stability associated with soft suits (e.g. the Apollo A7LB).

2.2.2 An Elegant Compromise? The Mk-III

In 1981, NASA ramped up investigation into a series of hybrid Zero Prebreathe Suits (high internal pressures, 8 psi or more). These suits would integrate both hard and soft components, in an endeavor to utilize the advantages of each. Again, Gary Harris's book on spacecraft design has an excellent section on the MK-111, which was consulted during the writing of this section.



Figure 13: The MK-III Zero Prebreathe Suit [NASA.gov,Spaceflight.NASA.gov]

The first series of suits utilized a wide variety of mobility joints, in an attempt to isolate which joints would be most effective. The Mk-III (Figure 13) was the result

of these tests, and illustrated the eclectic approach that had been adopted by the designers. It incorporated rotary joints at the hip and thigh, rolling convolute shoulder joints, and flat pattern joints in the arms and legs. (The rolling convolute joint integrates metal rings to help control the behavior of the pressurized fabric, while flat pattern joints incorporate panels of additional fabric in an attempt to maintain a constant volume in the joint).

There is a hard upper torso reminiscent of the shuttle's HUT, and a hard brief (drawn from the AX-5) that allows significant lower torso mobility. The suit had a rear entry configuration, meaning that an astronaut climbs into the suit from the back, and then a hatch is closed behind him. After using the MK-III, astronauts remarked that this entry method was much easier than wriggling into the shuttle EMU.

Some advantages of the MK-III were its mobility (thanks to multiple bearings and well-designed fabric joints), its capability for zero prebreathe, and its ability to support some of its own weight, thanks to the inherent stiffness of its pressurized legs. This last feature was mentioned by suit subject Dean Eppler after a field trial at a lunar analogue site. His comments, echo statements about the shuttle EMU, which suggest an advantage to low compliance in the suit legs when standing and working, and to a higher flexibility when the astronaut is working close to the ground [10].

However, because the suit was designed to take 8.3 psi, it was relatively heavy (over 200 lbs). A mixed gas life support system would add complexity, and potentially weight, to the system. Proponents of the suit believe that this weight could be reduced significantly, if the internal pressure of the suit was lowered.

Another issue with the suit was its relatively low adjustability. Because of the hard upper torso, there is little flexibility in repositioning scye bearings for varying sizes of people. Resizing rings can be used to shorten or lengthen some sections of the suit, but the multiple-bearing mobility joints have a minimum length that cannot accommodate small suit subjects.

Again, any hard components on the suit will be threatened by the dust on the surface of the moon. The waist and hip bearings in particular, would need some type of protective cover to minimize dust intrusion. These hard components could also prove uncomfortable during launch and reentry, unless sufficient padding were provided.

Although the suit's hard components lent it some flexibility, there is also a degree of programming inherent in the briefs and hard upper torso. The joint can only swing through a set series of angles, occasionally complicating motions that would normally be intuitive. For instance, the knees of the suit tended to rotate outwards as they are lifted.

Although the MK-III was designed for use on the space station (hence its high operating pressure), a redesign could make it a strong candidate for a planetary suit. However, engineers at ILC Dover have recently revisited the idea of an all-soft suit, and developed another promising suit prototype that should be examined as a potential planetary suit: the I-Suit.

2.2.3 I-Suit: Perfecting the Art of Soft Mobility Joints

The I-Suit is an all-soft suit with integral bearings, featuring fabric components that are connected to metal interfaces (e.g. the helmet ring and the quick disconnects at the wrists). This prototype suit is available in two configurations: waist entry (as in the shuttle EMU) and rear entry (as in the MK III). Both are shown in Figure 14.

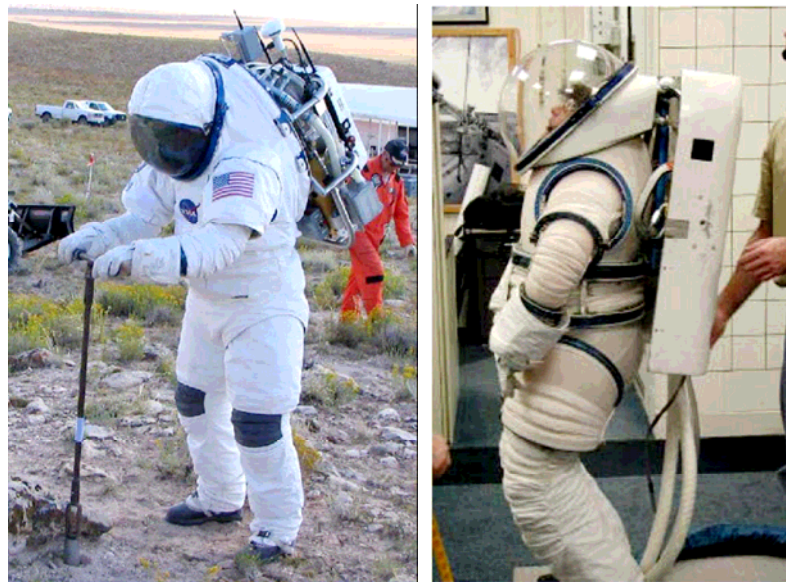


Figure 14: Rear Entry (Left) and Waist Entry (Right) I-Suit [DRATS,I Suit Advanced]

The concept behind the suit is to focus on improvement of the soft joints, rather than attempting to integrate bleeding edge technology that would lead to increased weight and complexity (they're taking tested technology, and improving it through iteration). Because the suit limits the use of hard components, it should have improved comfort during launch and reentry, as well as during routine EVA, compared to systems with rigid pieces. It could also be extremely stowable, since the soft components could be folded up for storage.

Because the I-Suit employs soft mobility joints supplemented by bearings, a certain amount of torque is required to actuate any of the limbs. Nevertheless, it performs very well against other suits with legacy soft joints (e.g. the Apollo and shuttle EMUs). A 1999 study by ILC Dover [11] pitted these three suits against each other, to compare their range of motions, actuation torques, and ease in performing routine tasks (e.g. walking on a treadmill, rising from a prone or supine position). The shuttle EMU had slightly higher mobility than the older Apollo A7L, but fared worst in functional performance evaluation: the suit subject had difficulty even standing in the suit in 1-g, and was unable to rise after falling to his stomach. It should be noted, however, that the Apollo suit was not sized for the suit subject, and that its over-long legs may have contributed to its relatively poor performance.

Because the I-Suit is noticeably more flexible than the MK-III in the legs, one suit subject had a unique issue with the soft suit. He found working in the suit just as exhausting as working in the MK-III, even though it was a lighter suit, because he could not let the stiffness in the legs take the weight of the suit. Instead, he found himself bearing the entire weight on his shoulders, which are less capable of load bearing for extended periods. For this reason, the suit subject suggested that the high leg mobility could be a detriment during planetary operations [12].

Although resizing of the I-Suit is nominally conducted by switching out modular suit components, the soft suit lends itself to a more advanced concept of reconfiguration. Because the suit's shape is dictated by its restraint system (fabric components and webbing links that hold the internal pressure), the configuration could be changed by altering the shape of this restraint system. The suit's upper torso

could conceivably be reconfigured to adjust the location of the scye bearings before donning, or to tilt down the helmet ring if the astronaut wants to see in front of him.

2.3 Hard Suit or Soft?

Three candidate next generation suits have been suggested, but the question remains: which would be most appropriate for planetary operations? The AX-5 has amazing flexibility (perhaps too much), but is heavy and would likely be uncomfortable during launch and reentry. The MK-III is flexible, but exhibits some of the downsides of hard suits: some joints exhibit ‘programming,’ and the hard upper torso and brief sections limit the ability to reconfigure the suit. An all soft suit (e.g. the I-Suit) would be lightweight, comfortable during launch and reentry (except perhaps at the bearings), and could conceivably be reshaped based on suit subject size or task requirements. This functionality alone, makes the I-Suit a strong candidate for the next planetary suit.

2.4 The Properties of a Soft Suit

If a soft suit is going to be used for the next generation of suits, there are several unique properties that must be kept in mind. A soft suit generally has three layers, which may or may not be integrated (as in the Apollo suit). The first, internal layer is the pressure bladder: a coated nylon fabric whose only purpose is to form an airtight seal, enclosing the pressurized volume and minimizing leakage. The next, ‘restraint’ layer provides the shape and structural integrity of the suit, taking the load of the internal pressure. This layer is built from fabric with high tensile strength (usually ripstop nylon or an equivalent) that takes circumferential pressure loads, and

has integral ‘restraint lines’ that run along the neutral axes of joints to take the longitudinal loads. The final layer is a removable outer cover known as the TMG (Thermal and Micrometeoroid Garment). This outer coverall is a lay-up of many layers of material that serve to break up meteorites and provide a layer of thermal insulation. Figure 15 shows the layers of fabric that form the soft components of the shuttle EMU.

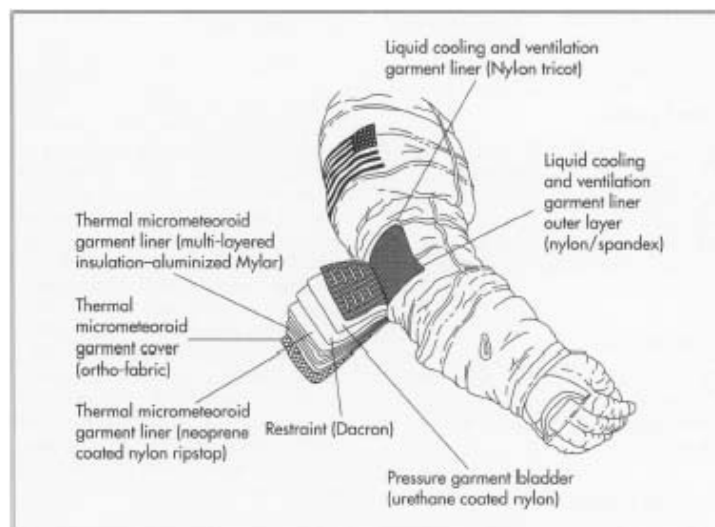


Figure 15: The Layers of a Shuttle EMU [madehow.com]

Much research has been done into quantifying the behavior of these suits, and determining what factors will limit its performance. One important property, brought to light during EVA’s by the Apollo astronauts, is the importance of a suit fitting closely around its wearer.

2.4.1 The Importance of Fit

It has been suggested that an ability to resize the suit would be a major factor in choosing the suit architecture. Is suit fit really so important? Why can’t a five foot

tall woman wear a suit made for a six foot man? If a soft suit is not tailored properly, what kinds of problems can arise? How important is the ability to change the size on orbit, or between tasks? There are two categories of suit fit that lead to problems in a soft suits (or suits in general, for that matter): suits that are too big for the wearer, and suits that are too small.

Suits that are too small lead to chafing, irritation and general discomfort, as well as limiting mobility in extreme cases. A suit that was too small would also lead to major difficulties in donning for a waist entry suit, since astronauts must already struggle to climb into this type of suit. Before suit tailors removed excess material from an elbow joint, Neil Armstrong's sleeves were tight enough that he ruptured capillaries when he moved his arms [13]. Pete Conrad's suit legs were too short due to a rushed tailoring job, causing discomfort when he was sitting in the depressurized suit [14]. A contemporary memo mentioned that the astronauts also had trouble closing the zippers on their suits, because "the suits are custom fitted and, by necessity, must be tight to achieve good mobility" [15].

A suit that is too big will place major constraints on mobility, since the user will be forced to operate in a suit whose joints are not collocated with the joints in their body. Essentially, the reader can imagine the human as a motor that is actuating a machine that is built around them, and meant to act in parallel. If their elbow is offset several inches from the center of rotation of an elbow joint, the efficiency of their motion is reduced significantly. This problem is detailed in a 1993 paper by Menendez, et al [16]. In their paper, researchers from the ESA attempt to quantify the behavior of soft space joints, based on parameters such as internal pressure and

range of motion. They point out that ‘[f]or a manned joint the lowest flexion/extension torque (for a range of mobility) occurs when the crew articulation instantaneous centre of rotation coincides with the joint instantaneous center of rotation.’ [16]

Another problem arises at the Scye bearings; if these are too far apart, the insides of the astronaut’s arms will contact the edges of the bearing, preventing them from bringing their arms any closer together.

Contradictorily, a suit would best serve astronauts if it was large enough to be donned easily, but tight enough that it moved in concert with the wearer.

2.4.2 The Behavior of Soft Mobility Joints

High joint torques have been mentioned, as a downside to soft suits. Why are these torques so high, and what methods have been used to reduce these loads in the past?

A soft space suit is a pressurized volume with an inherent compliance, because of the elasticity of the fabric. The simplest possible suit segment is simply a pressurized cylinder, closed at both ends. When this cylinder is bent, it kinks at the axis of bending, and further flexion will reduce the internal volume. By definition, compressing a volume of pressurized air requires work (equation 1).

$$W = \int (pdV)$$

The ideal joint would maintain a constant volume throughout its entire range of motion, minimizing the torque necessary for actuation. Otherwise, the torque required to move will be proportional to the internal pressure, and to the amount of

volume change as the joint swings through its range of motion. A hard suit is inherently a constant volume system, since it eliminates the ‘pinching down’ that occurs in soft mobility joints. The sections simply rotate and swivel with respect to each other, maintaining the internal envelope.

A variety of soft mobility joints have been developed, in an effort to minimize actuation torque. These joints attempt to maintain a constant volume by either providing additional material that ‘unfurls’ as the joint flexes (so-called ‘flat pattern’ joints, or by providing rigid segments (e.g. circumferential rings) that prevent the joint from closing down during bending. The most common examples of the first joint type are ‘convolute’ joints and joints with ‘gores.’

Convolute joints (Figure 16) involve the insertion of folds in a fabric panel, to artificially introduce slack. A long piece of fabric is folded in an accordion pleat, to match another panel in length. These panels are then sewn together along the sides, leading to additional fabric that can unfold as the joint moves.

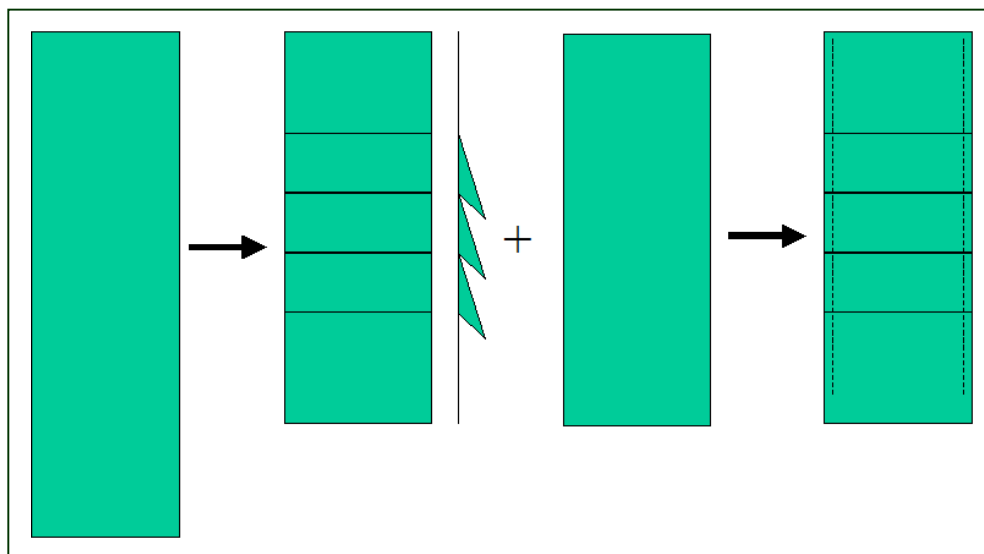


Figure 16: Convolute Joint

Gored joints (Figure 17) have a similar idea but a different execution: bowed fabric panels are sewn together to form a panel, leading to a ‘puckered’ appearance when depressurized. Using this method, the panels have the same length, and additional fabric is only provided along the center of the joint.

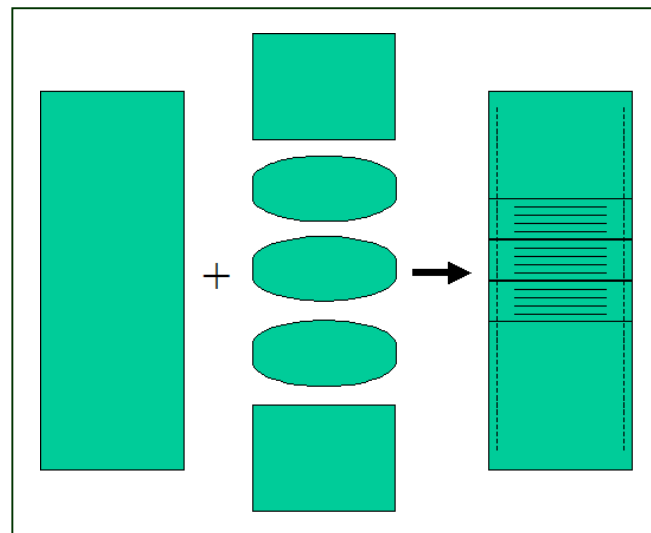


Figure 17: Gored Joint

The more complex soft joints integrate metal rings to maintain the shape of a joint during bending. For instance, a rolling convolute joint uses overlapping metal bands that overlap as the joint is actuated.

The shuttle EMU makes use of these so-called flat pattern joints for mobility in the knees, elbows and shoulder. In a 2001 paper [17], students at the Massachusetts Institute of Technology attempted to quantify the amount of torque required to actuate joints on this suit. The study suggested that the elbow flexion torque (imagine stretching your arm out in front of you, and then curling the lower arm back towards the chest) could exceed 15 N-m (11 ft-lb) at an angle of 105

degrees (at this angle, the lower arm is fifteen degrees past orthogonal from the upper arm). Flexing the knee could take as much as 25 N-m (18 ft-lbs), while hip abduction (spreading the leg outward from the body centerline) was clearly the most energy intensive movement. Swinging the leg out by 17 degrees took a torque of more than 160 N-m (118 ft-lbs).

An ideal suit would minimize this inflexibility, since astronauts must always apply a significant portion of their available strength towards moving the suit (and maintaining it in the desired position, once it is achieved). Because they are continuously applying loads to their suits, the astronauts lose some capacity to apply loads for external tasks. This phenomenon was examined in a 1996 study [18], which compared unsuited and suited strengths for six subjects. In this experiment, subjects were asked to flex joints at a constant angular velocity, and the amount of applied torque was measured using a LIDO joint testing unit. The study found that the most severe reduction in available torque occurred in shoulder flexion/extension (swinging the arm upwards or downwards in the front-back plane), where it was degraded by 40% from the unsuited values. Similarly affected were shoulder abduction and adduction (swinging the arm to the side, away from or towards the body), with an average of a 29% drop in strength.

Because such high loads are required to move the joints on a soft space suit, astronauts are also in danger of fatigue, which could compromise their ability to accomplish mission goals, or even to reenter their spacecraft at the end of an EVA. In a 2001 study [19], employees of NASA's Anthropometrics and Biomechanics Facility investigated the fatigue properties of subjects working in street clothing, and

compared these to their fatigue limits while wearing suits. Their research showed a 25% decrease in time to fatigue, if they worked at 100% of their muscles' Max Voluntary Contraction in a suit, compared to working at 80%. There was only an 8% decrease in time to fatigue, when completing the same test without a suit.

2.4.3 Constraints on Internal Pressure

An observer might suggest lowering the internal pressure of the suit, to decrease the amount of work required to move. However, suit designers must preserve a delicate balance between mobility, and the physiological needs of the astronaut. Specifically, a human requires an atmosphere with an oxygen partial pressure of at least 3 psi. A standard Earth atmosphere is approximately 14.7 psi, 79% nitrogen and 21% oxygen. Therefore, the standard partial pressure of nitrogen is 79% of 14.7, or about 11.6 psi. This leaves around 3.09 psi of oxygen for human consumption. Because humans are optimized for this amount of oxygen, lower partial pressures will lead to oxygen starvation (hypoxia), or oxygen toxicity (hyperoxity). Too little oxygen will starve the brain and cause a human to pass out (and eventually die, if the condition is not reversed), while hyperoxity can affect the central nervous system and even lead to blindness.

Nitrogen, on the other hand, is a physiologically inert gas, meaning that we do not need it to survive. However, nitrogen collects in our tissues and bodily fluids as we breathe. If we suddenly reduce our atmosphere's partial pressure of nitrogen (by breathing pure oxygen, for example), the nitrogen begins to come out of solution and form bubbles in the blood. These bubbles can collect in joints and lead to intense pain, or in serious cases, could obstruct blood flow to the brain or gas exchange in the

lungs. When these bubbles cause complications, the condition is known as ‘Decompression Sickness’ (DCS).

Although the onset of DCS cannot be excluded completely, its likelihood of incidence is affected by several factors. The most dominant factor is the ratio of nitrogen partial pressures, which will determine the propensity for bubble formation. For instance, if an astronaut goes from a nitrogen-rich atmosphere to a pure oxygen atmosphere, there will be a drastic change in nitrogen partial pressure, and a related risk of seeing DCS symptoms. This relationship is quantified in the famous Haldane equation, where P_{N_2} is partial pressure of nitrogen, and $P_{Ambient}$ is the atmospheric pressure. Note that P_{N_2} is the nitrogen partial pressure of the air the astronaut has been breathing, while $P_{Ambient}$ is the pressure that he will be breathing.

$$R = \frac{P_{N_2}}{P_{Ambient}}$$

Because standard atmospheric pressure is 14.7 psi, with a nitrogen partial pressure of 11.6 psi, R is generally .79. Studies have shown that DCS onset occurs at R values of 1.6 to 1.8, but a conservative estimate is 1.4. So, assuming a lunar habitat was maintained at standard Earth atmospheric pressure and composition, what would be the minimum acceptable suit pressure? To keep an R value of 1.4, the new ambient pressure (suit operating pressure) would have to be 11.6 psi / 1.4, or about 8.3 psi. To maintain the correct oxygen partial pressure, the suit could be operated at 36% oxygen and 64% nitrogen.

However, there are ways of getting around this limitation in pressure differential. The ‘prebreathe’ is a common practice in modern EVA operations, where astronauts and cosmonauts must move from the high operating pressure of the ISS or shuttle (kept at standard Earth atmosphere), to the lower operating pressure of their EVA suits. In this lengthy procedure (over two hours, for donning a US suit), astronauts breathe oxygen at high pressure and then slowly step down to lower pressures, while exercising to speed the ‘flush’ of nitrogen from their system. In this way, there is no abrupt change in nitrogen partial pressure, leading to a significantly lower risk of decompression sickness. A 2005 paper by Prisk, et al [20] details this process, while attempting to judge the incidence of nitrogen bubble formation during the process. They hoped to judge the effect of these bubbles on pulmonary function following operations in a space suit, but time constraints precluded the astronauts from taking medical data immediately following EVA.

A 1994 paper [21] by Russian suit designer Isaak Abramov highlighted this delicate balance between mobility, prebreathe time and risk to the astronaut. Increasing the internal pressure of a suit would decrease the prebreathe time and the risk of decompression sickness, but would also reduce the mobility of the suit. The AX-5 and MK-III suits, as previously mentioned, were designed for an 8.3 psi operating pressure, meaning that no prebreathe would be required.

2.5 Upgrades to the Soft Suit

In recent years, several attempts have been made to augment soft suits, since their compliance lends itself to external actuation. For example, the shape of a suit is dictated primarily by its restraint layer, which is a flexible fabric layer that is only

rigid once pressurized. If the restraint layer and the integral restraint lines are resized between pressurizations, the overall suit shape will change. If this change in shape could be done while the suit was pressurized, the suit could be actuated to move in concert with the wearer, reducing the need for an astronaut to apply high torques at joints.

2.5.1 Joint Actuation Assistance

Because the internal pressure of a suit cannot be reduced below 3 psi, and because soft mobility joints can only be improved to a certain limit (which doubtless has not yet been reached), it seems unlikely that joint torques will ever be completely eliminated. However, mechanical assistance could be used to help an astronaut actuate a joint, reducing their work load and allowing them to apply larger loads to external tasks.

This concept was explored in a 1997 paper [22] by E. A. Sorenson et al of the University of Maryland's Space Systems Laboratory (SSL). In concert with ILC Dover, a group of students at the SSL designed a system (Figure 18) that would actuate the metacarpophalangeal or "MCP" joint (the main 'hinge' joint along the base of your fingers, which allows you to close your hand). A glove was built specially by ILC Dover, to settle into a preferred configuration with the MCP joint bent down (hand closed) when pressurized. A motor and a system of cables applied loads to counteract this bias, opening up the hand and extending the fingers. When the control system sensed the wearer attempting to close their hand, it decreased the tension on the cables, allowing the glove joint to gently flex in parallel with the subject's hand.

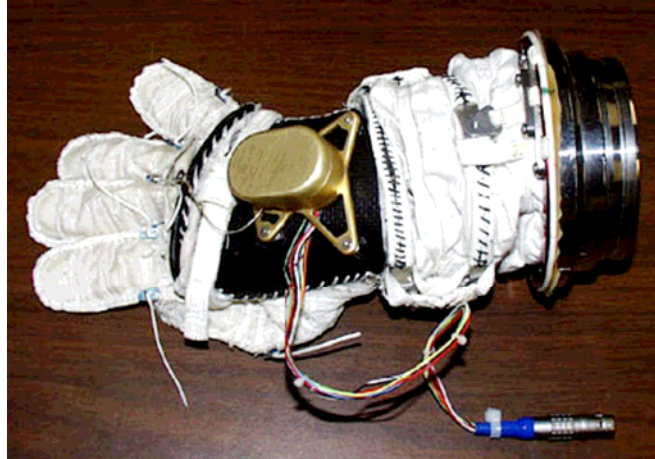


Figure 18: Power Assisted Glove [00635330]

Measurements of subject muscular activity (correlated with EMG readings) suggested a 30% reduction in so-called ‘task effort’ when the power assist function of the glove was used. The range of motion of the glove MCP joint also quadrupled, when motion was assisted by the actuation system.

2.5.2 A System for Active Resizing and Motion Assistance

It has been shown that resizing is an important feature for spacesuit functionality, and that soft suits (which are arguably the most easily reconfigurable), require high torques to actuate joints. Therefore, the ideal spacesuit would conceivably be resizable, lightweight, and actuated to move with the astronaut (instead of forcing the astronaut to apply large torques for movement). One concept, as previously mentioned, is the so-called ‘Morphing’ suit. The idea was developed jointly by ILC Dover and the University of Maryland Space Systems Laboratory, and several prototypes have been developed and tested.

In a 2004 paper on the subject [23], Dave Graziosi of ILC Dover described the initial testing conducted at ILC Dover. A simple set of requirements had been laid

out, and the suit designers built a prototype Soft Upper Torso (SUT) to gain a better understanding of several properties of the system. This prototype is shown in (Figure 19), in its undeformed and resized configurations.



Figure 19: SUT Shape when Undeformed (Left) and Reconfigured (Right) [SUT]

The researchers observed the change in shape of the SUT as the envelope was manipulated, and calculated the force needed to reposition the scye bearings while the SUT was pressurized. They initially incorporated a manual system to adjust cable lengths, in the interests of determining the load capacity and stroke length requirements for an actuator.

In the interests of better characterizing the system, ILC Dover lent an ‘expanded’ version of their I-Suit upper torso (in the rear entry configuration) to the University of Maryland’s Space Systems Laboratory. This upper torso was significantly larger than the baseline SUT, so that the researchers at Maryland could attempt to shrink the envelope to match the I-Suit’s natural size. In their 2006 paper, the researchers outline the results of their testing. They used cables to connect the

hard components of the torso, and then used turnbuckles to manually adjust their lengths (Figure 20).

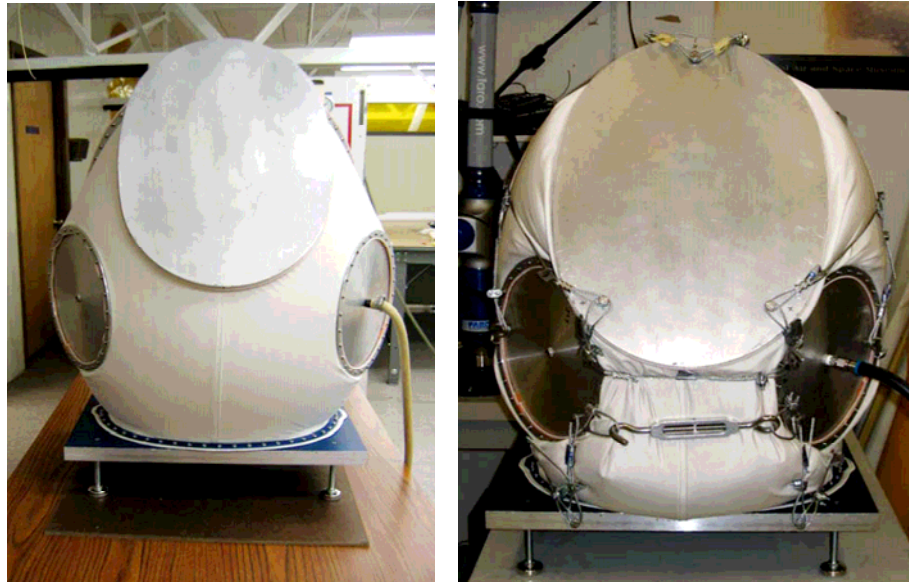


Figure 20: Resizing of the I-Suit SUT [MUT]

The tests showed that the concept of the Morphing Upper Torso (MUT) was feasible, but illustrated the need for future research to better characterize the system. For instance, the pressurized fabric has a non-trivial effect on the flexible links between the plates. This effect is difficult to quantify, because it is dependent on everything from localized bulges in the fabric, to the degree of slip between the fabric and the wires. In general, the fabric expands circumferentially and deflects the wires into a curved shape. This effect is visible to a certain extent in Figure 21, which shows the wires bowing out on a small-scale mockup of the soft upper torso.

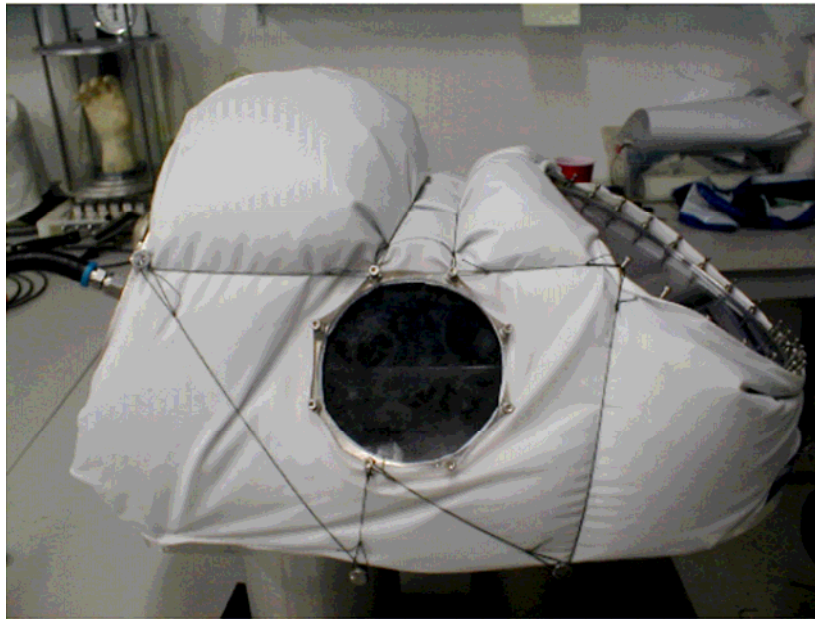


Figure 21: Influence of Fabric on Wire Shape [MUT]

The difficulty in quantifying the system also arises from the complexity of the linkage connection scheme. In the Morphing Upper Torso, the helmet ring (for example) is connected to the back plate, but also to the two scye bearings. Because of this, the entire system is interconnected and is very difficult to simplify.

When taken together, the wires and plates form a collection of interconnected parallel manipulators. (A parallel manipulator, is by definition a “closed-loop mechanism in which the end-effector (mobile platform) is connected to the base by at least two independent kinematic chains,” according to the Parallel Mechanism Information Center [24]). Specifically, the wires connecting each plate are arranged in a so-called Stewart Platform configuration. When the position and orientation of two plates are known relative to each other, it is relatively simple to determine the

lengths of the links connecting them. However, if only the wire lengths are known, it is extremely difficult to determine the precise separation and orientation of the two plates. This is a problem common to parallel manipulators, since there is generally more than one ‘solution’ (given a series of link lengths, there are generally several places the platform could be in relation to the base). However, parallel manipulators generally have excellent positioning accuracy and stiffness, which would make them ideal for holding the rings and plates of a space suit at their desired locations.

2.6 The Stewart Platform

The concept of the so-called Stewart Platform parallel manipulator was actually first proposed by a man named Dr. Gough, but the credit (and the name) for the design were given to an R. Stewart who published a paper in an engineering journal in 1965. In 1947, Dr. Gough had developed a tire testing machine that used six linear actuators to position a moving platform above a fixed base. The actuators are attached by spherical joints to the platform and universal joints to the base, so that the links can swivel as they change in length. Gough was eventually given credit for the inception of the idea, but the name stuck, and positioning platforms with six legs are still generally designated as “Stewart” platforms. An article on Parallelic.com also gives credit to designer Klaus Cappel, who submitted a patent for the same type of system (see Figure 22), several years before Stewart wrote his paper [25].

The multitude of links connecting the platform to the base give the manipulator considerable strength and rigidity, as well as very high positioning accuracy. Because of these traits, the early Stewart Platforms were often used for the purpose Stewart proposed in his paper: to control flight simulators. Essentially, the

simulated cockpit would be situated on top of the platform, which could then be moved around dramatically, swiveling and swinging in relation the base – but always under control. Amusement park simulators still use essentially the same system to actuate many rides.

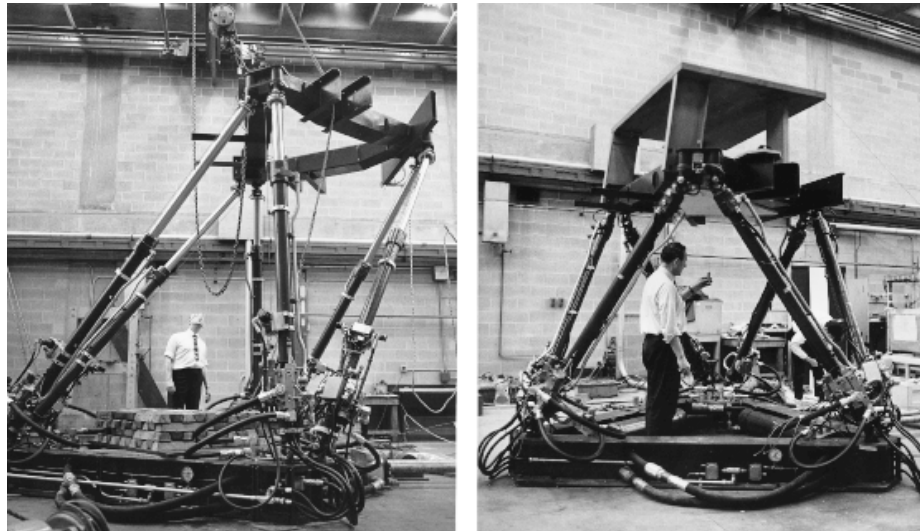


Figure 22: A Cappel Flight Simulator [Parallemic.com]

One of the strengths of the Stewart Platform, in addition to its rigidity and positioning accuracy, is its high number of degrees of freedom. A simple change in link lengths can cause the platform to slide from side to side, or rotate about any axis. Each of these potential changes in position and orientation are degrees of freedom associated with the Stewart Platform. In all, the manipulator has six degrees of freedom (yaw, pitch, roll and translations in the x, y and z axes. This functionality is illustrated in Figure 23, which shows adjustments in platform position (Left) and orientation (Right).

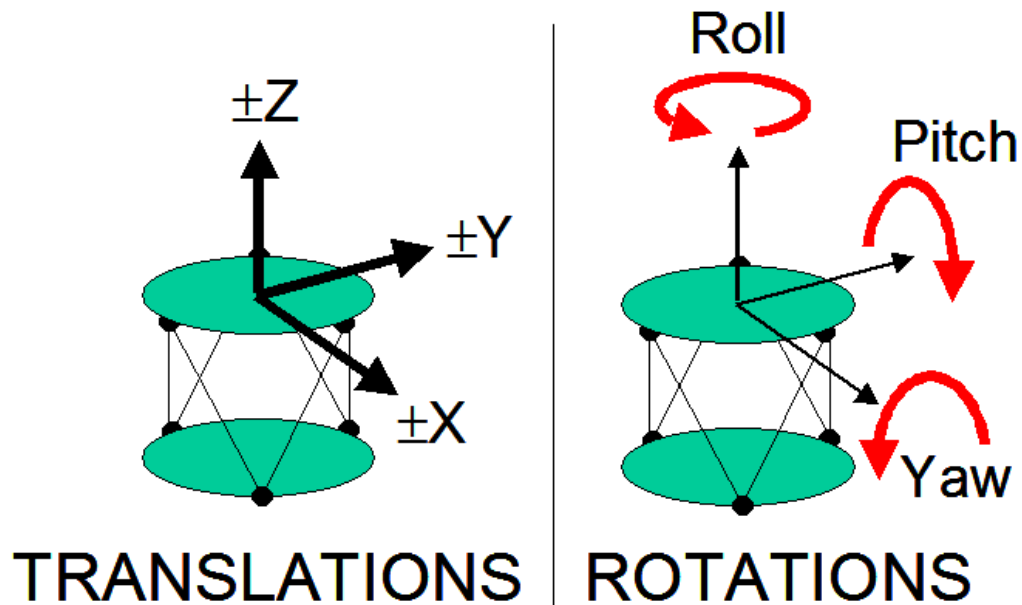


Figure 23: Platform Degrees of Freedom

As previously mentioned, it is relatively trivial to determine the links lengths once the platform position and orientation are known, since there is a unique solution that is only dependent on simple geometry. It is harder to determine where the plate is, if only the link lengths are known. This problem is complicated further when a Stewart Platform is asymmetric (meaning that no links are connected at the same point, and the attachment points are not equally spaced around the perimeter of the ring).

This phenomenon is discussed in a 2002 paper [26] by Jakobovic and Jakobovic, who combine several analytical models with optimization schemes to solve the forward kinematics. Their goal was to find a method that would approximate the position and location of the platform, as it was in motion, while maintaining minimal errors. They estimate the platform's trajectory at each time step,

in an attempt to give the solver an initial guess for the platform's configuration in the next step. In this way, they attempted to avoid a serious problem that arises when quantifying the motion of the platform: the link lengths do not uniquely represent a position and orientation of the top plate, so an initial guess must be used to determine which configuration the platform is most likely to be in.

For a simplistic example, imagine a folding tray table with two U-shaped legs that are hinged together at the 'knee.' One leg is attached to the tabletop, but can rotate in the bushings shown in Figure 24.

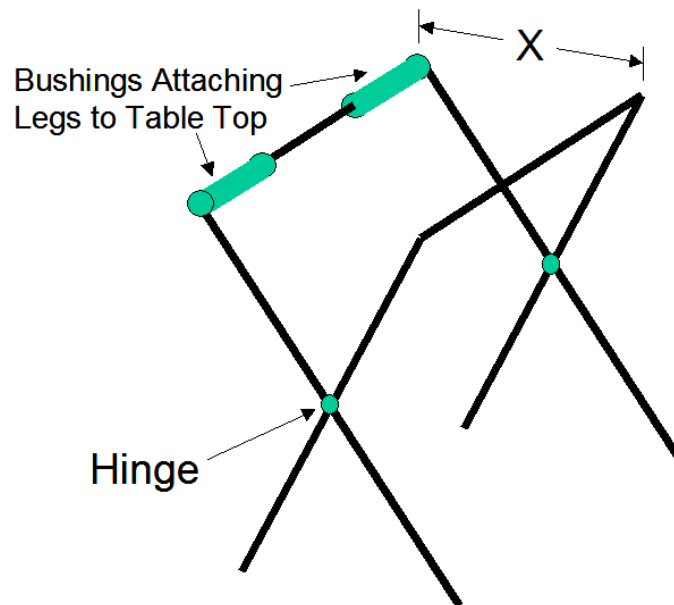


Figure 24: A Simple Example

Now imagine that you are told the length of the legs, and the separation between them (distance X). You cannot see the table, and are asked to guess the table's configuration. If the legs are X inches apart, you might assume that the table is in the desired configuration (both legs supporting the table). However, the legs may easily be in another configuration that is less optimal, as shown in Figure 25.

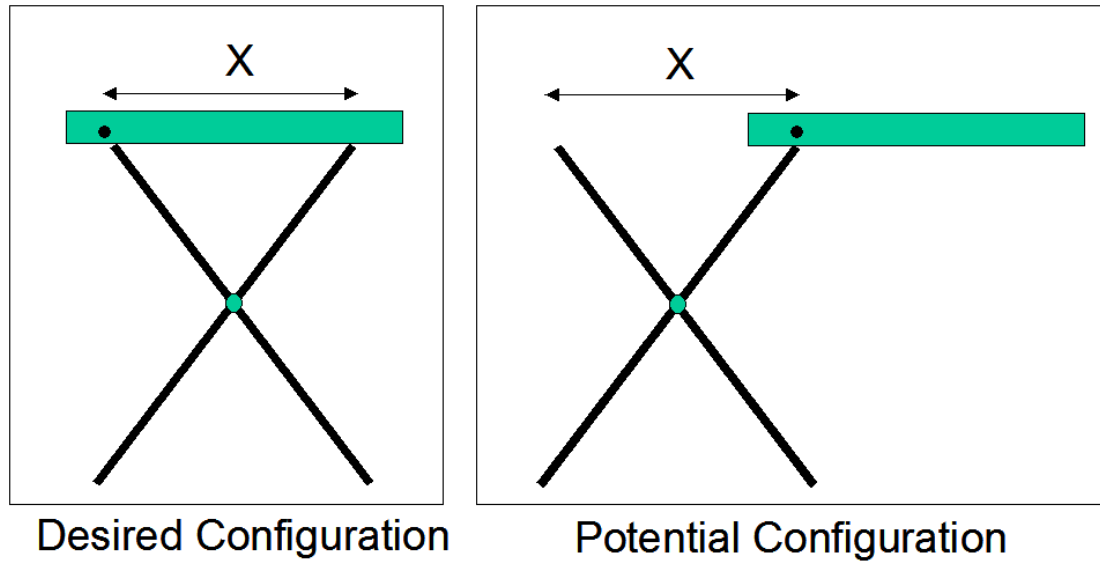


Figure 25: Possible table configurations

However, if you could be given status reports *as* the person unfolded the table, it would be easy to determine which of the two configurations the tray table had ended up in. If you know the trajectory (i.e. the direction of motion) of one of the legs, you will have a good idea of where it is going to end up, since you know what the final separation will be.

The Stewart Platform is far more complex because there are a total of six legs, each of which move in complex patterns. Because they are attached by spherical joints to the base, each leg can move in a spherical arc, as well as changing in length (although their movements are in actuality constrained by the motions of the other joints). The problem is simplified slightly by symmetry, and when multiple links are connected at the same point. However, the links in the Morphing Upper Torso were cables and not linear actuators. Therefore, a morphing suit would actually make use

of so-called “tendon based” parallel manipulators, which have their own complexities.

2.7 Tendon Based Parallel Manipulators

Although the classical Stewart Platform involves linear actuators attached between two rigid plates, research has also been done into using compliant links in parallel manipulators. In 2005, Miller et al published a paper [27] on “Tendon-Based Parallel Robots,” in which a number of flexible links are used to position a platform within a fixed frame (see Figure 26).

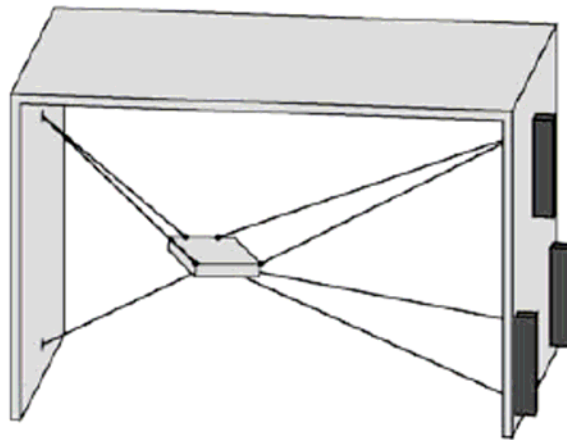


Figure 26: Example of a tendon-based parallel robot [Tendon Based]

There are a few additional considerations, when the links of a parallel manipulator are purely tensile. For one, the manipulator must provide a constraint to keep all of the cables in tension. This can be applied through a redundant cable, or can be provided by an external load (e.g. gravity, or internal pressure in the case of the morphing suit). The dexterity of the device will be proportional to the number of links. Specifically, a manipulator will need n wires for n degrees of freedom, or $n+1$

wires if one of the links is simply used to apply the constraint force. If a parallel manipulator requires an external load to guarantee tension in the links, it is known as an “Incompletely Restrained Parallel Mechanism.”

The workspace (set of all locations that can be reached by the manipulator) of a cable-based manipulator tends to be complex, because the system must keep tension on the cables at all times, and is therefore restricted in its motion. Because this workspace is complex, it is generally difficult (i.e. time consuming and computationally intensive) to find a path that lies within the manipulator’s allowable field of motion.

In the morphing suit, the external constraint on the links is provided by internal pressure, rather than by gravity or a redundant link.

Chapter 3 : Initial Investigations

To gain a better understanding of the dynamics of a morphing arm, and to judge the feasibility of the system, several simple prototypes were constructed. Initially, short sections of the arm were constructed and evaluated. Eventually an entire arm mockup was constructed, in an attempt to predict issues that might occur in a morphing arm.

3.1 Early Prototypes

One of the prototype arm sections used compliant links to connect rings of stiff foam board, sized to fit around the author's arm (Figure 27). The links were arranged in a symmetric Stewart Platform configuration, as discussed in the background section. Graduated lines were marked on the links, to obtain a qualitative understanding of how the link lengths changed during motion of the platform.



Figure 27: Initial Prototype of Manipulator

The links were sized by measuring the circumference of the body segments that the rings would be adjacent to. For instance, if a ring was to be placed around the wrist, the circumference of the wrist was measured and a margin of 1" or more was

added, to allow significant clearance around the arm segment. However, it soon became apparent that wrings could not be sized to fit the wrist, which is generally the narrowest portion of the arm. Instead, the wrist ring had to be sized to fit over the wearer's hand. Therefore, the author's hand was measured around its widest part, with the thumb pressed against the palm (Figure 28).

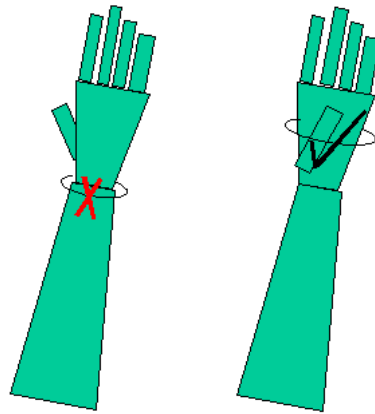


Figure 28: Correct Measurement Location for Wrist-Sized Ring

3.2 Single-Link Wrist Joint

Another early prototype used a single sliding link to connect two rings. In this configuration, the link could slide through attachment points located at the same six connection points associated with a symmetric Stewart platform. Figure 29 shows the prototype in its neutral position (with the same length of cable between each set of nodes) and rotated 90 degrees. The author's hand is applying the tension that would normally be supplied by internal pressure.

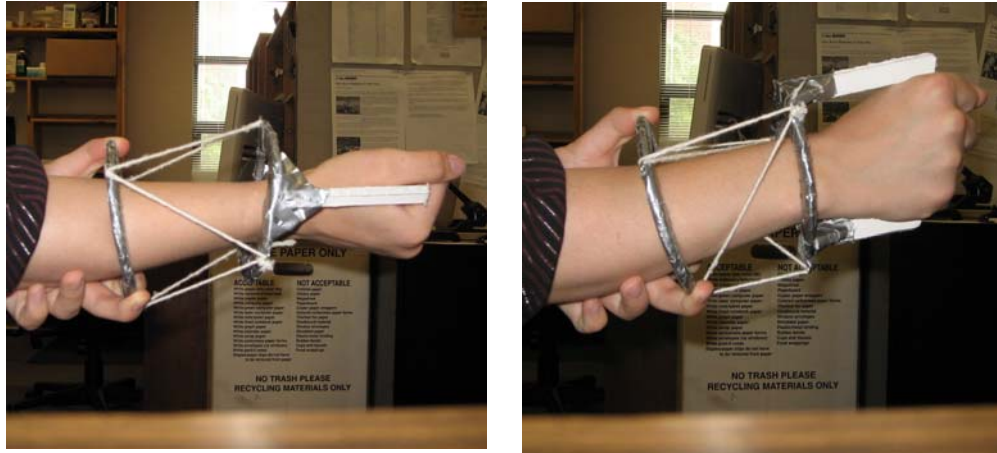


Figure 29: Single-Linkage Wrist at 0 and 90 degree Rotations

This configuration allowed significant rotational motion (roll), as well as excellent pitch and yaw. For example, when the ‘platform’ was tilted in relationship to the base, the platform could collapse down on one side, whereas a configuration of six linkages would be limited by minimum link lengths (assuming linear actuators were used to adjust the lengths of the links). Figure 30 illustrates the pitch and yaw flexibility of the system.

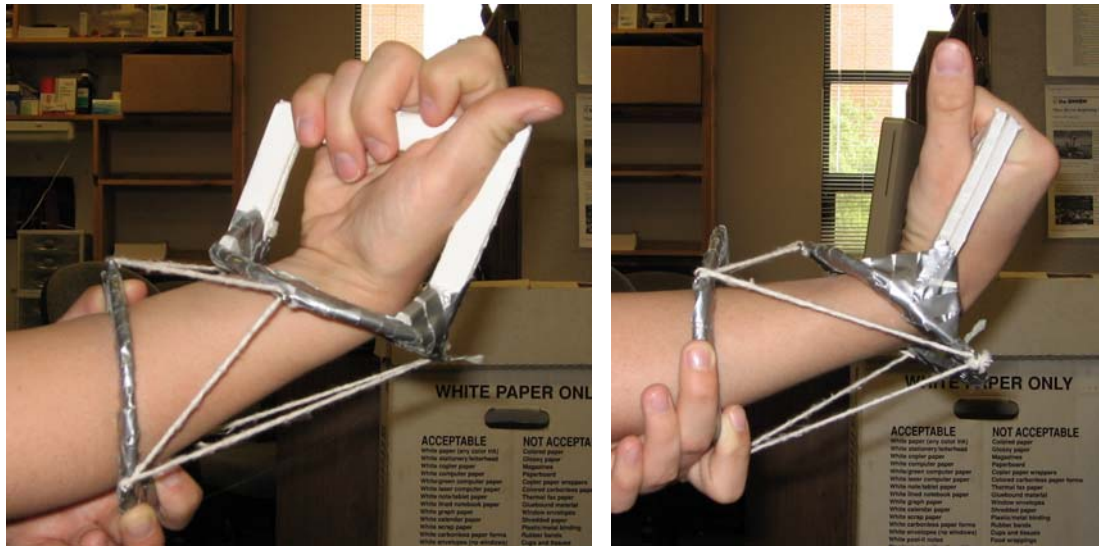


Figure 30: Pitch and Yaw Flexibility of Manipulator

If this single-linkage configuration were used in a wrist joint, the linkage could be allowed to slide freely (allowing manual rotation), or could be driven by one or more rotary actuators at the attachment points, to follow the motion of the astronaut. The inspiration for this joint came from observation of an Apollo A7L, which had cable-actuated mobility joints that allowed rotation without the use of bearings (Figure 31).

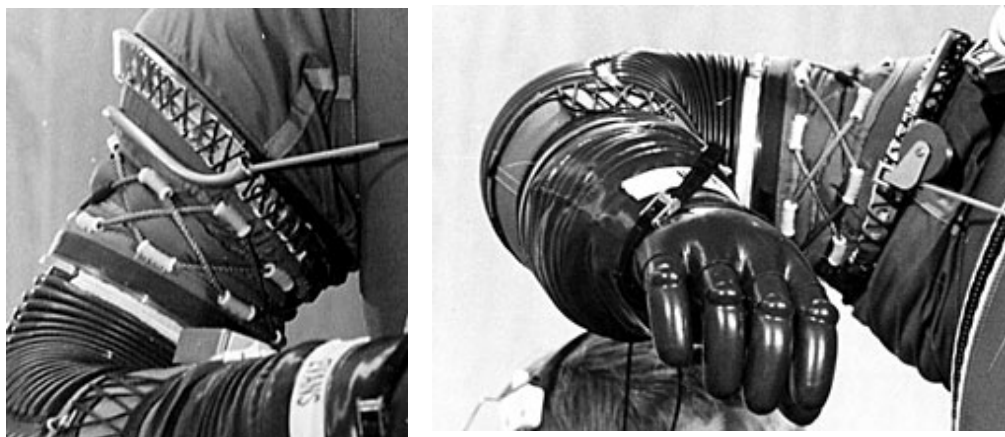


Figure 31: Novel Rotational Joint on the A7L Shoulder [ALSJ]

Investigation of the single-linkage joint led to a concern about contact between the cables and the wearer's arm. As the rings rotate, the attachment points rotate and the wires begin to enter the envelope of the rings. In the single-linkage prototype, the joint rotation (roll) limit was 90 degrees in one direction, at which point the cable contacted the subject's arm. This problem is best illustrated by a top view of the manipulator (Figure 32), showing the wires before and after rotation. At a 30 degree rotation, the wires (black lines) begin to cross into the interior of the ring.

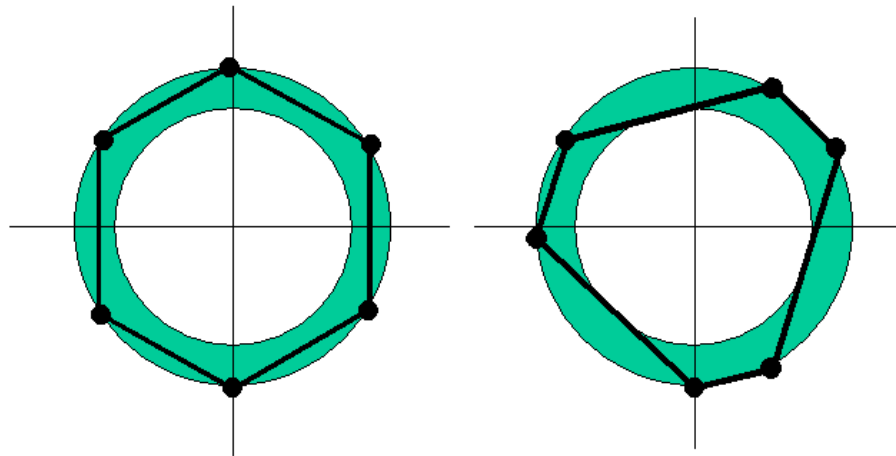


Figure 32: Wires Crossing into Interior of Ring (at 30 Degree Rotation)

The risk of impingement will be based on several factors, including the thickness of the ring (outside radius minus inside radius), the magnitude of the rotation, and the clearance between the inside of the ring and the outside of the arm segment. Impingement will occur at an earlier rotation angle for a thinner ring, since the attachment points are closer to the interior, compared to a wider ring. A MATLAB code was written to combine all of these factors, and determine the

maximum ring rotation for a given set of parameters (ring size, clearance between ring and arm, etc.).

3.3 Rotational Interference Model

Simple geometrical relationships were used in combination with MATLAB's graphing features, to check analytically and graphically for interference issues during rotation of the arm. Circular rings were assumed, while the arm sections were approximated as ellipses. Figure 33 shows a top-down view of the rings, with the cross section of the elbow and the arm. In this case, values have been set to match the author's arm and the rings of the single-cable wrist design.

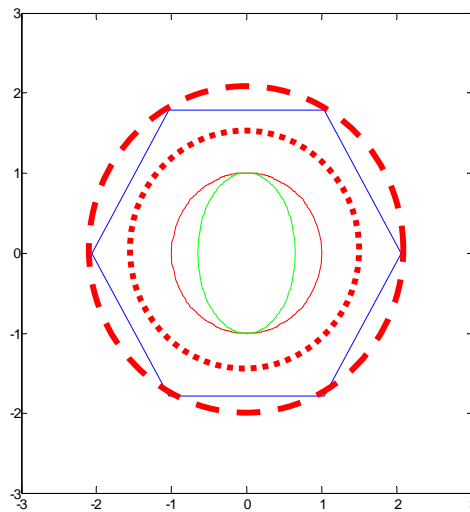


Figure 33: Top Down View of the Wrist (Ellipse), Forearm (Circle), Outer Rings (Dashed Line), Inner Ring (Dotted Lin) and Links (Solid Lines)

The inputs for the program were the dimensions of the arm segment (e.g. circumference of a circular segment, or major and minor axes of an elliptical segment), the minimum desired offset between the ring and the arm, and the spacing of the attachment points around the ring. Specifically, the user would give the angular

separation between the two points on each ring that are symmetric about the Y axis (as seen in Figure 33). The code took these values and treated the links as two dimensional lines connected to the perimeters of the rings (essentially looking at the system from the top down). It would then check for interference into the ellipses that defined the subject's arm.

Method Used to Check For Interference:

Equation for a Line:

$$y = mx + i$$

Equation for an Ellipse:

$$\frac{x^2}{a^2} + \frac{y^2}{b^2} = 1$$

Solving Ellipse Equation for y:

$$\frac{y^2}{b^2} = 1 - \frac{x^2}{a^2}$$

$$y^2 = b^2 \left(1 - \frac{x^2}{a^2}\right)$$

$$y = \sqrt{b^2 \left(1 - \frac{x^2}{a^2}\right)}$$

Solving for Intersection of Line and Ellipse

$$y = \sqrt{b^2 \left(1 - \frac{x^2}{a^2}\right)} = mx + i$$

$$(mx + i)^2 = b^2 \left(1 - \frac{x^2}{a^2}\right)$$

$$m^2x^2 + 2mxi + i^2 = b^2 \left(1 - \frac{x^2}{a^2}\right)$$

$$m^2x^2 + 2mxi + i^2 = b^2 - \frac{b^2x^2}{a^2}$$

$$\left(m^2 + \frac{b^2}{a^2}\right)x^2 + 2mxi + (i^2 - b^2) = 0$$

Plug into Quadratic Formula

$$\frac{-b \pm \sqrt{b^2 - 4ac}}{2a}$$

$$\frac{-2mi \pm \sqrt{2mi - 4 \left(m^2 + \frac{b^2}{a^2}\right) (i^2 - b^2)}}{2a}$$

An intersection exists only if the x coordinate of the intersection is real. In other words, if the value under the radical is negative, there is no intersection. For this reason, the MATLAB code only checks the sign of this quantity, and returns a value of 0 (no intersection) or 1 (intersection between the line and the ellipse).

$$\text{Check : } \left(2mi - 4 \left(m^2 + \frac{b^2}{a^2}\right) (i^2 - b^2)\right) > 0$$

In some cases, the nodes on the rings would be lined up, meaning that they would be at the same x location, creating infinite (vertical) slopes for the links and causing the code to blow up. A simple check was added, and when this condition occurred, the x location of the nodes was compared to the width of the ellipse, to check for interference in this way.

In the first iteration of the code, the user would input rotations of the rings (in the XY plane), and the program would check for interference, by determining if the links had crossed into the envelope of the arm. The second iteration only required the user to specify the dimensions of the arm, and the desired clearance between the arm and the rings. The program then varied the angular separation of the attachment points from 10 to 170 degrees, and checked each combination at angles of 10 through 45 degrees of ring rotation (swiveling the forearm ring relative to the wrist ring). At each iteration, the program output the number of links that were impinging on the envelope of the arm. This process allowed the user to determine the optimum node location on the rings, to allow the highest range of motion without interference.

The main goal of this simple code was to determine the feasibility of a Stewart Platform constructed around a person's arm. Would the wires interfere with the human's motion? Would only small rotations be possible, given this possibility of interference? This was deemed an important factor to determine, before further investigations were conducted.

Preliminary results from the code suggested that a human could rotate their arm more than 60 degrees in either direction (from a neutral position), before contact occurred between the wires and the arm. This would suggest 120 degrees of available

rotation, although a conservative estimate would be closer to 90 degrees (to allow for the material thickness between the arm and the wires). Without gross displacement of the shoulder, the human arm can complete about 180 degrees of roll about its long axis, (pronation and supination are the medical terms), but this amount of rotation could easily be achieved by connecting Stewart Platforms in series. Although bearings could also be integrated, common sense suggests that this could lead to issues, since instabilities could arise if the sections of the morphing arm were allowed to swivel freely in respect to each other.

3.4 Whole-Arm Mockup

Once it was determined that rotational motion would not cause unsolvable interference issues, a simple low-fidelity mockup of the morphing arm was created (Figure 34: Arm Mockup).



Figure 34: Arm Mockup

Foam board rings were sized to fit the author's arm (leaving approximately half an inch of clearance on all sides of an arm segment). The rings were connected with compliant links (narrow elastic cord), so that the lengths would change as the wearer moved. This setup allowed the author to gauge the behavior of the Stewart Platforms connected in series, as well as to check for interference issues during movement.

For this mockup, rings were spaced evenly along the arm to maintain approximately the same distance between the parallel rings. The ring adjacent to the Scye ring (placement seen in Figure 35), originally caused interference issues with the Scye ring, and led to an uncomfortable amount of bulk in the area of the armpit. For this reason, about $\frac{1}{4}$ of the ring was cut out for clearance (see Figure 35), forming a horseshoe shape. If this configuration were used, the remainder of the ring would have to be thickened for bending strength, (see Figure 36) since removing this section would greatly reduce its structural integrity.

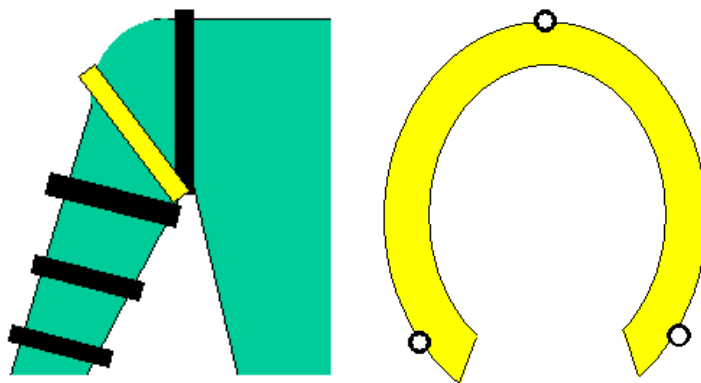


Figure 35: 'Horseshoe' Ring Placement and Shape

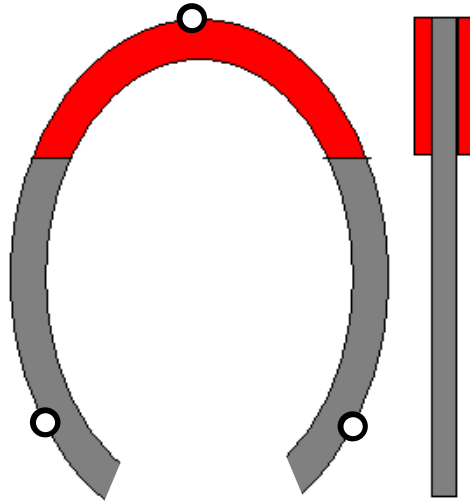


Figure 36: Horseshoe Ring, Showing Reinforcement

The arm mockup also revealed a potential concern associated with the morphing arm: the difficulty of actuating an elbow joint, which would require more than 90 degrees of flexion and extension. In the mockup, the elbow joint was a single-link joint with high mobility, but whose links would enter the envelope of a suit elbow (see Figure 37) during joint flexion.

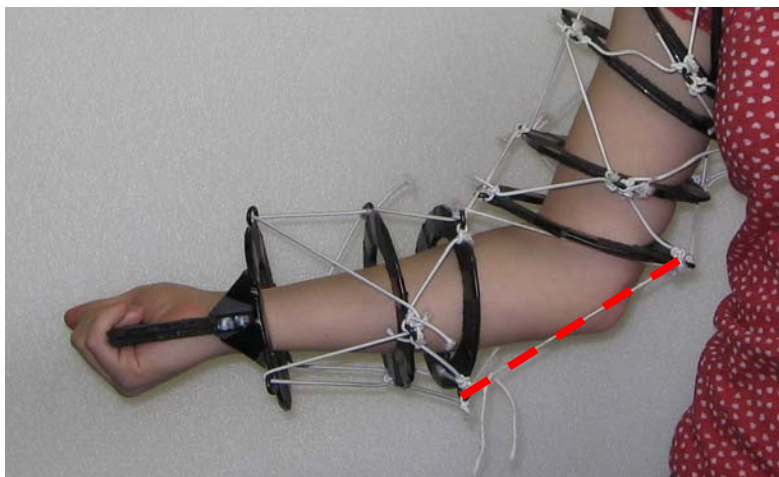


Figure 37: Elbow Joint Interference

Chapter 4 : Test Setup

Up to this point, mockups had been developed purely for proof of concept, and to gain a qualitative understanding of the system's behavior. These mockups had revealed potential issues in the construction of an arm (for example, the actuation of an elbow joint), and suggested a desired ring spacing along the arm. However, to obtain quantitative data, (and to include the effects of the fabric), a higher-fidelity, pressurized test platform would have to be developed. This system could be used to determine fabric effects on wires, test methods for reducing these effects, measure loads transmitted through the cables, and determine the accuracy and precision with which the platform could be positioned. All of these factors would have to be quantified, before a control system could be applied.

4.1 Construction of the Test Section

The test section would consist of a section of pressurized sleeve with end caps, to approximate a segment of the morphing arm. Because it would be pressurized and depressurized multiple times, it would have to be durable and relatively airtight. It would require locations to attach the cables that would connect the end caps, and provide the constraints on location and orientation of the top plate when pressurized.

Figure 38 shows the test section when pressurized, without the cables attached.



Figure 38: Pressurized Test Section

The following materials were used to construct the test segment:

- Pre-drilled aluminum Plate, 9" in diameter
- Pre-drilled Lexan Plate, 8.625" in diameter
- Nylon parachute material
- Urethane coated nylon
- O-Rings, to fit channels in plates

4.1.1 Fabricating the Pressurized Sleeve

As mentioned in the background section, a soft space suit generally has a total of three layers: a pressure tight internal layer (the pressure bladder), a high-tensile-strength “restraint layer” that gives the suit its shape, and a “Thermal and Micrometeoroid Garment” that protects the wearer from thermal extremes and micrometeoroids. The test section will consist of a pressure bladder and a restraint layer, both constructed of nylon. The pressure bladder material has a coating of urethane, which gives it its airtight properties. The restraint layer is made of a ripstop nylon with a high tensile strength, developed for use in parachutes. The restraint layer is made slightly smaller than the pressure bladder, so that it will take any pressure loads (the pressure bladder is only provided to keep the suit airtight, not for structural integrity).

4.1.2 Method for Connecting a Fabric Cylinder to a Metal Plate

The standard method for attaching a cylindrical sleeve to a flat plate, is to construct a fabric flange that will lay flat against the plate, and which will attach via tabs around the bottom of the sleeve (see Figure 39).

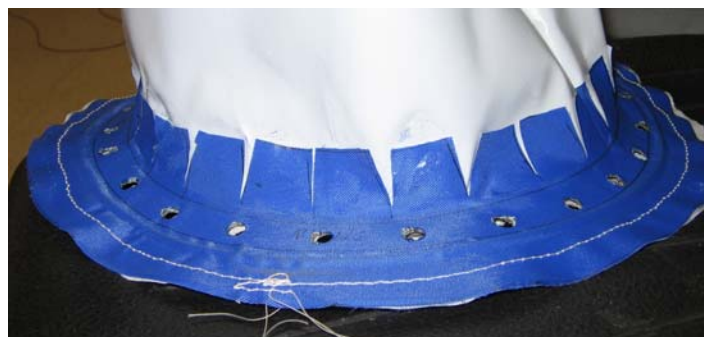


Figure 39: A test sleeve, turned inside out to show flange tabs

Figure 40 shows how the fabric flange should be fabricated, given the metal plate that must be interfaced with. The dotted line on the flange and the solid black line on the plate show the location of the O-Ring, which fits in a channel in the plate (within the circle of bolt holes). The fanned-out lines on the interior of the flange show where cuts should be made, to construct the tabs that will connect to the cylinder. Once the cylinder is attached to the flange, and the flange and the plate are lined up, a metal ring with the same hole pattern is bolted over the flange, clamping down the fabric and compressing the O-Ring.

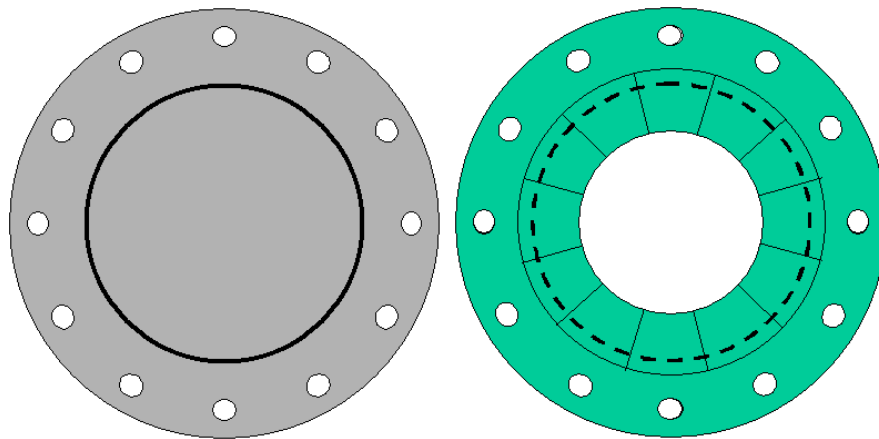


Figure 40: End Plate (Left) and Flange (Right)

Two pieces of fabric, one 12” and one 6” long, were cut from each of the two types of fabric. The sections were sized to match the internal circumference of the clamping rings, with an inch of additional fabric for the seam. Next, four flanges were cut from each of the two materials. Tabs were cut in each flange, and the cylinders were constructed and attached to the flanges. Although the restraint material sleeve

could be fabricated by sewing, the pressure bladder required a careful process of heat sealing.

4.1.3 Heat Sealing the Pressure Bladder

Because punctures would destroy the pressure integrity of the urethane-coated nylon, sections of the material could not be joined by sewing. Instead, a heat sealing iron was used (Figure 41). The method for heat sealing described in this document, was arrived at through trial and error by Jeff Braden and Shane Jacobs of the University of Maryland Space Systems Lab, as they heat sealed pressure bladders for a space suit analogue, the Maryland Advanced Research and Simulation (MARS) suit.



Figure 41: Heat Sealing Tool

The iron was allowed several minutes to heat up, before test sections were adhered together. These test sections were generally about an inch wide and two to three inches long, folded in half to mate two urethane-coated surfaces (only the coated surfaces will adhere together; the nylon will not bind with the urethane layer). The iron was placed against the fabric for 10-15 seconds, before being repositioned farther along the intended seam. When the width of the section had been treated with

the iron, the piece was quickly cooled, by rubbing it against the metal tabletop. After the piece was sufficiently cool to the touch, an attempt was made to separate the two surface (by grabbing opposing sides and tugging). If the seam ripped apart, the iron was allowed more time to heat up, before the process was repeated. The process of heat sealing a test strip is shown in Figure 42.

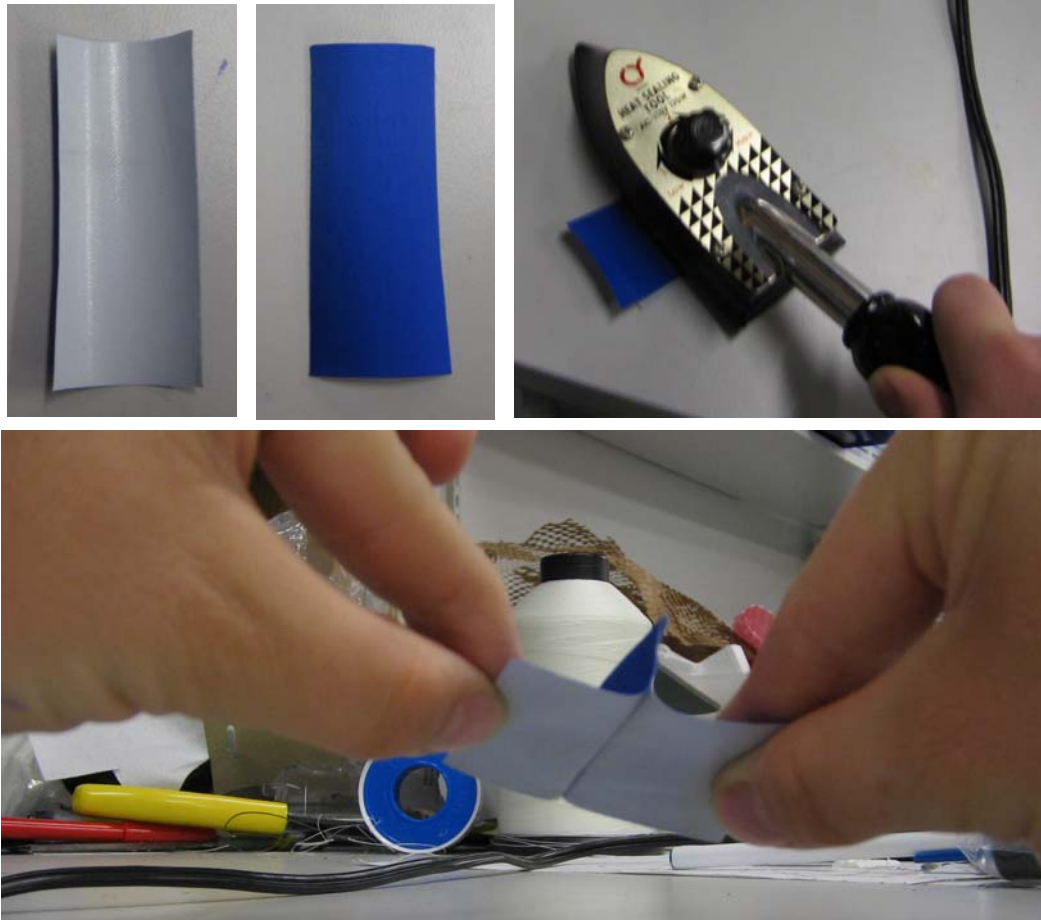


Figure 42: Top Left: Urethane coated (white) and uncoated (blue) sides of fabric. Top Right: Heat Sealing the Test Section. Bottom: Testing the seam of the test section

Sealing the seam of the nylon cylinder was relatively straightforward, but attaching the flange to the cylinder was a very difficult process. The attachment was accomplished by first sealing the tabs at opposing sides of the cylinder, and then heat

sealing the intervening tabs. The process was simplified slightly by pulling the edge of the cylinder down around a metal tube, and clamping it in place. The flange could then be pulled into place as each successive tab was attached, without having to reposition the cylinder. This technique is shown in Figure 43. Note that the iron is being applied to the non-treated side of the fabric; touching the heat sealer to the urethane-coated side will damage the fabric (some of the coating material will come off on the iron).

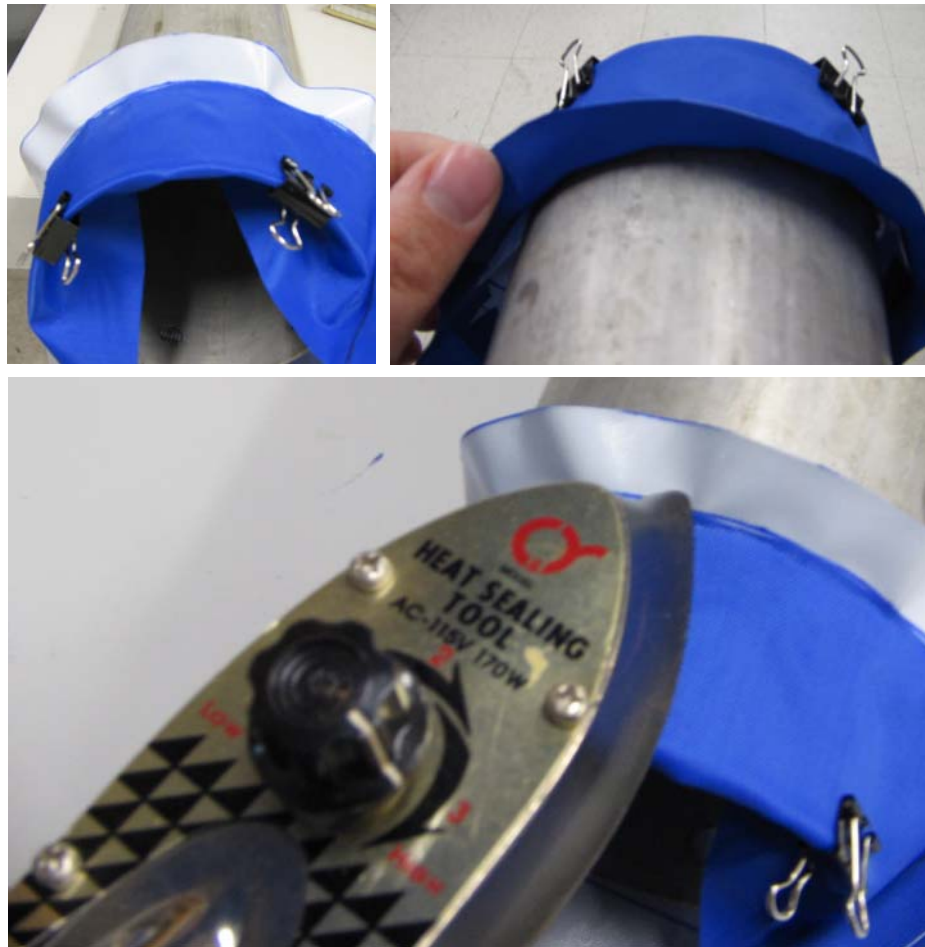


Figure 43: Heat Sealing the Flange

Inevitably, there will be some error between the circumference of the cylinder and the internal circumference of the flange. The resulting excess of fabric will lead

to a crease in the pressure bladder, which will form a leak point to the exterior of the cylinder. This is generally unavoidable, but can be reduced by attempting to take out the slack as you heat seal around the perimeter of the cylinder.

4.1.4 Assembling the Test Section

Once the pressure bladder was successfully heat sealed, the restraint layer was sewn together, and both were attached to their respective flanges, the system was assembled.

The two end plates were legacy of an earlier experiment conducted by the Space Systems Laboratory, so were predrilled for **4-40** metric bolts, and had machined channels for O-rings. The bottom plate was aluminum, 10 inches in diameter, ½in thick, with drilled and tapped bolt holes. The top plate was clear Lexan, 9in in diameter, ½ in thick, with through holes for bolts. The aluminum clamping rings had the same bolt patterns as the top and bottom rings, respectively, but were 1/8 in thick.

Before the fabric cylinder could be attached to the top and bottom plates, O-Rings had to be placed in the machined slots. The slots were first pretreated with vacuum grease, and then the O-rings were laid down. Because the plates did not have standard-sized O-Rings, these had to be fabricated for the test section. A long cord of O-Ring material was cut to length using a razor blade, and then two ends are glued together using cyanoacrylate (e.g. Super Glue[®]). Next, the cylinder was attached to the two endplates.

There is generally some difficulty in attaching a fabric flange to a metal plate, because the fabric tends to shift and cover the bolt holes. The ring is generally placed

over the flange, and then bolts are inserted through the holes in the ring, flange, and plate. If a hole in the flange has been made too small to simply push the bolt through, rotating the bolt will generally allow the bolt's threads to pull it through the fabric. Once the flanges have been securely attached to the end plates, the test section can be pressurized.

4.2 Pressurizing the Test Section

The test section was pressurized using a Craftsman 150 psi compressor (Figure 44). The regulator on the compressor was used to step down the supply pressure to 40 psi. A second regulator, with attached digital pressure gauge, was used to control the pressure in the test section. During initial pressurizations of the test section, the internal pressure was maintained at .5 psi for safety reasons. This precaution was taken because pressurized sleeves generally have one or more 'restraint lines' of high-tensile strength webbing that take longitudinal loads along the section. In the test section, the pressure load was being taken only by the restraint material.



Figure 44: Compressor, Pressurized Line into Test Section, Regulator and Pressure Gauge

The test section was pressurized, and then the air flow was shut off. The sleeve went slack, but did not deflate entirely until the relief valve on the pressure line was opened, meaning that the sleeve had reasonable pressure integrity. It took about $1/10^{\text{th}}$ of a psi to inflate the cylinder, lifting the top plate away from the table. The cross sectional area of the cylinder, and hence the surface area over which the pressure acted, was approximately 64 in^2 . This suggests that the top plate and fabric sleeve weighed approximately 6.4 lbs.

4.3 Attaching Links to the Plates

Once the pressure integrity of the test section was determined, lengths of fishing line with a 100 lb breaking strength were attached to bolts on the top and bottom plate. To begin with, all line lengths were chosen to hold the top plate parallel to the bottom plate, with just enough separation to place the cylinder in compression. In Figure 45, this configuration is compared to the test section without cables attached.

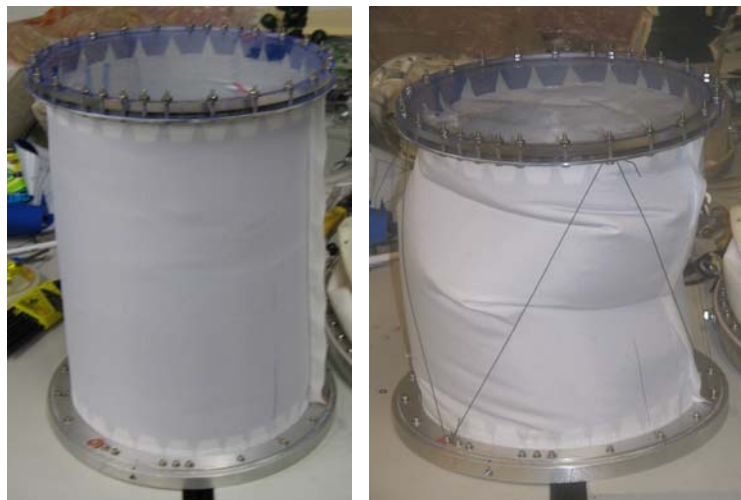


Figure 45: Link Attachment

Initially, the method of changing link lengths was to untie the fishing line connecting the bolts, and retie the line at a different length. However, this process was time consuming because the bolts had to be removed to retie the links (since washers were used to capture the loops on the ends of the lines, and the only way to lift the washers was to loosen the bolts).

The greatest difficulty occurred when affixing the lines to bolts on the base, since these bolts were threaded into the aluminum plate. As the bolt was tightened down (after the link had been looped around it), the link would be captured by the bolt and rotate around, whereas the lines would optimally extend from below opposite sides of the washer. This problem is illustrated in Figure 46.



Figure 46: Line Extending from Either Side of Washer

To simplify adjustment of the line lengths, turnbuckles (see Figure 47) were attached in series with the links. Turnbuckles consist of two clevis-headed bolts that screw into a central connector.



Figure 47: Turnbuckle

One of the bolts is right-handed, and the other is left-handed. Because the bolts have opposite directions of tightening, the central connector can be rotated to adjust the length of the link, without rotating the link. Figure 48 shows the test section with turnbuckles integrated. The links have also been given more rigidity, so experience different deformation than fishing line alone. This behavior will be examined in detail in the results section.



Figure 48: Test Section, with Turnbuckles Integrated

Once the wires were attached to the test section, some initial qualitative results were gained from observing the test section. However, in order to gain quantitative results, a method would be needed to accurately determine the position

and orientation of the platform. The selected measurement method was to track node locations in 3D using a FARO Technologies Inc. Platinum FAROArm® (see next section), and to use this data to determine the platform configuration.

4.4 Node Measurement Setup

The Platinum FAROArm® is a “Coordinate Measuring Machine” that allows measurement of points in 3D space to an accuracy of .0005” (according to a FAROArm® brochure). The arm has encoders in each of its joints, so it can track the location of its probe at all times. This probe has a ceramic tip, which is touched against the component whose location is to be measured.

The FAROArm® is supplied with CAM2 Measure®, a program that interprets information from the encoders and supplies 3D information on the probe location. This software allows measurement of points, lines, ellipses, and other complex shapes, and has several calculation functions that allow the user to find angular separations, radii, and other valuable information. Figure 49 shows the FAROArm® with its associated workstation, the FAROArm® in its extended configuration, and a close up of the probe.



Figure 49: Left: FAROArm with Workstation. Top Right: FAROArm in Use. Bottom Right: FAROArm Probe

When using the FAROArm, it is important not to allow the tubular sections to line up (causing singularities, which prevent measurements from being taken). When the sections do line up, a red light will flash on the probe, and the program will alert the user with a brief error message. It is preferable to maintain the joints at approximately 90 degree angles, to prevent these singularities from occurring.

4.4.1 FAROArm Calibration

Before use, the FAROArm must be calibrated using the CAM2 Measure program. The calibration option can be accessed by going to ‘Devices’ in the menu bar. Scroll down to Probes, then hit Calibrate on the menu that pops up. A graphic

shows the motion that should be used for calibration, and a help file describes this in more detail. If the Hole method of calibration is used, the user will apply the ceramic tip of the probe to a provided calibration fixture (see Figure 50), which must be fixed to the workstation (near the component that will be measured). The user must sweep the arm through a series of proscribed motions (shown in the popup window), while gathering data by pressing the green button on the probe.



Figure 50: Calibration of FAROArm

When a significant number of data points have been taken (usually 150+), the user will press the green button (to end the measurement), and then the red button, to accept the measurement. If the calibration is successful, the program will alert the user to this fact. Otherwise, the calibration must be performed again. It is important not to allow the ceramic tip to slip from the fixture (or else the measurement must be ended and restarted). The location of the calibration fixture will become the reference point (x,y,z origin) for all future measurements. It is recommended that you repeat the calibration at the beginning of each day of measurements, or if the measurement station has been jarred.

Once the calibration is complete, the FAROArm is ready to collect data. In the current research, the Point measurement function was used to find the location of nodes on the top and bottom plates.

4.4.2 Taking Measurements Using the FAROArm

To take a measurement, the user touches the probe against the component to be measured, and presses and releases the green button. The arm will continue to take data points until the green button is pressed again, ending the measurement. If more data points are desired for this location, the green button is pressed again, and then again once the additional data points have been taken. The red button is then pressed to keep the data points. A dialogue box will pop up, providing the average X,Y, and Z values, as well as the RMS of the data. If the measurement has a high error, a warning tone will be given (this sound is slightly different than the confirmation beep, that occurs whenever a measurement session is concluded by pressing the red button).

To end a measurement session and return to the CAM2 Measure user interface (e.g. to access any of the menus), the red button must be pressed again, while the arm is extended from the base. While the arm is standing upright (with the lower section perpendicular to the base), the arm will not exit the measurement mode.

The FAROArm allowed precise measurements of actual node locations, which could be used to calculate link lengths. These actual link lengths could then be compared to desired link lengths, calculated from an inverse kinematics code (Chapter 5). This code would take the desired platform location (defined as the center location, relative to the center of the base) and orientation (defined as Euler

angle rotations about the platform local axes), and output the necessary link lengths to arrive at this configuration.

4.5 Load Measurement Setup

Next, to allow measurement of loads in the links, a load cell was obtained and calibrated. The signal was scaled up using a transistor-based amplification circuit, and read using a multi-meter.

4.5.1 Amplification of Load Cell Signal

The majority of the credit for the load cell amplification circuit should be given to fellow graduate student Joseph Gland, who spent a great deal of time assisting with the design of this circuit. Setup, calibration and debugging were performed by the author.

The circuit uses ‘matched’ TPQ2222 transistors on a single chip, to obtain the greatest similarity and therefore the greatest accuracy in load amplification. A current source (third transistor attached to two resistors in series) was integrated into the circuit to maintain approximately constant current through the circuit and increase the accuracy of the amplifier. The output voltage had an offset of approximately 6.5 V, so the signal was compared to a steady 6.5 V signal from a DC power supply.

The load cell has a differential output proportional to the load, which was amplified by the load cell. The positive lead from the load cell was attached to Vin1, while the negative lead was attached to Vin2.

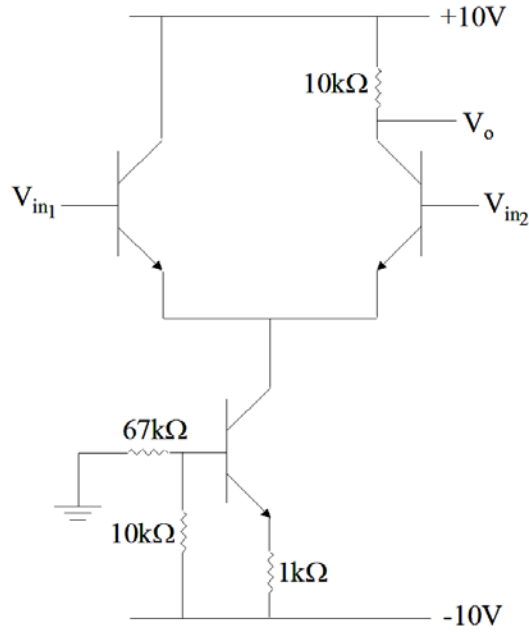


Figure 51: Amplification Circuit

The load cell calibration curve is shown in Figure 52. It was found by applying known loads to the load cell, and measuring the ratio of the measured voltage (in mV) to the excitation voltage of the load cell (in this case, 10 V).

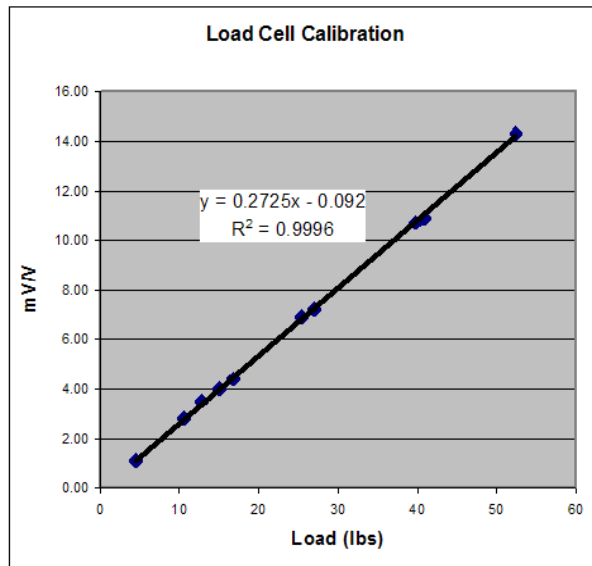


Figure 52: Load Cell Calibration Curve

A linear trend line was fit to the data, and resulted in the following equation relating measured voltage to tension:

$$y = 0.2752x - 0.092$$

Where x is the load (in lb) and y is the ratio of the measured voltage to the load cell supply voltage.

This was rearranged to find the simple linear relationship between the ratio of applied to measured voltage (unitless) and the load on the load cell:

$$x = (y + .0.092) / 0.2752$$

Where x is, again, the load in lbs, and y is the voltage ratio. This equation approximated the load on the load cell with a max error of 3% (average error: 1.15%).

Once calibrated, the load cell was linked in series with a link on the test platform (Figure 53). The load cell could be disconnected and reconnected, to allow measurement of tension in any of the six links.

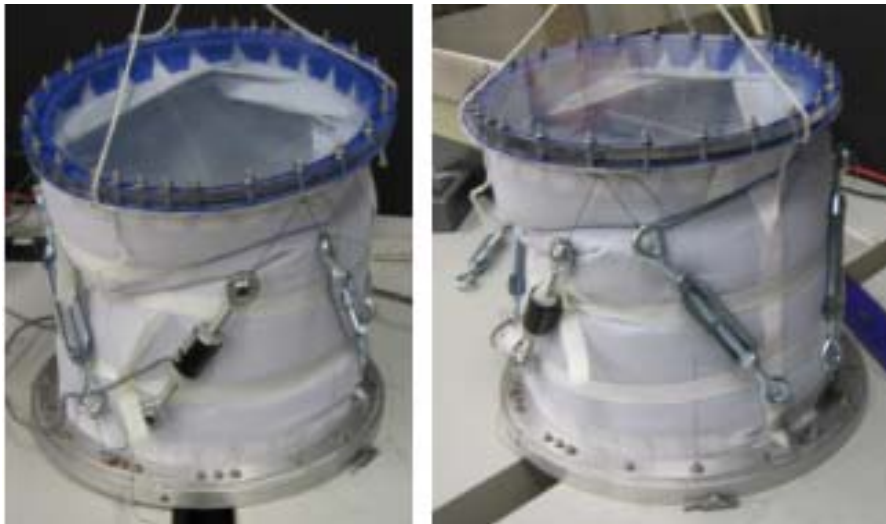


Figure 53: Load Cell Integration

Chapter 5 : Inverse Kinematics for the Stewart Platform

Although the forward kinematics for a Stewart Platform tend to be computationally intensive, and may not lead to a unique solution, the inverse kinematics are relatively straightforward. In other words, if the location and orientation of the platform are known, unique link lengths can be calculated.

5.1 Definition of Coordinate Systems

The inverse kinematics code takes node locations in the coordinate system affixed to the platform (hereafter designated as coordinate system B), and finds their locations in a coordinate system fixed at the center of the base (coordinate system A). Since the locations of the bottom nodes are already known, the link lengths can be calculated by finding the distance from the bottom nodes to the top nodes, in the base coordinate system.

The platform and base coordinate systems are illustrated in Figure 54, which shows the cylinder in its 'neutral' position (e.g. centers of platform and base have no horizontal offset, and node 1 is opposite from node 5, when viewed from the top down). In this configuration, the x axis of the platform coordinate system is rotated 60 degrees about the z axis, in respect to the x axis of the base (represented as a wide dotted line in the figure at the far right). As shown in the figure, the X axis of the base is lined up with node 4 on the base, and centered between nodes 5 and 6. The X axis on the platform goes through node 1, and bisects nodes 2 and 3.

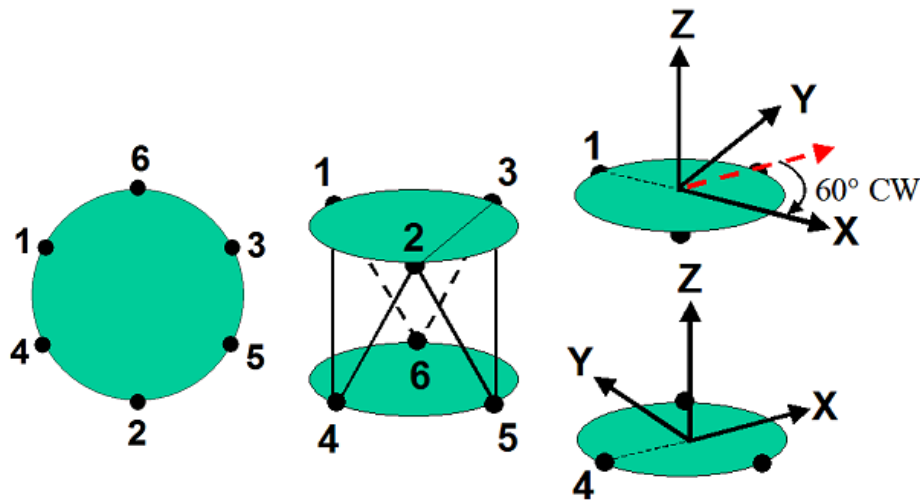


Figure 54: Left: Top Down View of Platform in Neutral Position. Center: Node Numbering Right: Base and Platform Coordinate Systems

Figure 55 shows the vectors that are used to find the distance between nodes in the A (Base) and B (Platform coordinate systems).

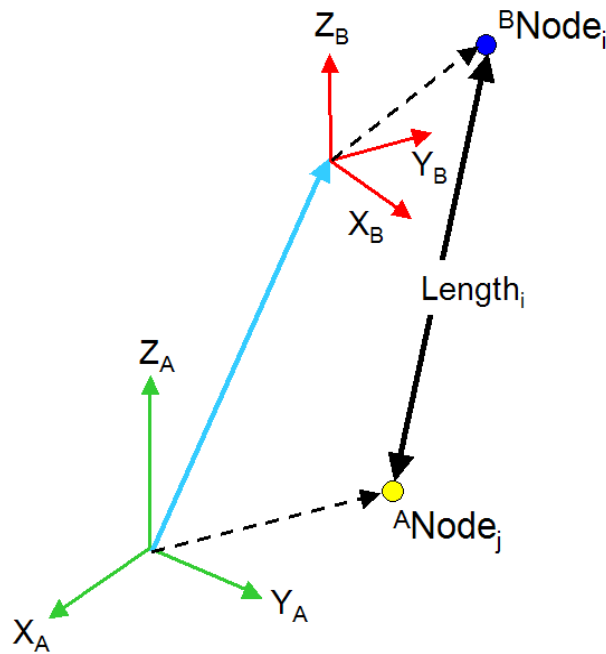


Figure 55: Relationship Between Nodes in A and B Coordinate Systems

The figure also shows the naming convention that will be used in the inverse kinematics computation. For example, ${}^B\text{Node}_i$ represents the vector from the origin of the B (Platform) coordinate system, to Node i . Length_i is the vector distance from Node j to Node i . The graphic shows the most general case, where the nodes are not necessarily in the XY planes of the A and B coordinate systems.

5.2 MATLAB Code

A code was written in MATLAB to perform the inverse kinematics calculations. The program asked for the radii of the top and bottom plates, the x, y , and z separation of their centers, and the orientation of the platform. The orientation of the platform was supplied in Euler angle rotations, which are rotations about local axes that change orientation as the platform rotates. The assumed order of rotation was: 1. Rotation about the initial Z axis (α), 2. Rotation about the new Y axis (β), and 3. Rotation about the new X axis (γ).

5.2.1 Vector Representations of Node Locations

MATLAB was then used to find the vectors ${}^A\text{Node}_i$ for $i=4$ through 6. These vectors represented the locations of nodes 4 through 6 in the base coordinate system. The same calculations were completed for the platform nodes, to find their coordinates in the platform coordinate system.

5.2.2 Transformation of Platform Nodes to Base Coordinate System

Now that all node locations were known in their respective coordinate systems, the locations of all nodes could be represented in the base coordinate system.

Two things were needed to represent the platform nodes in the base coordinate system: the location of the platform origin with respect to the base origin, and the orientation of the platform in relation to the base. The first could be found in terms of a vector (using data already supplied to the program), and the second could be represented by a rotation matrix based on the Euler rotation angles (also already specified). By definition,

$${}^A Node_i = ({}^A P_{BO}) + {}_B^A R \cdot ({}^B Node_i)$$

Where ${}^A P_{BO}$ is the vector connecting the origin of the two coordinate systems, and R represents the rotation matrix that will rotate a vector from frame B to frame A. This equation will provide the vector from the origin of coordinate system A, to Node i (whose location is defined in the B coordinate system).

Rotation Matrix: (Graphic from Shane Jacobs)

$$R = \begin{vmatrix} c\alpha c\beta & c\alpha s\beta s\gamma - s\alpha c\gamma & c\alpha s\beta c\gamma + s\alpha s\gamma \\ s\alpha c\beta & c\alpha c\gamma - s\alpha s\beta s\gamma & -s\alpha s\beta c\gamma - c\alpha s\gamma \\ -s\beta & c\beta s\gamma & c\beta c\gamma \end{vmatrix}$$

Where $c = \cos$ and $s = \sin$

The next step, after determining the location of Node “i”, is to find its distance from node “j”. The magnitude of this vector difference will give the length of link ij.

$$Length_{ij} = |{}^A Node_i - {}^A Node_j|$$

The lengths calculated here are the ideal wire lengths that will place the platform in a desired configuration. In reality, the wires will be warped by the internal pressure of an arm segment, so the distance between nodes can be slightly less than the length of a wire connecting those nodes.

The next chapter begins by outlining qualitative results, gathered from observing the section once it was pressurized. These included the behavior of the fabric, deflection of the links, and repeatability of the test section's shape. Once these initial observations were made, the inverse kinematic model was used to choose platform orientations and locations, and to determine the accuracy with which the platform could be positioned.

Chapter 6 : Results

Observation of the test platform was combined with node locations and load measurements, to determine the behavior of the test section and the practicality of implementing a morphing arm (based on parameters mentioned in the introduction).

6.1 Qualitative Results

One of the first results obtained from this experiment was a better appreciation of the complexity of the arm segment's behavior. Because the shape of the segment is relatively simple, there is an expectation of how the cylinder should deform, but the pressurized shape actually tends to be rather complex, with localized fabric buckling and noticeable deformation of the wire links. A few test runs were conducted initially, to gain a qualitative understanding of how the test section was behaving.

However, before these results are discussed, a node numbering scheme will be applied to the platform, for easier reference (see Figure 56), and the difference between 'link length' and 'node-node distance' will be explained.

6.1.1 Node Numbering Convention

Nodes 1 through 3 are located on the top plate (the 'Platform'), while nodes 4 through 6 are connections on the bottom plate (the 'Base'). This convention applies when viewing the section from the front, as shown in Figure 56. As a reference point, all figures include the slot between adjacent tables, through which the pressure hoses were passed. When the camera is looking down this slot, the image is taken from the front (as shown).

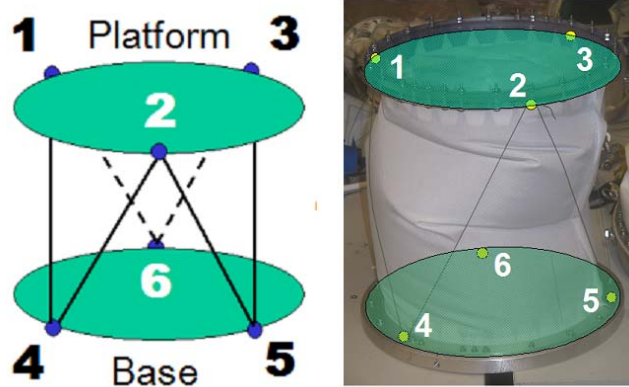


Figure 56: Node Numbering Convention

At each configuration of link lengths, multiple pressurizations were conducted to determine if the section would change drastically in shape. For each pressurization, a label was placed below the test section for future reference (see Figure 57).

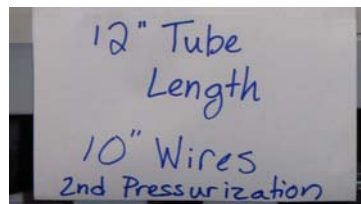


Figure 57: Test Section Labeling

There will be much discussion in this document about ‘node-node distance’ in relation to ‘link length’. The distinctions between these values are discussed in the following section.

6.1.2 Labeling Convention: Link Length vs. Node-Node Distance

There are three crucial parameters that define the wire links in the pressurized Stewart Platform. These are the *desired link length*, the *actual link length*, and the *node-node distance*.

The *desired link length* is the parameter that is output from the inverse kinematics code, given a desired platform location and orientation. This is an ideal length, and serves as a goal length when wires are being measured.

The *actual link length* represents the length of a physical wire link, including some inaccuracies due to measurement error. The precise magnitude of the actual link length is an unknown, because the distance between nodes is only measured when the system is pressurized, once the wires have already been deformed.

The *node-node distance* is the magnitude of a vector in 3D space connecting two nodes. This distance will be shorter than the *actual link length*, assuming that the pressurized fabric expands circumferentially and impinges on the wires. The node-node distance may in some cases be larger than the desired link length, if there is significant error between the *desired* and *actual* length of the link.

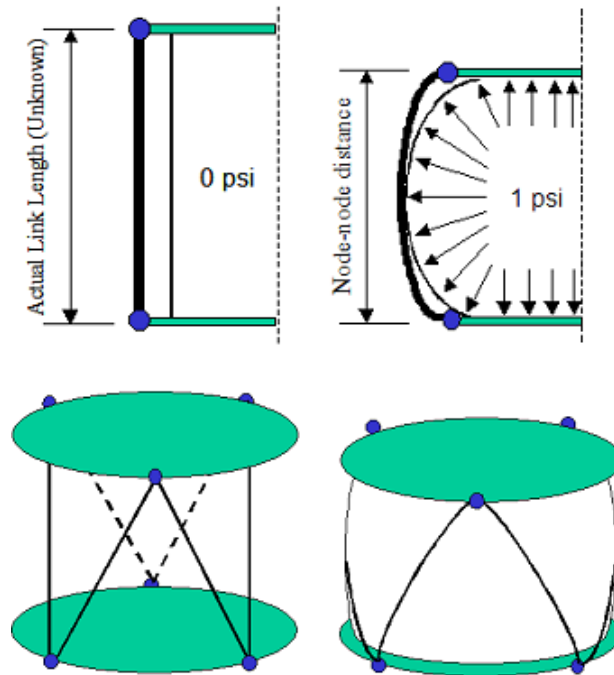


Figure 58: Exaggerated cross section of undeformed (left) and pressurized (right) test segment

As shown in Figure 58 , the wire links are deformed outward by the pressurized fabric. This deformation is not necessarily uniform, because there are bound to be asymmetrical bulges and creases in the fabric sleeve. The node-node distance will almost always be shorter than the actual wire length. The graphic on the previous page gives a simple 1D example of this phenomenon, where the node-node distance shrinks as the section is pressurized (although the *actual link length* remains the same).

For example, assume that two plates are being placed parallel to each other, 10 inches apart. In this case, according to the inverse kinematics code, the *desired link length* is 11 inches. The wire links are tied off at approximately 11 inches in length, but there is some error in measurement. Let’s assume now that we somehow know the *actual link lengths* (which cannot normally be measured). These hypothetical values are presented in . Some will probably be too short, while others will doubtless be too long.

Table 1: Sample errors in measured link lengths

Link IDs	Desired Link Length (in)	Actual Link Length (in)
14	11	10.89
42	11	10.91
25	11	11.09
53	11	10.87
36	11	11.15
61	11	10.79

Now assume that the section is pressurized, and node-node distances are measured. Because the bulging of the fabric is not uniform, some links will shrink in apparent length more than others. This change in apparent link length is apparent in the node-node distance, which is measured with great accuracy (hypothetical values are seen in Table 2).

Table 2: Example node-node distances

Link IDs	Desired Link Length (in)	Node-Node Distance (in)
14	11	10.84
42	11	10.81
25	11	11.04
53	11	10.68
36	11	11.05
61	11	10.67

The only comparison that can be made with significant accuracy, is between the desired link length (from the inverse kinematics) and the magnitude of the vector connecting a pair of nodes (node-node distance). This is the error that will be described in the following sections as ‘link length error.’ It is the summation of an unknown error associated with measurement, combined with an error due to the deflection of the wire, which has the effect of shortening the apparent length of the link (the node-node distance). However, when the same set of links are used between successive pressurizations, the error due to the pressurized fabric can be better quantified (since the measurement error will be constant). Note: because the measurement error can lead to links that are initially too long, the final node-node distance can actually be longer than the desired link length.

6.1.3 Pressurization with Parallel Plates

During the first pressurization, link lengths were adjusted so that all would remain in tension, and so that the top and bottom plates would be approximately parallel. The section showed significant bulging where the wires were not constraining the fabric, and noticeable deformation in the wires. This bulging was most noticeable when viewing the section from the ‘back’. The thin dark line along

the length of the section would generally run vertical, if the sleeve were standing upright.

The fabric tended to pucker inward at the seam (along the right side of the section, when viewed from the front - Figure 59 b), and bulge out on the opposite side.

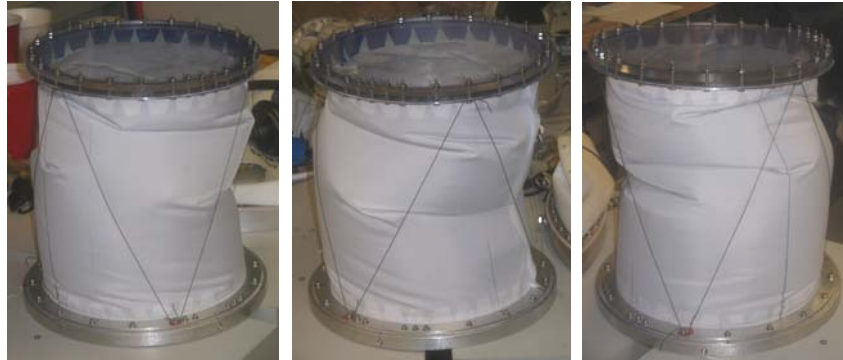


Figure 59: Initial Pressurization of Test Section. A.) Section Viewed from the Left. B.) Section Viewed from the Front. C.) Section Viewed from the Back

The wire lengths were shortened to 10" and the process was repeated: the section was pressurized, and observed for its deformation behavior. The results of this pressurization are shown in Figure 60.



Figure 60: Pressurization with 10" Wires

As seen in the figure, one of the wires was actually slack in this case. This proved to be a common problem when attempting to position the two plates parallel with each other, with equal link lengths. This lack of tension has a few potential causes, the most likely of which is simply inaccuracy in measuring the links. If four of the six links are the correct length, they will successfully hold the top plate in the desired configuration. The other wires will remain slack, since they are slightly longer.

This slack in the wire is also potentially caused by the bulging of the fabric, which forces some of the wires outwards and may cause an uneven tension distribution across the links.

Positioning the plates in an exactly parallel configuration may be a difficult proposition, since several of the wires can potentially be slack. Whereas in the Morphing Upper Torso the tension in the links had a preferred direction (e.g. pulling a ring back towards the back plate), the current configuration has no bias direction (is being controlled from all sides, and will not have a preferential direction of motion). This lack of preferred direction could potentially lead to problems with controlling the system, and concerns about its stability.

To determine how much the section's shape would change between pressurizations, the section was deflated and then repressurized without adjustment of the link lengths (Figure 61).

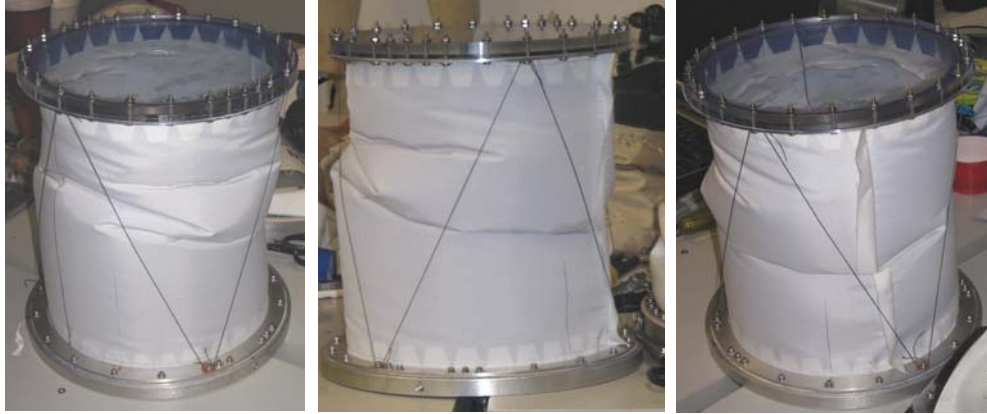


Figure 61: 10" Wires, Pressurization 2

The cylinder has actually fallen into a very different deformed shape than in its first pressurization. Specifically, there seems to be more general folding of the fabric, rather than the wholesale bulging of the initial pressurization. The two pressurizations are compared side by side in **Figure 62**.

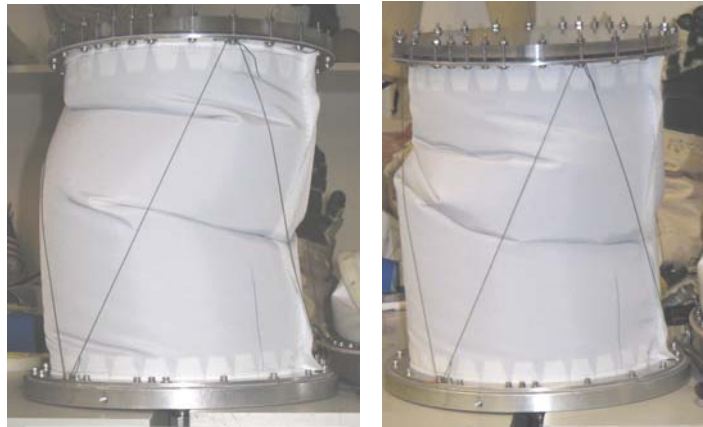


Figure 62: 1st and 2nd Pressurizations Compared

The ‘fronts’ of both sections are shown in the image, revealing the very different buckling behavior seen between pressurizations. Nevertheless, both seem to crease inwards at the seam, which likely has slightly higher stiffness than the remainder of the section.

Interestingly, there appears to be less deflection of the wires in the 2nd pressurization, suggesting that the folds in the fabric are reducing the impingement on the wires. This leads to the idea of introducing folds and creases in the fabric, to reduce the effect of the fabric on the wires.

Another potential method for reducing the influence of the fabric was to simply place the plates farther apart, reducing the amount of additional material, and hopefully the amount of puckering. For the next pressurization, 12” wires were used to reduce the amount of compression in the sleeve. The results of this test are shown in Figure 63.



Figure 63: Pressurization w/ 12" Wires, Showing Slack

When 12” wires were used, there was significant slack in 2 of the wires. The remaining four seemed to be providing the positioning for the platform, suggesting that the two slack wires were redundant. Figure 64 shows the location of the slack wires, links 25 and 36, represented as dotted lines. The Stewart platform will behave like the one shown at the right, until the two slack wires become tight (as the platform moves).

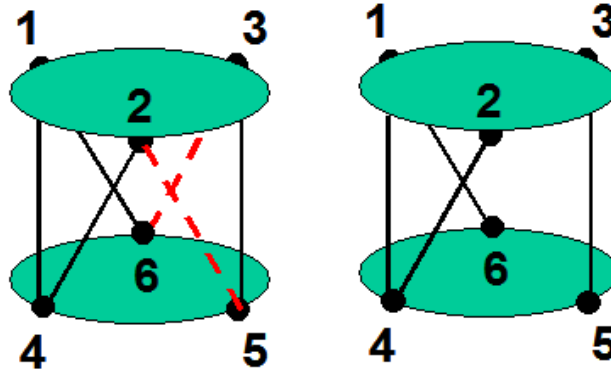


Figure 64: Location of Slack Wires, and Resultant Behavior

Now that some pressurizations had been conducted with the plates parallel to each other, some test pressurizations were done with the plates at a more complex configuration. The inverse kinematics code was used to select link lengths that would place the platform at a given location and orientation, and then the section was pressurized.

6.1.4 Pressurization at More Complex Configurations

An initial attempt was made to position the plate at a ten degree angle from horizontal (rotation of γ , about the local x axis), with a plate center separation of 9.625". However, due to an error in the first version of the inverse kinematics code, the link lengths for a 45 degree rotation were provided. This rotation led to an interesting result: the proscribed wire lengths were longer than the fabric sleeve, so the fabric took the resultant longitudinal load, leaving all but two of the wires slack (Figure 65). This result revealed another factor that had to be included in the inverse kinematics code: the maximum separation between the plates. If this separation

distance exceeded the length of the fabric sleeve, the sleeve (and not the wires) would take the resulting load.



Figure 65: Plate at Drastic Angle Led to Loading of Fabric Sleeve

The plate was next repositioned to a less drastic angle: 13 degrees about the local y axis (beta) and then 3 degrees about the platform x axis (gamma). The image below (Figure 66) shows the shape of the section, when in this configuration.

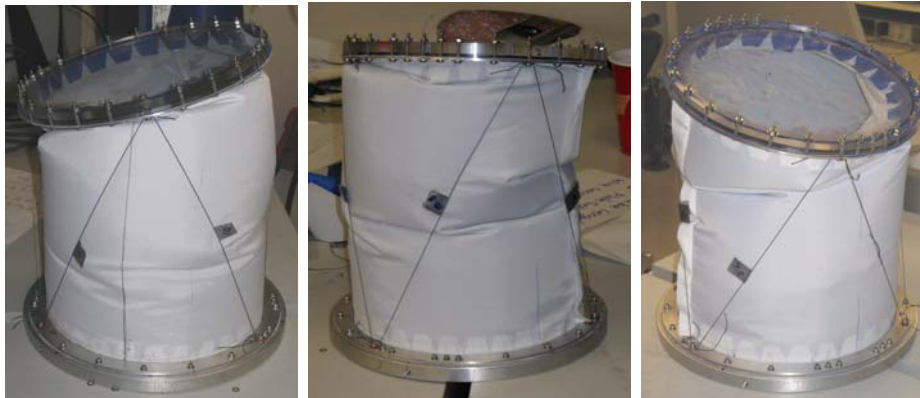


Figure 66: Pressurized Section at 13 degrees beta, 3 degrees gamma

The section was depressurized and repressurized using the same link lengths, and appeared to take approximately the same configuration on successive pressurizations. However, a more accurate way to check the repeatability of the

platform's configuration was to use the FAROArm, and find the change in platform configuration between pressurizations. The next section of this document discusses the quantitative results obtained through measurement of the platform.

6.2 Quantitative Results

For each of a series of pressurizations in various configurations, measurements were taken of the node locations of the top and bottom platforms. For the first set of pressurizations, the center of the platform was recorded and compared to the desired location. The distances between nodes were also taken, and compared to desired link lengths. The error between these values would indicate the amount of deformation in the links, since any outward perturbation would shrink the apparent length of the wire. Later measurements would involve both the position and orientation of the platform.

6.2.1 Error in Platform Center Location

The error in locating the center of the platform was found for a variety of configurations. First, the plates were placed in an approximately parallel configuration, and the node locations were found using the FAROArm. These node locations were used to find node-node distances and the platform center.

6.2.1.1 Parallel Plates

The first measurements involved parallel plates placed 10" apart. The test section was pressurized at .5, 1, and 2 psi, and data was collected at each pressure. Table 3 gives a summary of link length errors, for all three pressurizations. The error

in link length is calculated by connecting the nodes with wires of known lengths, pressurizing, and then measuring the distance between nodes. There will be some initial measurement error in the length of the link, in addition to the error associated with the fabric impingement. For this test case, the largest total error was in Link 52, with an average error of nearly $\frac{1}{2}$ ", or approximately 4.5% of the link length. However, these errors had a minimal effect on the positioning accuracy of the center of the platform, which was maintained within $\frac{3}{8}$ " of its intended location, as show in Table 4. All errors are absolute values, unless otherwise indicated.

Table 3: Errors in Link Lengths

Error in Link Length			
Link	Min	Max	Average
41	0.159	0.222	0.187
24	0.019	0.240	0.159
52	0.299	0.571	0.439
35	0.232	0.319	0.273
63	0.069	0.186	0.120
16	0.210	0.265	0.238

Table 4: Errors in Platform Location

Error in Platform Location			
Axis	Min	Max	Average
X	0.233	0.259	0.243
Y	0.179	0.338	0.271
Z	0.045	0.165	0.112

In general, link lengths were maintained within $\frac{1}{4}$ " of their desired value ($\frac{1}{2}$ " at worst), and the platform location was maintained within $\frac{3}{8}$ " of its desired location, even as pressure was increased. Again, it should be noted that wire lengths

are approximated when setting up the test section, so some portion of the error is likely due to minor errors in measuring links. To better determine the amount of error caused by the pressure, an effort was made to reduce the impingement of the pressurized fabric on the wires. The results of this effort are seen in the next section.

6.2.1.2 Addition of Convolutes to the Pressurized Test Section

In an attempt to reduce the influence of the fabric on the wires, gathered sections were introduced to the cylinder. This was accomplished by tying pieces of narrow webbing around the test section at approximately even intervals, to cinch down the pressurized tube and force more uniform deformation.

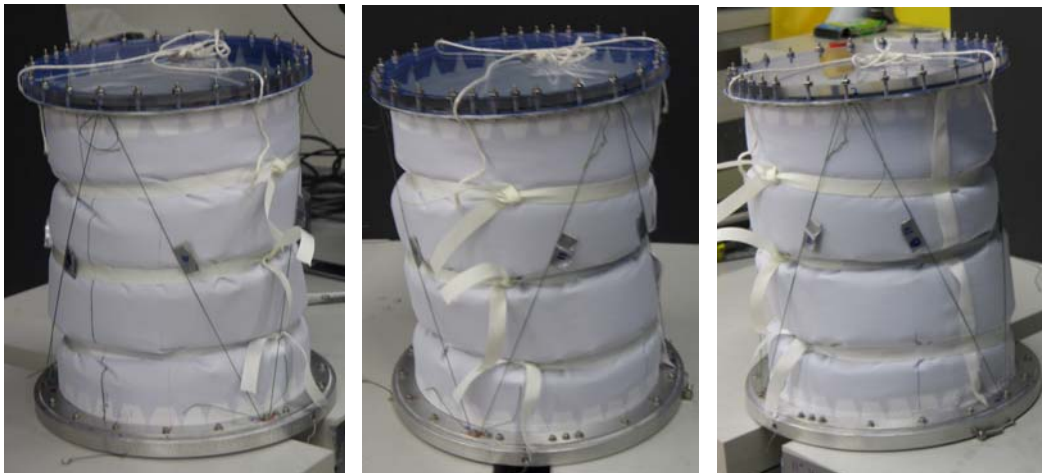


Figure 67: Uniform Deformation Forced by Introduction of Convolutes

As seen in Figure 67, the fabric does not appear to contact the wires at all. This was a very promising result, since it suggested that the influence of the fabric could be lessened, if not eliminated entirely.

Again, the locations of all nodes were measured, and this information was used to find the center of the platform and the actual node-node distance. A summary

of the error in link lengths is given in Table 5. In this case, it seems likely that the majority of the error is simply due to measurement – meaning that initial errors in link length could potentially be as high as ¼”.

Table 5: Error in Link Lengths

Error in Link Lengths (in)			
Link	Intended Link Length	Node-Node Distance	Error
41	11	10.76	0.237
24	11	10.87	0.133
52	11	10.92	0.079
35	11	10.90	0.103
63	11	10.75	0.253
16	11	10.76	0.236

Table 6: Errors in Platform Center Location

Error in Platform Location (in)			
Axis	Intended	Actual	Error
X	0	0.157	0.1565
Y	0	0.2	0.2002
Z	10	10	0.0017

In the case of the platform center, the largest error was less than a ¼” from the intended location. To better determine if there was a decrease in error due to the convolutes, the results of this test case were compared to the results for the previous test at 1 psi.

6.2.1.3 Comparison of Results with and without Convolutes

As can be seen in the following set of tables, the convolutes had a dramatic effect on the accuracy of positioning the platform. This is likely due to the decrease in impingement on the wires, because the fabric is being forced into a uniform shape.

Table : Errors with Convolutes (Left) and without Convolutes (Right)

Error in Link Lengths (in)			
Link	Desired Link Length	Node-Node Distance	Error
41	11	10.76	0.237
24	11	10.87	0.133
52	11	10.92	0.079
35	11	10.90	0.103
63	11	10.75	0.253
16	11	10.76	0.236

Error in Platform Location (in)			
Axis	Intended	Actual	Error
X	0	0.157	0.157
Y	0	0.200	0.200
Z	10	10.00	0.002

Error in Link Lengths (in)			
Link	Desired Link Length	Node-Node Distance	Error
41	11	10.84	0.159
24	11	10.78	0.219
52	11	10.43	0.571
35	11	10.68	0.319
63	11	10.93	0.069
16	11	10.76	0.238

Error in Platform Location (in)			
Axis	Intended	Actual	Error
X	0	0.259	0.259
Y	0	-0.298	0.298
Z	10	9.874	0.126



Figure 68: Section with convolutes (Left) and without (Right)

With convolutes, the average error in link length decreases from .263” to .173”. In other words, the link is not experiencing as much of an outward perturbation when the convolutes are constraining the expansion of the fabric. Again, some of the error in link length is associated with measurement error. The average error in positioning the center of the platform decreased from .228” to .119”. In other words, the average error in positioning the plate, and the average deformation of the wires, decreased by approximately half. This result suggested that convolutes could

be used to position the platform more predictably, at least when a simple parallel plate configuration was desired.

Next, the platform was placed in a slightly more complex configuration, and the center and link lengths were measured as before.

6.2.1.4 Angled Platform

The platform was set at a separation distance of approximately 9.5", at a slight angle from horizontal, as seen in Figure 69 . The section was deflated and pressurized a total of three times, and data for the center of the plate was collected. On the second and third pressurization, 3D node locations were noted and recorded using the FARO arm. Due to data collection issues, node locations are not available from the first pressurization. However, photographs were taken of each test for comparative purposes. The following figure, Figure 69 , shows the deformed shape that resulted from each pressurization. The cylinder appears to buckle in approximately the same locations in each case.



Figure 69: Change in Shape Between Three Successive Pressurizations

The node locations were used to find the center of the platform and the displacement between nodes. The distance between nodes is compared to desired

link lengths for the 2nd and 3rd pressurization, in Table 7. The largest error between the desired link length and actual node to node distance is ¼”, or approximately 3% of the length of the link.

Table 7: Error in Link Lengths

Link ID	Desired Link Length (in)	Pressurization 2		Pressurization 3	
		Node-Node Distance (in)	Error (in)	Node-Node Distance (in)	Error (in)
53	9.5	9.23	0.27	9.33	0.17
36	8.75	8.85	-0.10	8.85	-0.10
61	9.75	9.79	-0.04	9.8	-0.05
14	10	9.94	0.06	9.91	0.09
42	11	10.9	0.10	11	0.00
25	10	9.95	0.05	10	0.00

The change in platform center between pressurizations is given in Table 8. The platform only shifts by a maximum of a tenth of an inch, in the largest dimension that is being controlled. This error in plate location would likely be scaled down for a smaller diameter section (e.g. the cross section of an arm).

Table 8: Location of Platform Center

Change in Center Location			
Pressurization	X (in)	Y (in)	Z (in)
2	0.934	0.075	9.41
3	0.914	0.089	9.521
Error	0.020	0.014	0.112

To obtain data points for a different configuration, the section was depressurized and the link lengths were changed. During this test, the platform was oriented with approximately 6 and 10 degree rotations about the X and Y axes, respectively (Figure 70).

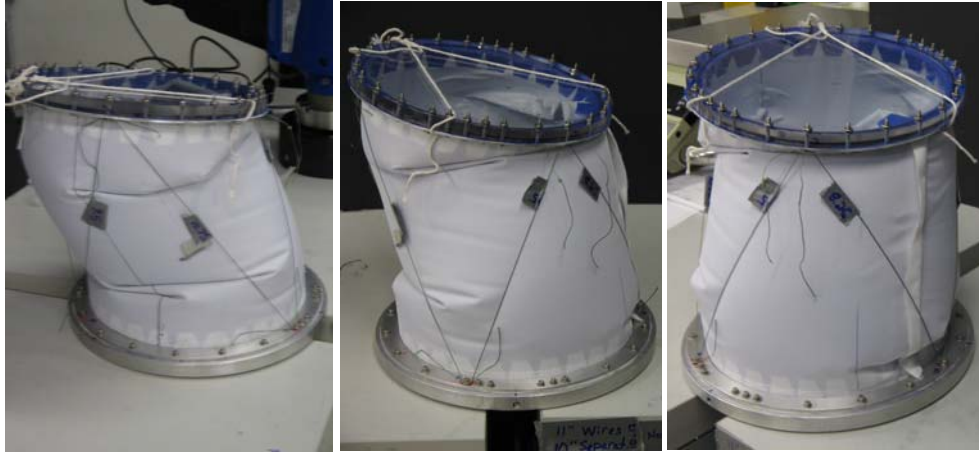


Figure 70: Pressurization at 6,10 and 60

The resulting link length errors are provided in Table 9. The maximum error in link length is over $\frac{1}{2}$ "', while the average is approximately $\frac{1}{3}$ ". Some of the actual node-node distances are longer than the desired link length, because of measurement errors.

Table 9: Errors in Link Length

Error in Link Lengths (in)			
Link	Desired Link Length	Node-Node Distance	Error
41	10.78	11.39	0.602
24	8.29	8.18	0.102
52	8.25	7.89	0.356
35	10.17	10.03	0.142
63	8.95	8.82	0.132
16	9.51	9.09	0.422

The errors in platform location are provided in Table 10. The maximum error in platform location is $.28$ "', and the average is approximately $\frac{3}{16}$ ".

Table 10: Errors in Platform Center Location

Error in Platform Location (in)			
Axis	Intended	Actual	Error
X	1	1.28	0.2803
Y	1.5	1.551	0.0512
Z	8	7.795	0.2051

To better determine how much of the error was caused by the pressurized fabric, convolutes were again introduced in an attempt to force a more uniform deformation behavior.

6.2.1.5 Angled Plate with Convolutes

As before, narrow strips of high-tensile-strength webbing were tied around the section before pressurization. The convolutes did change the deformed shape, but actually caused more pronounced bulging in some areas. This effect is best seen in Figure 71 , which shows the section after pressurization.

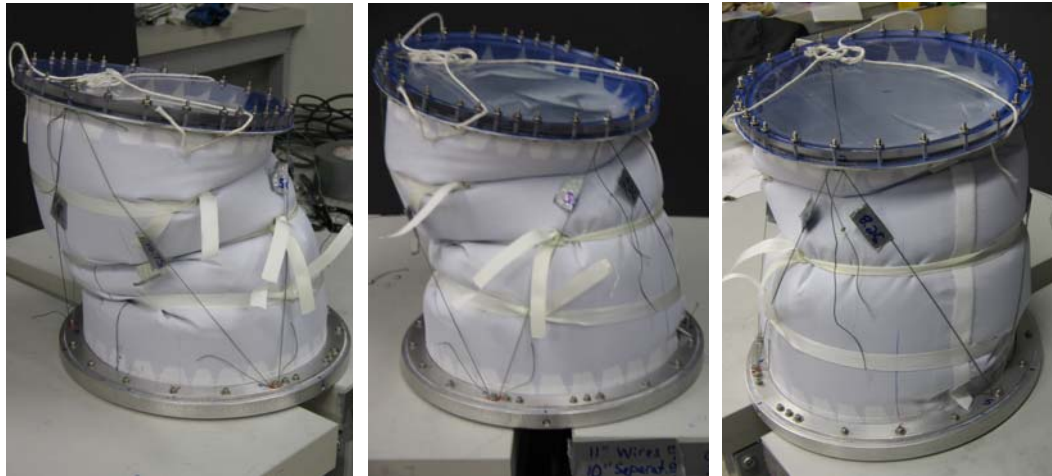


Figure 71: Angled Platform with Convolutes Added to Force Uniform Deformation

The errors in link lengths are given in Table 11 . The maximum error is $\frac{1}{2}$ " and the average error is $\frac{3}{8}$ ". In other words, the maximum error in link lengths decreased after convolutes were added, but the average error increased.

Table 11: Errors in Link Lengths

Error in Link Lengths (in)			
Link	Desired Link Length	Node-Node Distance	Error
41	10.78	10.55	0.239
24	8.29	8.19	0.094
52	8.25	7.77	0.477
35	10.17	9.66	0.512
63	8.95	8.58	0.367
16	9.51	9.08	0.424

The errors for the center of the platform are given in Table 12. The maximum error in platform location was .29”, and the average error was .197”.

Table 12: Errors in Platform Position

Error in Platform Location (in)			
Axis	Intended	Actual	Error
X	1	1.220	0.2201
Y	1.5	1.414	0.0858
Z	8	7.714	0.2858

Interestingly, the errors with and without the convolutes were essentially the same, if not slightly higher for the section with convolutes. This result suggests that the fabric is still deforming the wires, but that bulges are simply occurring in different areas, due to the influence of the webbing bands. The convolutes could conceivably increase the error in the link lengths, if there is a large protrusion at one location because the straps are tightening down on one section.

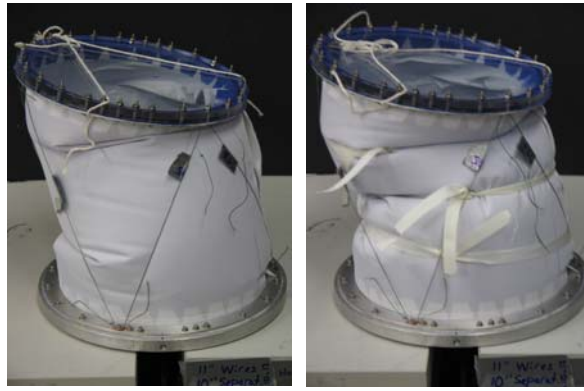


Figure 72: Deformation of Section With and Without Convolute

Figure 72 shows the difference in deflection behavior for the section, with and without convolutes. The section with convolutes appears to pucker outward more towards the top (at the left side of the test section), because the webbing has cut into the pressurized envelope quite deeply on the right.

Although determining the location of the platform was important, more useful data could be obtained through knowledge of both its location and orientation. For this reason, a code was developed to calculate the Euler angles of the platform in its pressurized configuration.

6.2.2 Euler Angle Calculation

Because the solution of the forward kinematics for a Stewart Platform is beyond the scope of this thesis, a simpler method was used to find the orientation of the platform.

First, the CAM2 Measure software associated with FAROArm was used to find the normal vector of the plane representing the top plate, in the base coordinate system. (Figure 73a) Next, a line was found along the x axis of the platform (passing through the center of the platform, and pointing away from Node 1, as shown in

Figure 73b). These two parameters provided the Z and X axes, respectively, of the coordinate system attached to the top plate (in the base coordinate system). The Y axis of coordinate system was found by taking the cross product of the Z vector with the X vector (Figure 73c). The unit vectors of this coordinate system were calculated next, by dividing the X,Y and Z vectors by their magnitudes (Figure 73d).

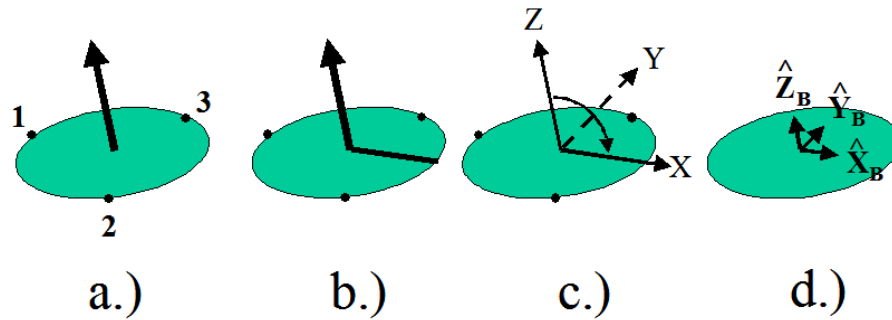


Figure 73: Calculation of Unit Vectors for Platform Orientation

The unit vectors could now be used to represent the orientation of the top plate in the base coordinate system. Specifically, the rotation matrix that represents the difference in orientation between the base (A) and platform (B) coordinate systems, is represented by the unit vectors of the platform coordinate system, in the base coordinate system (see). Each column in the matrix represents the unit vector of one axis of A in the B coordinate system.

$${}^A_B R = [{}^A X_B \quad {}^A Y_B \quad {}^A Z_B]$$

Given the known relationship between the rotation matrix and the Euler angles of the platform, the Euler angles can be calculated with relative simplicity.

$$R = \begin{vmatrix} c\alpha c\beta & c\alpha s\beta s\gamma - s\alpha c\gamma & c\alpha s\beta c\gamma + s\alpha s\gamma \\ s\alpha c\beta & c\alpha c\gamma - s\alpha s\beta s\gamma & -s\alpha s\beta c\gamma - c\alpha s\gamma \\ -s\beta & c\beta s\gamma & c\beta c\gamma \end{vmatrix}$$

For example, r31 in the rotation matrix is $-\sin(\beta)$. Therefore, taking the arcsin of this entry of the rotation matrix will provide the angle Beta, which represents the orientation of the platform about the local Y axis (which is preceded by a rotation of α about the z axis, and followed by a rotation of γ about the local X axis).

However, care should be taken in maintaining the correct quadrant for each Euler angle. For instance, .5 is the sine of two separate angles: 30° and 150° , as shown in Figure 74.

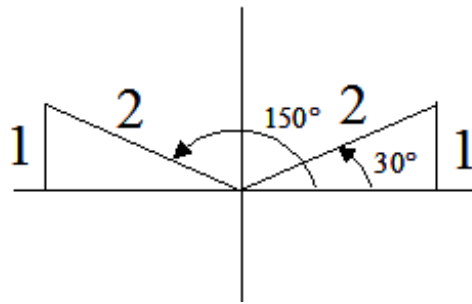


Figure 74: Calculation of Correct Angle

In cases where the quadrant of the Euler angle is not immediately apparent (for instance, the rotation of the platform should generally be about 60 degrees about the z axis), the arctan2 function of MATLAB, or atan2 of EXCEL, can be used to maintain the correct value of the angle.

A method was desired for verifying the rotation matrix that had been calculated for the platform, and which would be the basis for the Euler angle calculations. Therefore, the platform nodes were plotted in MATLAB, and compared

to nodes that had been moved from the base to the platform plane (via the rotation matrix and the vector connecting the origins of the two coordinate systems). The result of this transformation is shown in Figure 75 .

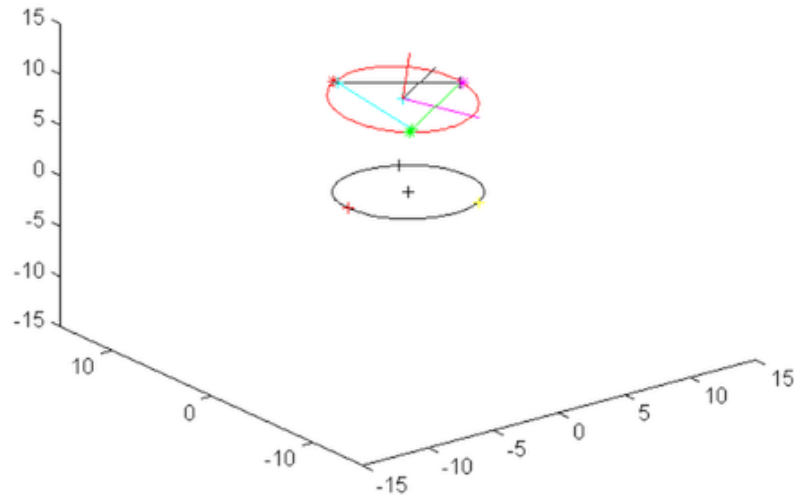


Figure 75: View of Platform and Nodes Relative to Base, for Verification

The measured locations of the platform nodes are displayed as asterisks (*), while the locations of the translated and rotated nodes are displayed as pluses (+). Because the base nodes are originally at a larger radius, they are placed just outside the platform nodes, in the same plane. The top ellipse in the image represents the shape of the base, if it were moved to the same location and orientation as the platform. Top, front and side views were available for further clarity.

The code was used to graphically verify the rotation matrix, to determine if there were any gross errors in calculation of the rotation matrix or platform coordinate system (for example, flipped directions of X and Y axes). It was also used for later pressurizations to graph node locations, and to visually verify calculated

Euler angles. For example, if the location of one node was imported incorrectly, it would not fall on the plane of the platform.

Now that a method had been developed for determining the orientation of the platform, the accuracy and precision of the positioning the platform could be determined.

6.2.3 Accuracy and Precision in Position and Orientation of Platform

Now that the location and orientation of the platform could be derived from simple node measurements, several tests were done to measure the precision and accuracy with which the platform could be located.

6.2.3.1 Initial Measurements of Plate Orientation and Position

The inverse kinematics code was first used to find the required link lengths for the following platform orientation: 10 degrees about the local y axis, followed by 6 degrees about the local x axis.

The resulting pressurized shape is seen in Figure 76 . At this point in testing, the turnbuckles had been introduced for easier resizing of the links. The slack lines in the image were used to hold the section upright while tying webbing strips around the section (when introducing convolutes). The plates had a center separation of 1.5” in the x direction, 1” in the y direction, and 8” in the z direction. Henceforth this will be known as Separation “A” for clarity.

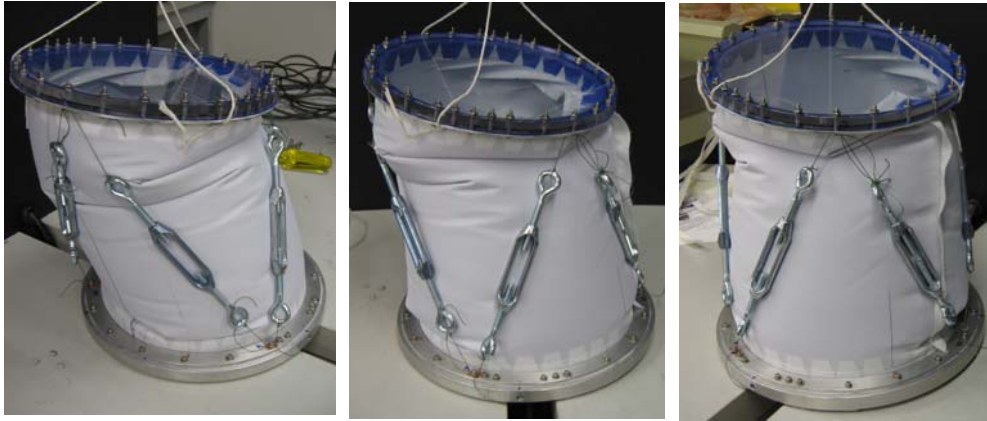


Figure 76: Initial Pressurization, Separation A

As before, the node-node separations and center locations were found using the FAROArm. However, in this case the plate Euler angles were also found. The results of three successive pressurizations are summarized in the following tables.

Table 13: Errors in Link Lengths

Link	Desired Link Length (in)	Node-Node Distance (in)	Error (in)
L41	10.78	0.127	0.068
L24	8.32	0.244	0.218
L52	8.22	0.371	0.139
L35	10.24	0.252	0.115
L63	8.92	0.057	0.056
L16	9.51	0.067	0.032

As seen in Table 13 , the maximum error in link lengths was less than 3/8", and the average error was less than a 1/4" for each link.

Table 14: Errors in Platform Center Position

Axis	Attempted Location (in)	Max Error (in)	Average Error (in)
X	1	0.284	0.225
Y	1.5	0.113	0.090
Z	8	0.196	0.171

All errors in platform location were less than 3/8", and the average error in platform location was less than 1/4", for the three pressurizations completed.

Table 15: Errors in Euler Angle

Platform Euler Angles	Attempted (Deg)	Max Error (Deg)	Average Error (Deg)
Beta (About y)	10	1.54	1.03
Alpha (About z)	-60	2.82	1.33
Gamma (About x)	6	3.29	1.56

As seen in Table 15 , the average error in plate orientation was 1.5 degrees or less. However, there were errors of more than 3 degrees in Beta, which occurred when there were large errors in two of the link lengths (3/8" in one, and 1/4" in the other).

Now that the accuracy of positioning had been examined for orientation of the plate, convolutes were introduced, to learn their effects on accurate and repeatable positioning.

6.2.3.2 Plate Orientation and Position: Influence of Convolute

As before, convolutes were added to the pressurized section by tying lengths of narrow webbing around the sleeve before pressurization. The restraints tended to slip when the section was deflated, so the repeatability in positioning the convolutes is relatively low. Figure 77 shows the deformed shape of the section with convolutes.

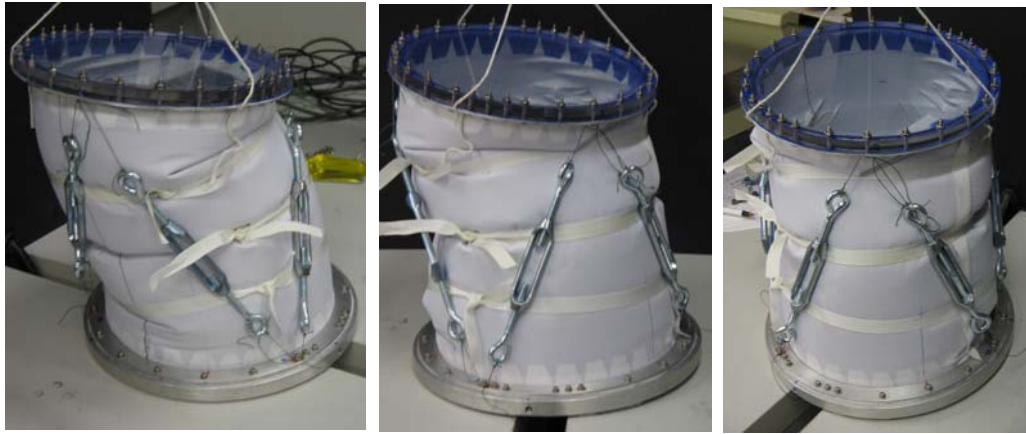


Figure 77: Separation A, Pressurized with Convolutes

Again, data was taken to determine the link lengths, center location and orientation of the platform relative to the base. This data is summarized in the following tables.

Table 16 : Errors in Link Length

Link	Desired Link Length (in)	Node-Node Distance (in)	Error (in)
L41	10.78	0.265	0.162
L24	8.32	0.371	0.254
L52	8.22	0.269	0.208
L35	10.24	0.243	0.134
L63	8.92	0.241	0.129
L16	9.51	0.063	0.050

As seen in Table 16 , the maximum error in link length is less than 3/8", while the average error is generally less than 1/4".

Table 17: Error in Platform Center Location

Axis	Attempted Location (in)	Max Error (in)	Average Error (in)
X	1	0.315	0.187
Y	1.5	0.134	0.074
Z	8	0.406	0.280

As is shown in Table 17 , there is a maximum error in plate center position of about 2/5” and an average error of more than ¼”. This is slightly higher than the error without convolutes, but still relatively minor given the size of the plate that is being positioned.

Table 18: Errors in Plate Orientation

Platform Euler Angles	Attempted (Deg)	Max Error (Deg)	Average Error (Deg)
Beta (About y)	10	4.46	2.65
Alpha (About z)	-60	3.65	2.90
Gamma (About x)	6	2.06	0.80

Given the data in Table 18 , there actually seems to be a significantly higher error in Euler angle, for the platform configuration with convolutes. Specifically, the average error can approach 3 degrees for both beta and gamma, and max errors of nearly 5 degrees are achieved. The highest error occurred when their were errors of more than a ¼” in two separate links: 41 and 52.

Once verifications had been done on the precision and accuracy of positioning the platform, the loads on the links was investigated.

6.2.4 Measurement of Link Tension

While the platform was in the position and orientation mentioned in this section (Separation A, angles of 6, 10 and 60), a load cell was attached to each wire in turn.

6.2.4.1 Measurement of Link Tension: Separation A

The test section is shown with load cell attached in Figure 78 . The load cell had threaded clevis pins at each end, but these only allowed less than a 1/16” of adjustment in length. Because of this, the wires on the test section had to be untied and shortened or lengthened, to adjust their length when the load cell was attached (there was not sufficient link length to attach the load cell in series with a turnbuckle). This method of adjustment necessarily led to errors in link length, because there was less fine tuning of link length available.

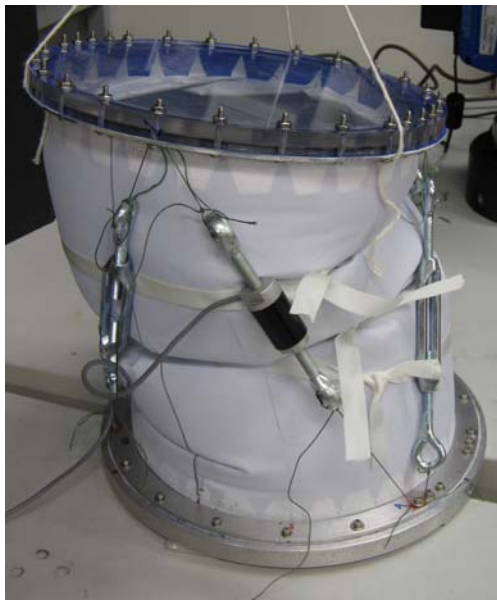


Figure 78 : Test Section with Load Cell Attached

The load cell was moved to each successive link, and the load on the cell was found for each pressurization to .5 and then 1 psi. This method of measuring the load was a result of having only one load cell, which did not allow measurement of load on more than one link simultaneously. In each case the voltage across the load cell

was measured before pressurization, at a pressure of .5 psi, at a pressure of 1 psi, and then again when the pressure was reduced to zero.

The results of the load measurements are summarized in Table 19 . As seen in the table, the maximum load occurred on Link 24, while the minimum load was on Links 41 and 35.

Table 19 : Loads on Links (lbs)

Link Loads(lbs)		
Link	Actual	Predicted
L41	2.17	4.35
L24	13.18	10.82
L52	10.98	11.98
L35	2.54	5.13
L63	9.51	17.70
L16	4.37	18.57

All of the link tensions are lower than predicted, and the sum of all tensions was only 40 lbs, where it should have been at least 60 lbs (based on the internal pressure and the area of the plates). Therefore, the tests with the load cell on Link 14 and 35, respectively, were reexamined.

Observation of the wires in these cases led to an interesting discovery: on these load cases, there were high side loads on the load cell, due to the high angle of the wire. This perturbation was a result of the significant bulging in these areas, which pushed the load cell relatively far away from the nodes at either end of the wire. This observation is shown in some detail in Figure 79 . This issue was

observed to a smaller degree on Link 16, and did not seem to occur at all on the other links, which experienced less deformation from the fabric.

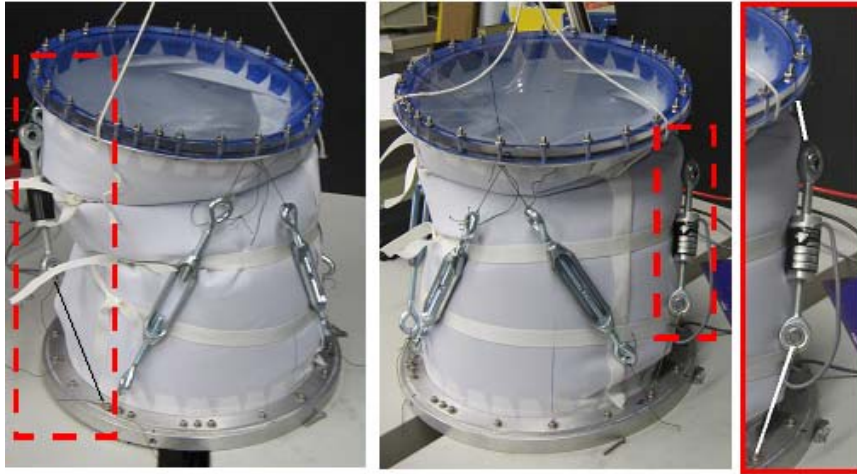


Figure 79: Deformation of Wire Links During Measurement of Load on Link 14 (Left) and Link 35 (Right and Center)

To check the measurement method on a simpler example, the link lengths were readjusted to place the plates parallel from each other, approximately 7” apart.

6.2.4.2 Measurement of Link Tension: Parallel Plates

Link lengths of 8.333” were attached to nodes on the top and bottom plates, and the load cell was attached successively to link 24 (at the front of the platform) and 36, where there was major deformation of the fabric sleeve. In each case, the test section was pressurized to .5 and then 1 psi.

A side view of the pressurized section is provided in Figure 80 , and shows the drastic bulging at the back of the segment. As seen in the figure on the right, the condition was worsened while measuring the tension in link 36, as the topmost band of webbing slipped upwards and allowed even greater bulging, and hence deflection of the lines attached to the load cell.



Figure 80: Bulging of Fabric Causing Large Side Loads on Load Cell

The results of the tension measurements are provided in Table 20. The apparent tension in link 36 (which exhibited large side loads) was only $\frac{1}{2}$ of the tension in link 24, for each of the two pressurizations.

Table 20 : Link Tensions for Parallel Plates

Link	.5 psi	1 psi
36	2.17	4.01
24	2.91	8.04

The results of this test led to significant concern about the accuracy of load data obtained using this method. In particular, a large portion of the load seemed to be directed into bending the load cell, rather than being directed down the barrel. This was verified by a simple test, conducted on the pressurized test section. As the load cell was pulled away from the pressurized wall of the section (increasing the eccentricity of the load), the load seen by the load cell decreased by 3X. The load cell was then pushed inwards, straightening the wires. In the latter case, the apparent load on the cell tripled. This seemed to confirm the hypothesis that a large side load

was affecting the accuracy of the measurement. This deformation, and resulting eccentricity of the load, is seen in Figure 81.

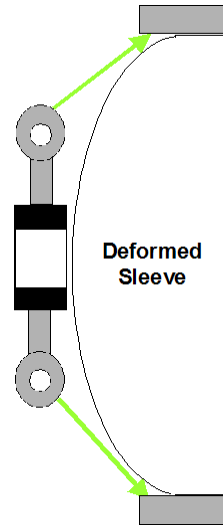


Figure 81: Wire Deformation

The load cell and clevis bolts create a very long, rigid section of the link, meaning that the short pieces of wire at either end are at very high angles, when there is large deflection in the wires. If a shorter load cell could be obtained, or if another method were used to reduce the eccentricity of the load, this method could perhaps be used with greater effect.

6.2.5 Application of Inverse Kinematics to Arm Length Changes

It has been suggested that the morphing arm concept could be used to resize the suit based on wearer. The wire lengths could be changed using linear actuators in series with the links, or rotary actuators mounted at the nodes. Before actuating the arm, it would be necessary to determine the required stroke length of the actuators.

For example, the rings in the arm would be drawn closer together to shorten the arm, or shifted farther apart to fit a longer wearer. The stroke length of each actuator would be determined by finding the maximum required change in link length. For instance, assume that the arm is sized to fit a 95th percentile man. How much would the link lengths have to change, if the same arm was resized to fit a 5th percentile woman?

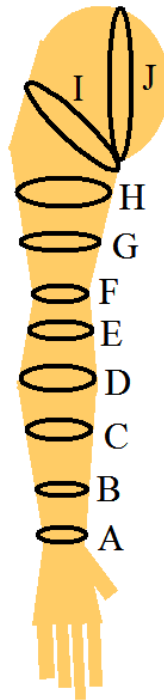


Figure 82: Example ring configuration

The first step of calculating link lengths in the morphing arm is to determine the number, size and spacing of the rings. Ring diameters are approximated by taking anthropometric data for arm sections from the Anthropometric Source Book [30], and then adding a margin of 1/2" around the arm cross section. The spacing of the rings is determined by finding the overall length of an arm section (e.g. wrist to elbow), and then splitting this into equal sections. For elliptical rings (e.g. the Scye bearing rings,

indicated as ‘J’), the aspect ratio of the ring was estimated using measurements of the author’s arm. The sizes and spacing of rings, as well as the node placement on the rings, were input into the inverse kinematics code. The result was a set of link lengths connecting each pair of rings (e.g. ring A and ring B). These link lengths were calculated for both sizes of arm (small woman and large man, assumed to be the extreme), and the change in link length were calculated.

The largest changes in link length were for the links connecting the scye bearing ‘J’ and intermediate ring ‘I’ and between the bicep ring ‘H’ and the intermediate ring ‘I’ (Table 21). The largest total change in link length was nearly 2.5” for the links connecting ‘I’ and ‘J’. All other link length changes were less than 1”.

Table 21: Changes in Link Length

	Link Lengths (in)						Link Lengths (in)						
	95th Percentile MN						5th Percentile WMN						Max Δ
	14	42	25	53	36	61	14	42	25	53	36	61	in
HI	5.83	3.19	4.39	4.39	3.19	5.83	4.01	2.16	2.97	2.97	2.16	4.01	1.82
IJ	7.20	3.22	5.14	5.14	3.22	7.20	4.85	2.20	3.45	3.45	2.20	4.85	2.35

The small required changes in link are encouraging, suggesting that it would be feasible to create significant changes in arm length by making small link length adjustments.

Chapter 7 : Conclusions and Future Work

7.1 Conclusions

Although more data would be essential in proving these generalizations conclusively, the following initial results have been obtained through testing:

1. The center of the platform can be positioned within 3/8” of its desired location.
2. The Euler angles for the platform are highly dependent on link lengths (errors of 3/8” in link length lead to errors upwards of 5°)
3. The link lengths will generally be within 1/4” of the desired length, despite the effects of the fabric.
4. Convoluters may actually detract from the accuracy of positioning, because they cause localized bulging that deflects the wires.
5. Several inches of slack fabric would be suggested, since the fabric length will place the strictest limitation on the amount of rotation the rings can achieve (wires, not fabric, must do the load bearing).
6. Measurements of link tension seem to be highly dependent on the angle of the links from the load cell

These conclusions all suggest that the morphing suit concept would be feasible, with some limitations. Convoluters would be useful for reducing impingement of wires in straight sections of the suit (for instance, a section of the arm that would not bend), but could tend to increase wire deformation at joints (where the

rings in the suit would not remain parallel). Certain joints (such as the elbow) will be difficult to actuate, because the wire links must not intersect the subject's arm.

7.2 Future Work

Future work will include further testing on the test cylinder, as well as application of this technology to the University of Maryland Space Systems Lab's neutral buoyancy space suit analogue, the MX-II.

7.2.1 Testing to be Conducted with the Test Section

The influence of aspect ratio on deformed shape should be examined, by comparing the short (6") cylinder length to the 12" cylinder in similar configurations. An optimal aspect ratio should be suggested, based on results from the experimental model and potentially, an analytical model of pressurized cylinder buckling. The trade will likely involve the need for slack fabric vs. the problems associated with an excess of bulk fabric, which when pressurized expands outwards and deforms the wires. The slack fabric is required to allow rotation of the platform (e.g. twisting the rings about the central axis of the cylinder, or adjusting the pitch and yaw (shifting one ring out of a parallel configuration with the next ring).

A more accurate way of measuring the tension in the links should also be determined. The problems with the current setup include the high sensitivity of the load cell to side loads, and the length of the load cell, which leads to high eccentricity of the applied load. A solution would be to obtain a much shorter load cell (in relation to the wire links), or to find a load cell that is less susceptible to side load.

Another method of analyzing the deflection of the wires, would be to approximate each link as a beam with an applied distributed load. The effective width of the link would be determined empirically, by determining the node-node distance, comparing this to the desired wire length, and using the FAROArm to find the max deflection of the wire. A correlation could then perhaps be found between the applied pressure load, and the change in apparent link length (node-node distance vs. desired link length).

7.2.2 Modifications to the Test Section

Once the behavior of a single section has been characterized, the test section should be extended to create a serial parallel manipulator (essentially, two test sections stacked on top of each other). Is the behavior still predictable, or do inaccuracies propagate to the point that the platform location is no longer repeatable and predictable?

Another, more sophisticated addition to the test section would be a specially constructed anisotropic fabric, with significantly different material properties in the longitudinal and circumferential directions. The fabric could be constructed to have minimal circumferential expansion, but enough longitudinal stretch to increase the ring-ring distance before donning. The excess fabric length could then be folded into a manageable accordion pleat, without fear of significant outward bulging that is normally associated with a pressurized section.

It should be noted that all experimental data is being taken at 1 psi, to maintain the structural integrity of the test setup. Because of the relatively low

operating pressure, gravity still applies a noticeable portion of the total load on the test section. In the lower gravity environment of the moon and Mars, given the generally high operating pressure of an EVA space suit, pressure loads will dominate. Therefore, the analytical model of link tensions will be useful in estimating actual suit requirements.

Example: an internal pressure of approximately 0.1 psi will support the weight of the test section and allow it to stand upright. The plate is approximately 9" in diameter, and a pressure of $1/10^{\text{th}}$ psi across this 64 in^2 surface applies approximately 6.4 lbs of force. This suggests that the plate and fabric sleeve weigh approximately 6 and a half pounds. Even on Mars, this weight would be reduced to around 2 lbs. If a space suit were pressurized to 3 psi (the requisite pressure to allow a breathable atmosphere at 100% oxygen), the load forcing the plates apart would be close to 200 lbs, a factor of 100X larger than the gravity load!

7.2.3 Application to the MX-II

Finally, the ideal next step would be to incorporate a section of morphing arm into the Space System Laboratory (SSL) neutral buoyancy space suit analogue, the MX-2 (see Figure 83). Jacobs, Akin and Braden [31] discuss the current configuration of this suit in their 2006 paper. Suit operations are conducted in the SSL's 368,000 gallon water tank, which allows simulation of microgravity on very large scales. Morphing arm sections could initially be used to change the length of the limbs and reposition joints, for different sizes of suit subject. A future iteration would ideally allow active motion assistance.



Figure 83: The MX-II [spacecraft.ssl.umd.edu]

Integration into a manned test bed would allow a subject to wear the arm and conduct a qualitative performance evaluation, potentially supplemented by more quantitative measures of flexibility.

The MX-II is a combination soft and hard suit, with a rear entry configuration. The helmet and soft goods are attached to a Hard Upper Torso (HUT) constructed out of fiberglass. Test subjects ranging from 5'8" to 6'3" have been accommodated within the suit, with a weight range of approximately 120 lbs [31]. The suit is supplied with air at 6 scfm (standard cubic feet per minute) via an umbilical. Weights are provided in pockets on the exterior, to offset the buoyancy associated with the pressurized internal volume.

To integrate a morphing arm into the MX-II, the current soft goods would have to be segmented to allow the insertion of a series of rings into the arm. This procedure is illustrated in the following figure (Figure 84).

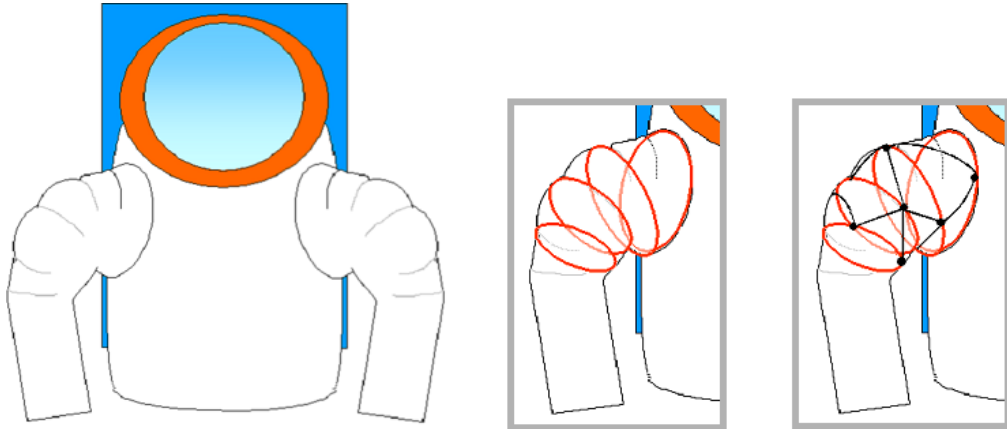


Figure 84: Addition of Resizing Rings to MX-II. Left: MX-II Torso. Center: Addition of rings. Right: Addition of links connecting rings

Either a new sleeve can be constructed, or the current sleeve can be sliced at the location of the rings. In either case, flanges would have to be added to integrate the rings into the sleeve.

Two different methods of sleeve construction are shown in Figure 85 . Flanges can be constructed in both the restraint layer and the pressure bladder (configuration at the center), or in the restraint layer alone (configuration at right). The pressure bladder flanges would be eliminated to minimize the number of leak points in the pressure bladder.

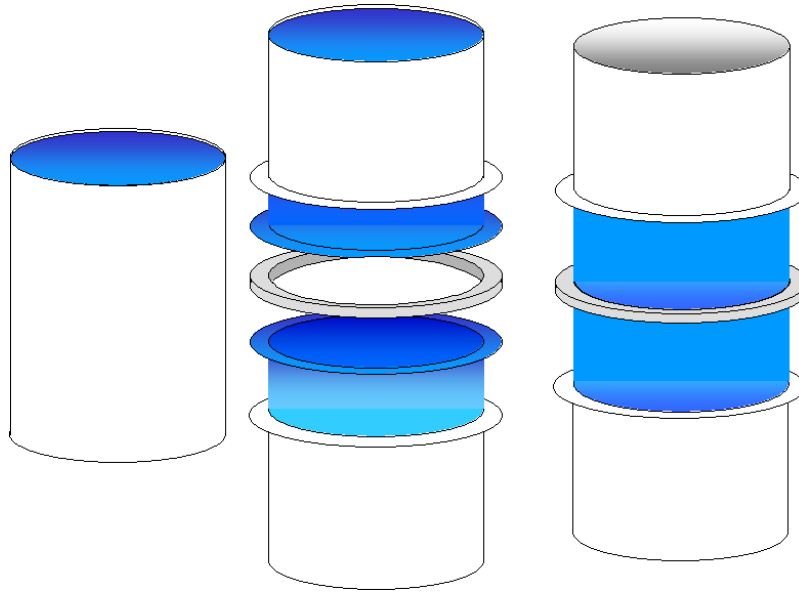


Figure 85: Sleeve segmentation (cutting the pressure bladder, or leaving it intact)

If the second configuration is chosen, the restraint layer must be ‘indexed’ to the pressure bladder to prevent relative motion. This is accomplished by stitching the internal seam of the restraint layer to the external seam of the pressure bladder, in at least one location. A simple example of indexing is shown in (Figure 86).

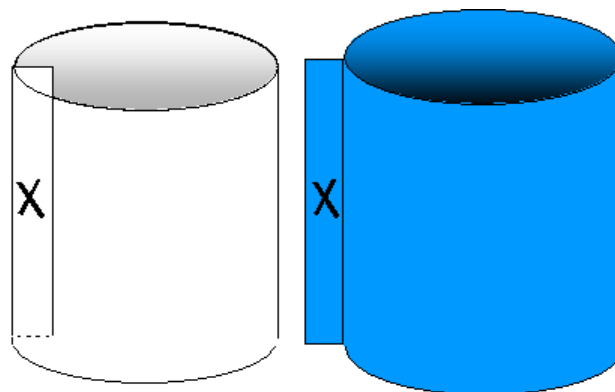


Figure 86: Indexing: Pressure bladder and restraint layer sleeves stitched together at 'X'

The rings would be actuated by either small rotary actuators at the nodes, or linear actuators in series with the links. The wire would then either be taken up on a reel, or drawn shorter and longer as the linear motor was driven through its stroke. If linear actuators are used, the wires should be attached to the integral rings through ‘bridges’ as shown in Figure 87 . Simply tying the links to bolts will not be sufficient for high-pressure (more than 2 psi) operation, because the fishing line will break at the washers (as was discovered during testing). The bridge can be attached to existing holes in the metal rings, which are required to attach the flanges.

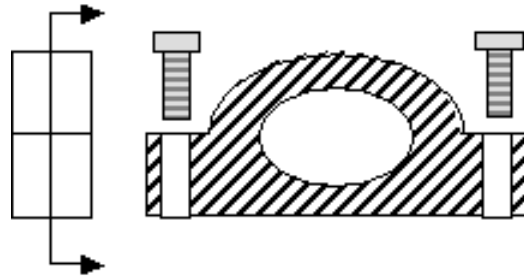


Figure 87 : 'Bridge' used to attach wires

The rotary or linear actuators integrated into the morphing suit would need the capability to change the link lengths while the suit was pressurized, and would need to be non back-drivable, to prevent unintentional changes in length under load.

For example, imagine a section of arm between the shoulder and elbow joints, which could be resized to efficiently position the elbow joint. At this location, the sleeve goes from a diameter of approximately 7.5 in at the base of the shoulder, to 5.5 in at the top of the elbow joint. This joint would be the simplest to construct, so would ideally be completed as a test joint before attempting the more complex configuration at, for instance, the shoulder. The current length of this section is 4.5

inches, which would require link lengths of approximately 5.5 inches. The arm is shown pressurized in Figure 88 , with the chosen section marked with rings at either end. Actuation of this section would allow the elbow joint to be positioned along the arm, in relation to the shoulder joint.

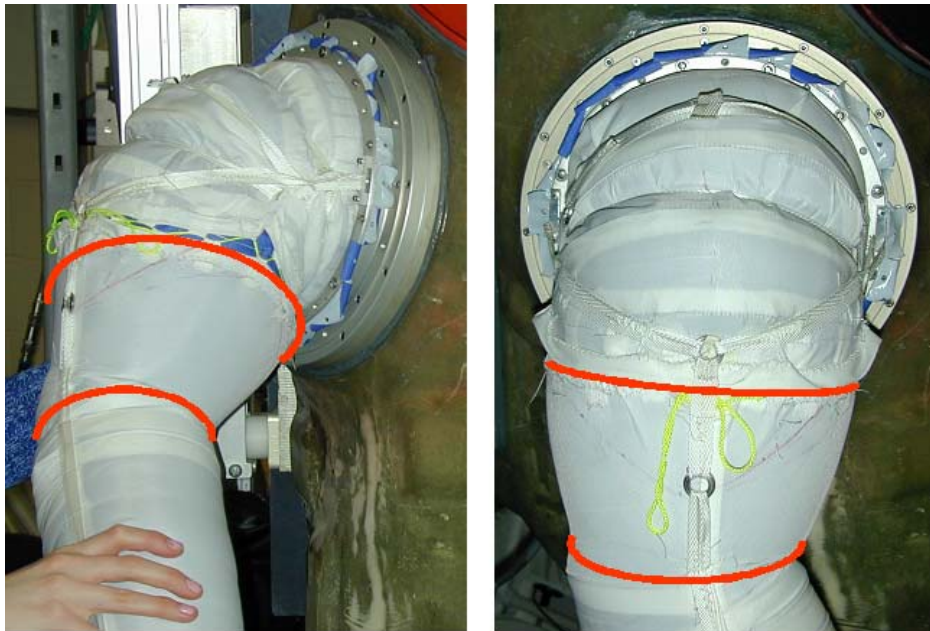


Figure 88: Pressurized MX-II Arm [spacecraft.ssl.umd.edu]

Now assume that the section must have the capability of either shrinking or lengthening by an inch from its nominal size. This would allow a total resizing capability of 2 inches, and require linear actuators with 1.59 inches of stroke. The minimum link length would be 4.85 inches, and the maximum would be 6.44 inches. At minimum separation, each actuator would take a load of approximately 23 lbs.

Note: this tension is calculated by looking at the Stewart Platform in static equilibrium, meaning that all forces and moments sum to zero. The direction of the pressure load is found by determining the normal of the top ring (in the coordinate system of the bottom ring), using the x,y and z coordinates of nodes 1, 2 and 3. The

magnitude of the pressure load is simply the internal pressure (3 psi was assumed in this case), multiplied by the average area of the rings. When the rings were farthest apart, the load would be decreased to 19 lbs. To account for possibilities of man loading (when the wearer applies loads to the suit, e.g. pushing out on the fingertips of the gloves and stretching the arm), an average load of 30 lbs will be used for actuator sizing estimates.

Table 22: Example actuator specs

Minimum Length	4.85	inches
Stroke Length	1.59	inches
Max Load	30	lbs

The power requirements for a linear actuator will depend on the applied load, and the speed at which the load is being moved. A passive resizing system would not require a high speed actuator, but an actively controlled morphing arm would need actuators with higher rates of motion, to effectively track the wearer's movement. Actuators with stroke lengths of 2 inches will be considered in this example.

The main concerns when selecting a linear actuator for this application, are overall length, and the high amperage normally required. Even the 'compact' linear actuators available on McMaster-Carr have lengths of more than 6.5 inches, and would require 2.8 A to move a 25 lb load, even at 24 VDC [32]. High amperages would be a major problem in an underwater environment, but would be seemingly unavoidable unless the voltage of an actuator was stepped up.

Another small linear actuator is the Danaher Motion Electrak 050 [33]. The retracted length is still too long (5.5 inches), and the current draw would still be half an amp, at 24 VDC, when pulling 30 lbs. (The length of the actuator must be *less*

than the link length, since there will need to be some length of wire on either end of the actuator.) Mounting the actuator would also be difficult, since there is only a clevis at one end of the cylinder.

Another linear actuator that is described as 'compact,' but which would be too long for this purpose, is the Motiotech Linear Electric Actuator [34], with a retracted length of 6.25 inches. At a load of 30 lbs (about 130 N), the actuator would draw about 2 A of current at 24 VDC. If a shorter version were available, it would be simple to mount this actuator because of the mounting holes at either end.

The concern here, is that the stroke length is very high compared to the required length of the actuator (in fact, it is nearly a third of the minimum link length). A smaller stroke length could be used (reducing the amount of resizing capability), but it is difficult to find a standard linear actuator with a stroke length of less than 2 inches.

Based on a survey of the available technology, it would seem that current draws are generally on the order of 2A, for a supply voltage of 24 VDC. This would suggest a power requirement of $(2A) \times (24V) = 48 \text{ W}$. If six actuators were used (one to change the length of each link), this would lead to a total power requirement of $48 \times 6 = 288 \text{ W}$! Again, there are also significant safety concerns associated with high currents in an underwater environment.

Although the single-link method could be used to minimize the number of actuators (use only one, to change the overall length of the link), there would likely be a danger of instability in the joint. This would occur if the single cable slid through the attachment points at the nodes, leading the section of sleeve to pitch and

yaw undesirably. This behavior would be more desirable in a joint, which would require rotational degrees of freedom, as opposed to a resizing section, which would only need to change in length.

This iteration of the morphing arm would allow a dynamic resizing capability (climb into the suit, and then shrink the size), while later iterations would ideally allow real-time motion assistance.

References

1. Shane E. Jacobs et al. "Morphing Upper Torso: A Novel Concept in EVA Suit Design." Proceedings of the 23rd International Conference on Environmental Systems. Norfolk, VA July 16th – 19th 2006.
2. National Aeronautics and Space Administration. "The Vision for Space Exploration." February 2004.
3. Charles C. Lutz, et al. "Apollo Experience Report – Development of the Extravehicular Mobility Unit." Lyndon B. Johnson Space Center, Houston TX. November 1997.
4. Connors, Mary M. Eppler, Dean. Morrow, Daniel G. "Interviews with the Apollo Astronauts in Support of Planning for EVA Systems Design." September 1994.
5. Jones, Eric M. "Genesis Rock." *Apollo 15 Lunar Surface Journal*. (Transcript) 1996. June 14 2006. <<http://www.history.nasa.gov/alsj/a15/a15.spur.html>>
6. Apollo 14 Mission Report. Houston, TX May 1971.
7. Apollo 11 Technical Crew Debriefing, Houston TX, July 31st 1969
8. David R. Williams, MD and Brian J. Johnson. "EMU Shoulder Injury Tiger Team Report." September 2003.
9. Harris, Gary L., "The Origins and Technology of the Advanced Extravehicular Space Suit" AAS History Series, Vol. 24, American Astronautical Society, 2001
10. "Learning to Work in the Suit: Interview with Dean Eppler".
<http://www.astrobio.net/news/article1738.html>

11. Graziosi, David. "Performance evaluations of an advanced space suit design for International Space Station and Planetary Applications." 29th International Conference on Environmental Systems, Denver CO July 12th -15th.
12. Weighing the Benefits of I-Suit: Interview with Dean Eppler.
<http://www.astrobio.net/news/article1748.html>
13. Courtney G. Brooks. James M. Grimwood and Loyd S. Swenson, Jr. Chariots for Apollo: A History of Manned Lunar Spacecraft. The NASA History Series. NASA SP-4205 National Aeronautics and Space Administration Scientific and Technical Information Office, Washington, DC, 1979.
14. Apollo 12 Mission Report. Houston, TX March 1970.
15. Apollo 16 Mission Report. Houston TX
16. Valentin Menendez, et al. "Performance of EVA Soft Suit Joints Influence of Driving Parameters." Proceedings of the 23rd International Conference on Environmental Systems. Colorado Springs, Colorado July 12-15 1993.
17. Schmidt, P.B., Newman, D.J., Hodgson, E., "Modeling Space Suit Mobility: Applications to Design and Operations". *Proceedings of the 31st International Conference on Environmental Systems*, July 2001.
18. Morgan, et al. Comparison of Extravehicular Mobility Unit (EMU) Suited and Unsuited Joint Strength Measurements. NASA TP-3613. Houston, TX June 1996.
19. Maida, et al. "Predicting Torque for Isolated Joints while Wearing an Extravehicular Mobility Unit (EMU)."

20. G. Kim Prisk, Janelle M. Fine, Trevor K. Cooper and John B. West. "Pulmonary gas exchange is not impaired 24 h after extravehicular activity."
21. Abramov, Isaak P. Stoklitsky, Anatoly Yu, Barer, Arnold S. Essential Aspects of Space Suit Operating Pressure Tradeoff.
22. E.A. Sorenson, R.M. Sanner, C.U. Ranniger. "Experimental Testing of a Power Assisted Space Suit Glove Joint." University of MD College Park, 1997.
23. Dave Graziosi, Jinni Ferl and Keith Splawn. "Development of a Space Suit Soft Upper Torso Mobility/Sizing Actuation System." SAE Transactions 2004, Journal of Aerospace Volume 113 no.1 pp. 516-522.
24. Bonev, Ilian. "General Terminology Related to Parallel Mechanisms."
Parallemic: The Parallel Mechanism Information Center. 27 February 2007.
<http://www.parallemic.org/Terminology/General.html>
25. Bonev, Ilian. "The True Origins of Parallel Robots."
<http://www.parallemic.org/Reviews/Review007.html>
26. Domagoj Jakobovic, Leonardo Jelenkovic. "The Forward and Inverse Kinematics Problems for Stewart Parallel Mechanisms."
27. Manfred Hiller et al. "Design, Analysis and Realization of Tendon-Based Parallel Manipulators." Mechanism and Machine Theory 40 (2005) 429-445.
28. "FARO: Platinum FaroArm." [Brochure]. Faro Technologies Inc. 2006.
29. Pickering, J. L. "72-H-298." Photo. Apollo 17 Lunar Surface Journal. 1995.
Accessed June 14th 2006. <<http://www.hq.nasa.gov/alsj/a17/a17.html> >

30. Staff of Anthropology Research Project. "Anthropometric Source Book Volume II: A Handbook of Anthropometric Data." Webb Associates, Yellow Springs, Ohio. 1978
31. Jacobs, Shane, Akin, David L., and Braden, Jeffrey R., "System Overview and Operations of the MX-2 Neutral Buoyancy Space Suit Analogue." 33rd International Conference on Environmental Systems. Norfolk, VA July 16th – 19th 2006.
32. McMaster-Carr.com
33. DanaherMotion.com
34. Motiontech.com.au